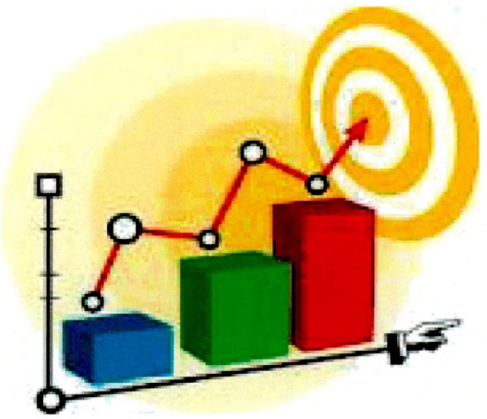

RESULTS AND DISCUSSION

CHAPTER - IV
RESULTS AND DISCUSSION

The results pertaining to present investigation on "Inhibitive Action of *Cocos nucifera* L. (Coconut palm) and *Borassus flabellifer* L. (Palmyra palm) - Shell, Leaf Stalk and Peduncle extracts on the Corrosion of Mild Steel in Acidic Media and their Adsorption Characteristics" are discussed under the following headings with the objectives set forth. Experiments have been conducted by varying the concentration of *Cocos nucifera* L. Shell (CNS), *Cocos nucifera* L. Leaf Stalk (CNLS), *Cocos nucifera* L. Peduncle (CNP), *Borassus flabellifer* L. Shell (BFS), *Borassus flabellifer* L. Leaf Stalk (BFLS) and *Borassus flabellifer* L. Peduncle (BFP) for different time intervals viz. ½ h, 1 h, 3 h, 6 h, 12 h and 24 h at room temperature and at elevated temperature (313 K – 343 K) using conventional mass loss methods. To learn the mechanism of inhibition, kinetic and thermodynamic parameters have been evaluated from temperature studies. To understand the nature of the inhibitors, electrochemical measurements were carried out. Efforts have also been taken to characterize CN and BF extracts.

- **Characterization of CN and BF extracts**

  The following techniques were carried out

  - FT-IR.
  - GC-MS.

- **Mass loss Measurements**

  The following parameters were investigated

  - Effect of concentration of CNS, CNLS, CNP, BFS, BFLS and BFP extracts and period of immersion on corrosion of mild steel in 0.5 M H_2SO_4 and 1 M HCl.
  - Influence of temperature on the corrosion of mild steel in the presence of CNS, CNLS, CNP, BFS, BFLS and BFP.
  - Adsorption isotherms.
  - Kinetic and Thermodynamic parameters.

- **Electrochemical Measurements**

  The following techniques were carried out

  - Tafel intercept method.
  - Linear polarization resistance method.
  - Electrochemical impedance measurements.

✶ **Surface Analysis Techniques**

The following surface analytical techniques have been used to study the surface of mild steel in the presence and absence of the inhibitors

- FT-IR.
- Scanning Electron Microscopy (SEM).

✶ **Statistical Analysis**

To investigate the inhibitor system is statistically significant or not by doing F-test by using the Analysis of Variance (ANOVA).

✶ **Theoretical calculation using Gaussian 03**

Quantum chemical calculations have been widely used to study reaction mechanisms and to interpret the experimental results with theoretical calculations.

4.1 CHARACTERIZATION OF CN AND BF EXTRACTS

4.1.1 FT-IR spectral analysis of CNS extract

A few drops of an aqueous extract of CNS were mixed with KBr. A solid mass was made into pellets. Its FT-IR spectrum is shown in Figures-17.a and Table-5. The broad peak at 3434.69 cm^{-1} is due to polymeric O-H group, the frequency at 2964.11 cm^{-1} corresponds to C-H stretching frequency and the C=O group presence is confirmed from the peak at 1714.97 cm^{-1}. The band observed at 1639.44 cm^{-1} relates to the C=C stretching. The presence of the functional groups C-N and C-O-C in CNS extract is confirmed from the bands at 1244.34 cm^{-1}, C-H bending frequency is noted at 1377.29 cm^{-1}. A notable band at 1054.39 cm^{-1} can be assigned to C-O stretching and O-H bending in phenolic derivatives. Aromatic ring present in the extract reflected the band appeared at 613.71 cm^{-1} **(Vinod kumar *et al.*, 2011)**.

4.1.2 GC-MS analysis of CNS extract

Gas chromatography (GC)–mass spectroscopy (MS) spectra of the product obtained on destructive distillation of CNS extract is shown in Figure-17.b. It contains 8 major peaks along with many small peaks indicating presence of more than 8 major compounds (Table-3). The small peaks may be attributed to the compounds present in small quantities as well as disintegrated major compounds. The peaks related to low retention times are mainly low polar plant compounds. The other peaks belong to naturally occurring phenolic dimers. Similar results were reported earlier by **Goh Meng Seng *et al.*, (2006)**.

4.1.3 FT-IR study of CNLS extract

From Figure 18.a, it is seen that the extract exhibited broad adsorption band at 3423.14 cm^{-1} indicating the presence of alcohol or phenol functional group (i.e., -OH). The band observed at 1711.65 cm^{-1} confirms the presence of –C=O stretching.

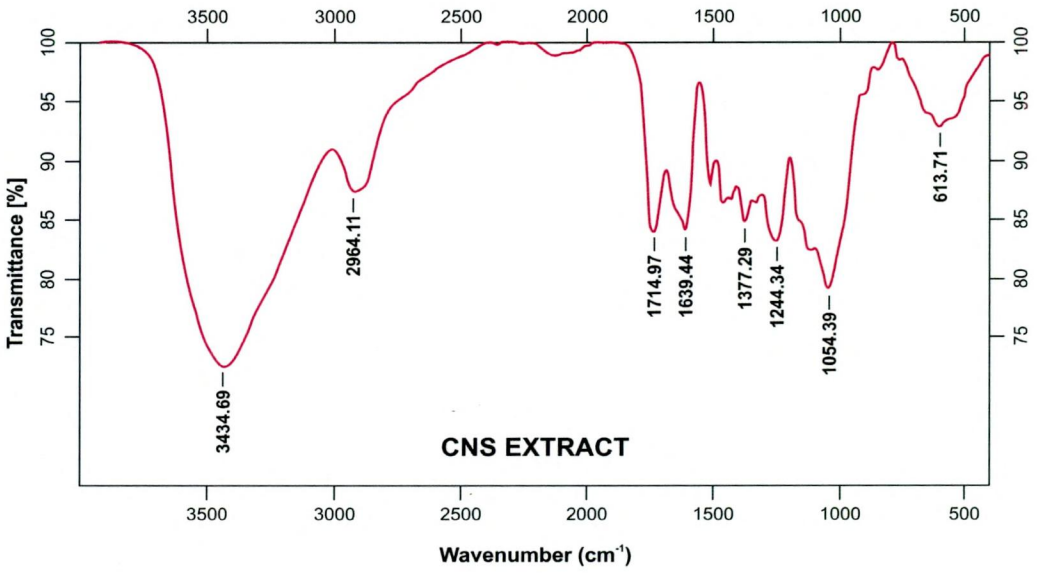

(a)

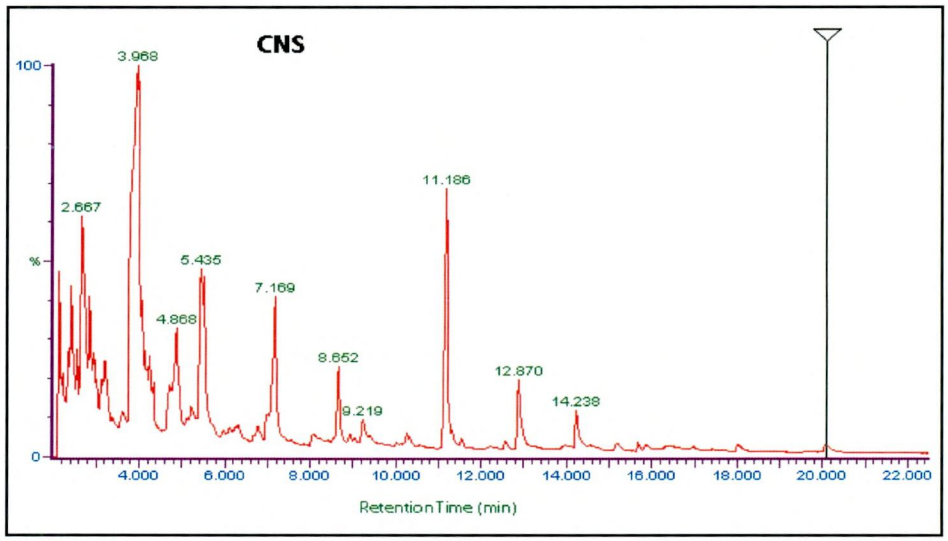

(b)

Figure - 17 Characterization of CNS extract by (a) FT-IR and (b) GC-MS Techniques

Table - 3 Phytochemical constituents identified in the aqueous distillate of CNS extract by GC - MS analysis

RETENTION TIME (min)	CHEMICAL COMPOUNDS	M.F	M.W
2.667	N-Methyl-N-Nitroso Ethanamine	$C_3H_8ON_2$	88
3.968	Phenol	C_6H_6O	94
4.868	4-Methyl-2-hydroxycyclopent-2-en-1-one	$C_6H_8O_2$	112
5.435	2-Methoxy phenol	$C_7H_8O_2$	124
7.169	2-Methoxy-4-methyl phenol	$C_8H_{10}O_2$	138
8.652	4-Ethyl-2-Methoxy phenol	$C_9H_{12}O_2$	152
9.219	1-(5-hydroxymethyl-2-furanyl)-1-Ethanone	$C_7H_8O_3$	140
11.186	2,6-Dimethoxy phenol	$C_8H_{10}O_3$	154
12.870	2,5-Dimethoxybenzyl alcohol	$C_9H_{12}O_3$	168
14.238	1,2,3-Trimethoxy-5-methyl benzene	$C_{10}H_{14}O_3$	182

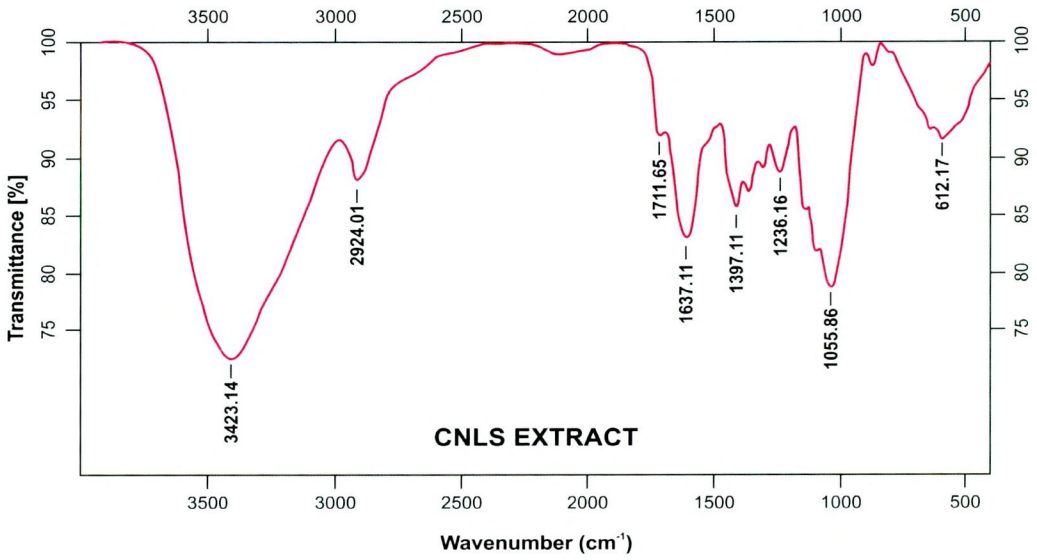

(a)

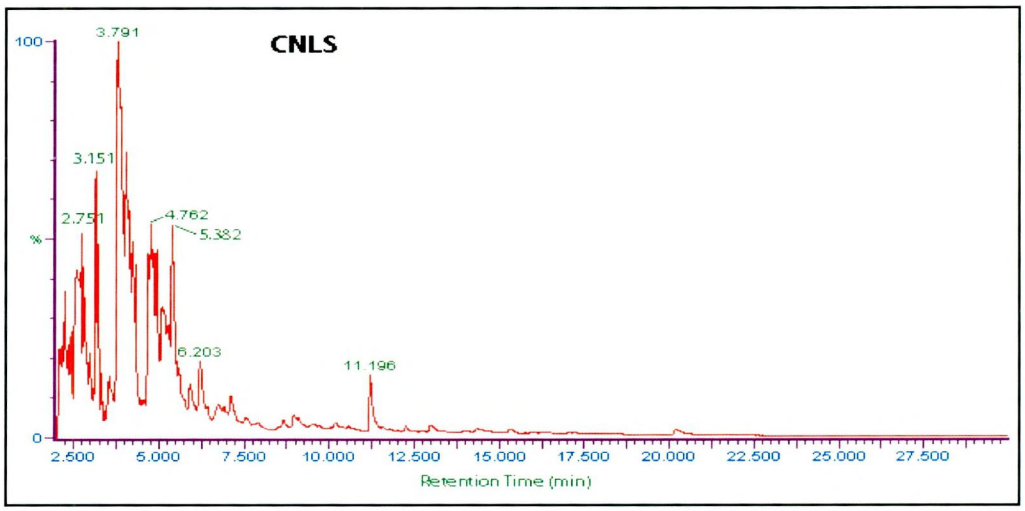

(b)

Figure - 18 Characterization of CNLS extract by (a) FT-IR and (b) GC-MS Techniques

Table - 4 Phytochemical constituents identified in the aqueous distillate of CNLS extract by GC - MS analysis

RETENTION TIME (min)	CHEMICAL COMPOUNDS	M.F	M.W
2.751	L-Histidine, Methyl ester, Dihydrochloride	$C_7H_{11}O_2N_3$	169
3.151	4,4-Dimethyl-2-Cyclopenten-1-one	$C_7H_{10}O$	110
3.791	1-(1H-Pyrrole-2-yl) Ethanone	C_6H_7ON	109
4.762	Cis-4-Hydroxy-2-Methyl-5-(1-Hydroxy-1-Isopropyl)-2-Cyclohexen-1-one	$C_{10}H_{16}O_3$	184
5.382	1-(2-Pyrazinyl)-1-Ethanol	$C_6H_8ON_2$	124
6.203	4A,5,6,7,8,8A-Hexahydro-8A-Methyl, 2(1H)-Naphthalenone	$C_{11}H_{16}O$	164
11.196	2,6-Dimethoxy phenol	$C_8H_{10}O_3$	154

A band at 1637.11 cm^{-1} suggests the presence of C≡C. A peak at 1397.11 cm^{-1} indicates the C-H bonding frequency. A small peak at 1236.16 cm^{-1} reveals the presence of C-N stretching frequency. The C-O stretching frequency and O-H frequency are also found in the CNLS extract (Table-5).

4.1.4 GC-MS analysis of CNLS extract

In order to identify the phytochemical constituents of CNLS, GC/MS was carried out. The analysis confirmed the identification of 7 components listed in the Table - 6.

4.1.5 FT-IR spectral results of CNP extract

The respective FT-IR peaks of CNP extract is given in Figure - 19.a and Table-6. The broad and strong bands at 3389.17 cm^{-1} is due to the presence of polymeric OH group. The band observed at 2927.85 cm^{-1} is assigned to –CH stretching. The peak at 1711.84 cm^{-1} arises due to carbonyl stretching. The peak at 1595.82 cm^{-1} corresponds to C=C stretching vibrations C-H bending vibrations are observed at 1403.08 cm^{-1}. 1057.61cm^{-1} is assigned to C-O stretch and OH bonding vibrations. Presence of aromatic ring is confirmed from the peak obtained at 668.75 cm^{-1} **(Satapathy *et al.*, 2009).**

4.1.6 GC-MS analysis of CNP extract

Structural assignment of GC retention data of compounds (Table - 6) is based on spectral matching with NIST library (National Institute of Standards and Technology). From the GC–MS analysis (Figure-19.b), it can be observed that the CNP extract consists of 6 major compounds. The peaks related to low retention times are mainly due to low polar plant compounds **(Satapathy *et al.*, 2009).**

Table - 5 FT-IR spectral data of CNS, CNLS and CNP extracts

Observed IR frequency, (cm^{-1})			Frequency range, (cm^{-1})	Assignment	Reference
CNS	CNLS	CNP			
3434.69	3423.14	3389.17	3500-3000	O-H stretch	Vinod Kumar, *et al.*, **2011**
2964.11	2924.01	2927.85	3000 - 2800	C-H stretch	Ebenso, *et al.*, **2008**
1714.97	1711.65	1711.84	1780 - 1650	C=O stretch	Nnabuk Okaon Eddy. **2009**
1639.44	1637.11	1595.82	1680 - 1580	C=C stretch	Silverstein and Basseler *et al.*, **1967**
1377.29	1397.11	1403.08	1465 - 1350	C-H bend	Eddy, *et al.*, **2009e**
1244.34	1236.16	1247.88	1235 - 1280	C-O-C	Pandian Bothi Raja, *et al.*, **2008**
1054.39	1055.86	1057.61	1300 - 950	C-O stretch	Eddy, *et al.*, **2009e**
613.71	612.17	668.75	900 - 650	C-H "oop"	Eddy, *et al.*, **2009e**

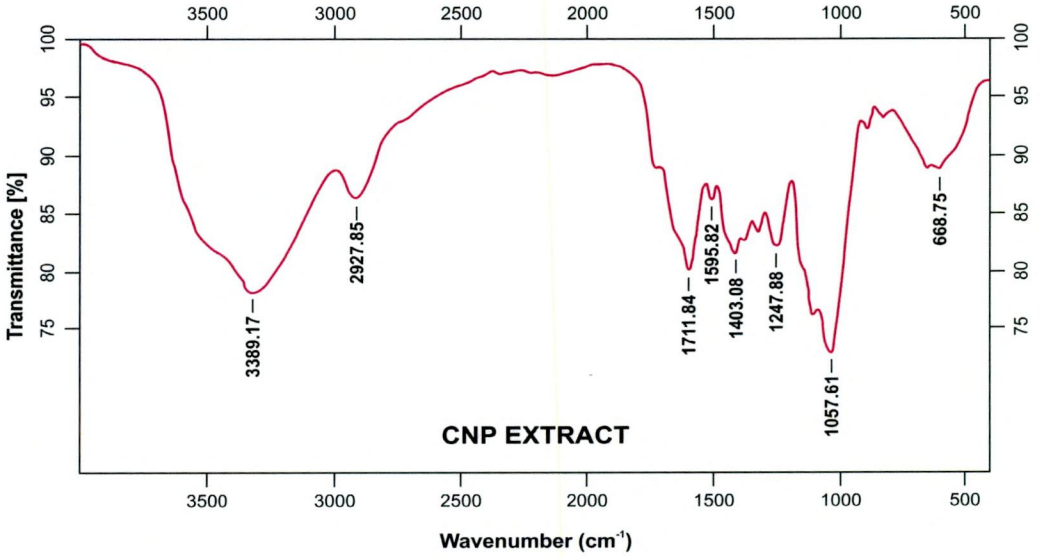

(a)

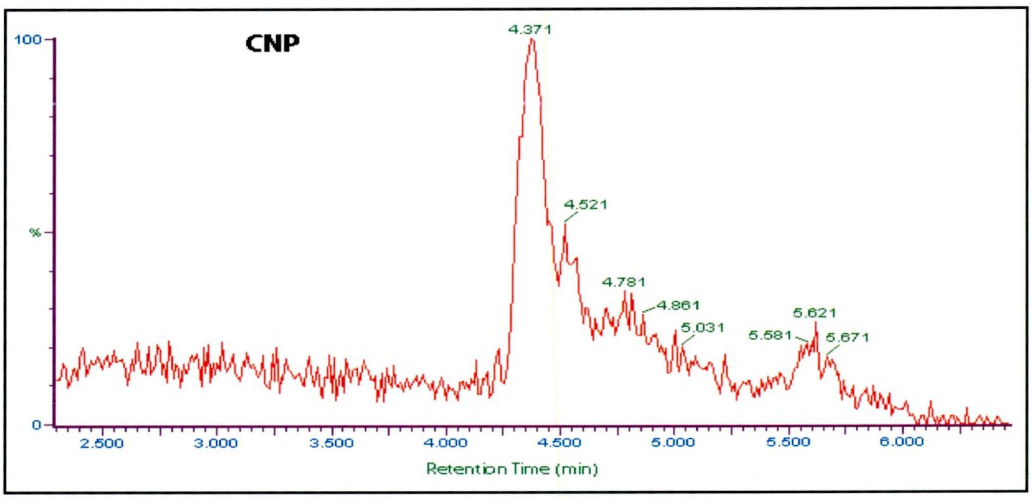

(b)

Figure - 19 Characterization of CNP extract by (a) FT-IR and (b) GC-MS Techniques

Table - 6 Phytochemical constituents identified in the aqueous distillate of CNP extract by GC - MS analysis

RETENTION TIME (min)	CHEMICAL COMPOUNDS	M.F	M.W
4.371	4-[2-(Methylamino)Propyl] phenol	$C_{10}H_{15}ON$	165
4.521	1-(1-Propenyl) Bicyclo[3.2.1]Octan-2-one	$C_{11}H_{16}O$	164
4.781	Tert-Butyl 3-Methyloxiranecarboxylate	$C_8H_{14}O_3$	158
4.861	4-Methyl-2-hydroxycyxlopent-2-en-1-one	$C_6H_8O_2$	124
5.031	Trisilane	H_8Si_3	92
5.581	2-Methoxy Phenol	$C_7H_8O_2$	124
5.621	2-(7'-Chlorohept-2'-Ynyloxy)Tetrahydro-2H-Pyran	$C_{12}H_{19}O_2Cl$	230

4.1.7 FT-IR spectral studies of BFS extract

FT-IR spectrum of BFS is shown in Figure-20.a. The broad and medium intensity band appear at 3408.94 cm^{-1} is due to the presence of polymeric O-H group. The intense band at 2931.69 cm^{-1} represents C-H stretching vibration. The bands at 1708.43 cm^{-1} is consistent with the C=O stretching vibrations. The adsorption band at 1596.36 cm^{-1} indicating the presence of C=C stretching. An adsorption band found at 1253.46 and 1053.45 cm^{-1} suggesting the presence of C-O stretching and O-H bending. The aromatic ring in the extract is established by adsorption at 616.94 cm^{-1} (Table-10).

4.1.8 GC-MS studies of BFS extract

Gas chromatography (GC)–mass spectroscopy (MS) analysis of BFS extract showed that the plant extract contains 10 different compounds (Table - 7). **(Chauhan and Gunasekaran, 2007).**

4.1.9 FT-IR spectroscopic study of BFLS extract

FT-IR spectroscopic analysis was used to identify the functional groups present in BFLS extract. The spectra of BFLS (Figure - 21.a) shows prominent peaks at 3409.38 cm^{-1}corresponding to polymeric O-H group. 2929.85 cm^{-1} corresponding to C-H stretching frequency. The peaks at 1713.10 and 1642.86 cm^{-1} correspond to C=O stretching of ketones, aldehydes, carboxylic acid and C=C stretching of alkenes present in the extract. The bands at 1399.40 cm^{-1} indicates C-H bending of alkanes. The C-O-C and C-O stretching frequency appears at 1250.24 and 1053.22 cm^{-1}.The aromatic ring in the extract established by adsorption at 623.15 cm^{-1}(Table-10).

4.1.10 GC-MS analysis of BFLS extract

The aqueous BFLS extract was analyzed with GC/MS. The GC/MS analysis detected all organic species quantitatively. Each peak area in the chromatogram was proportional to the amount of the organic compound(s) forming that peak. It can be observed that the BFLS extract consists of 7 major compounds listed in Table-8. **Fitch (1983)** also reported GC-MS results for the same compounds.

4.1.11 Analysis of FT-IR spectra for BFP extract

The FT-IR spectra (Figure-22.a) of the extract of BFP contains bands corresponding to phenolic hydroxyl groups (3452.62 cm^{-1}), C-H stretching (2943.76 cm^{-1}), carbonyl groups (1733.09 cm^{-1}), aromatic C=C bending (1639.54 cm^{-1}), two bands appear for the C-O stretching vibrations in esters in 1274.53 and 1055.18cm^{-1}, aromatic ring (664.39 cm^{-1}) (Table-10) **(Eddy and Mamza, 2009)**.

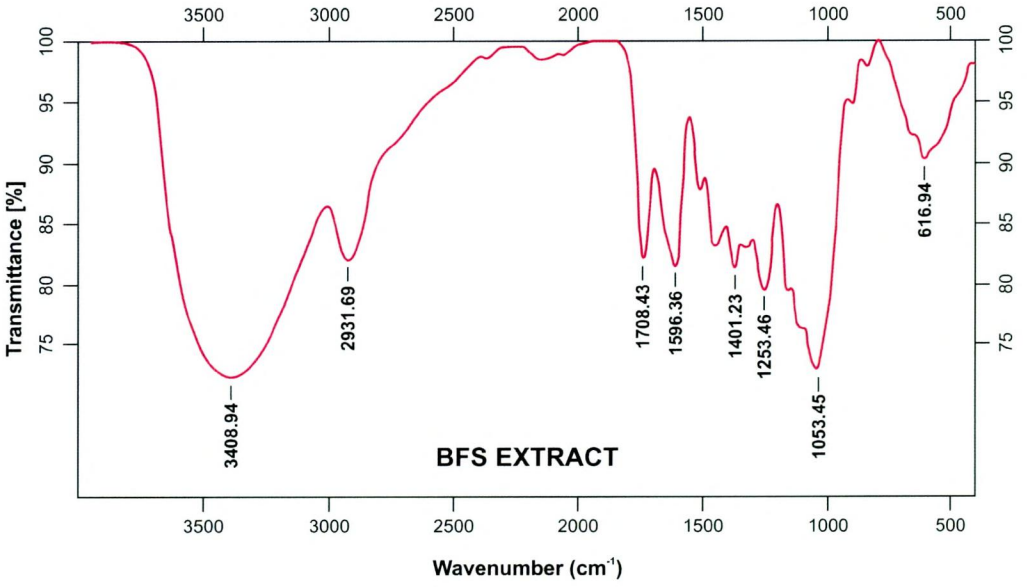

(a)

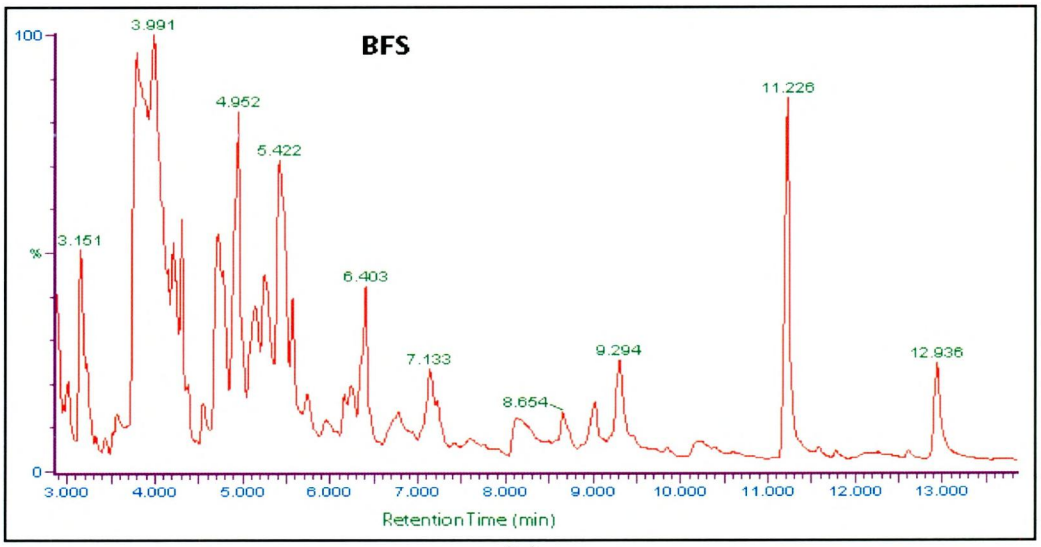

(b)

Figure - 20 Characterization of BFS extract by (a) FT-IR and (b) GC-MS Techniques

Table - 7 Phytochemical constituents identified in the aqueous distillate of BFS extract by GC - MS analysis

RETENTION TIME (min)	CHEMICAL COMPOUNDS	M.F	M.W
3.151	1,3-Dimethyl Cyclohexene	C_8H_{14}	110
3.991	Phenol	C_6H_6O	94
4.952	2-Cyclopenten-1-one	$C_6H_8O_2$	112
5.422	2-Methoxy-, Acetate phenol	$C_9H_{10}O_3$	166
6.403	1,6-Dimethyl,1,5-Cyclo octadiene	$C_{10}H_{16}$	136
7.133	2-Methoxy-4-Methylphenol	$C_8H_{10}O_2$	138
8.654	2,5-Cyclohexadiene-1,4-Dione,	$C_{10}H_{12}O_3$	180
9.294	3-Hydroxy-5-Methyl-2-(1-Methylethyl)2-Ethyl-3-Methoxy-2-Cyclopentenone	$C_8H_{12}O_2$	140
11.226	2,6-Dimethoxy Phenol	$C_8H_{10}O_3$	154
12.936	2,5-Dimethoxybenzyl alcohol	$C_9H_{12}O_3$	168

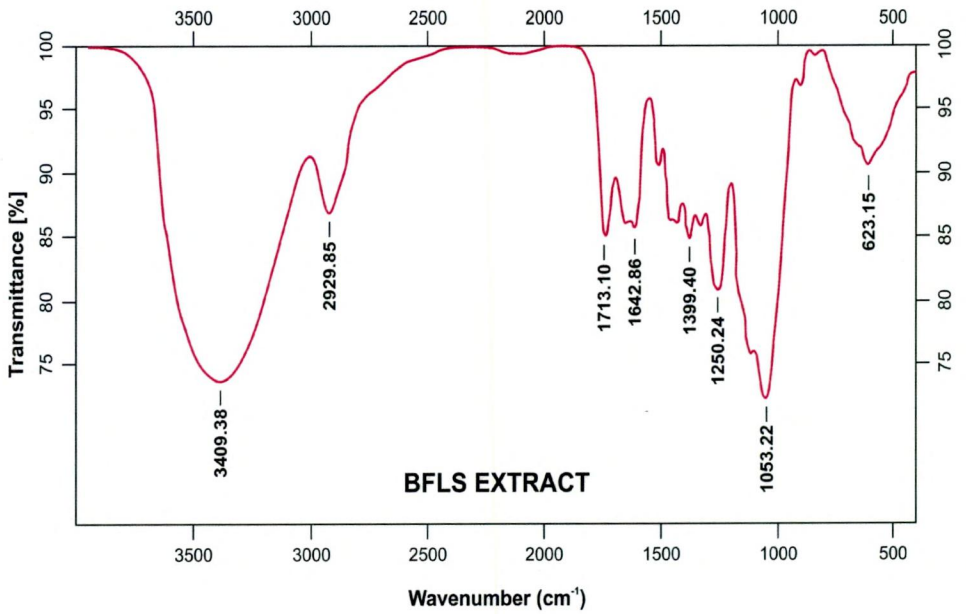

(a)

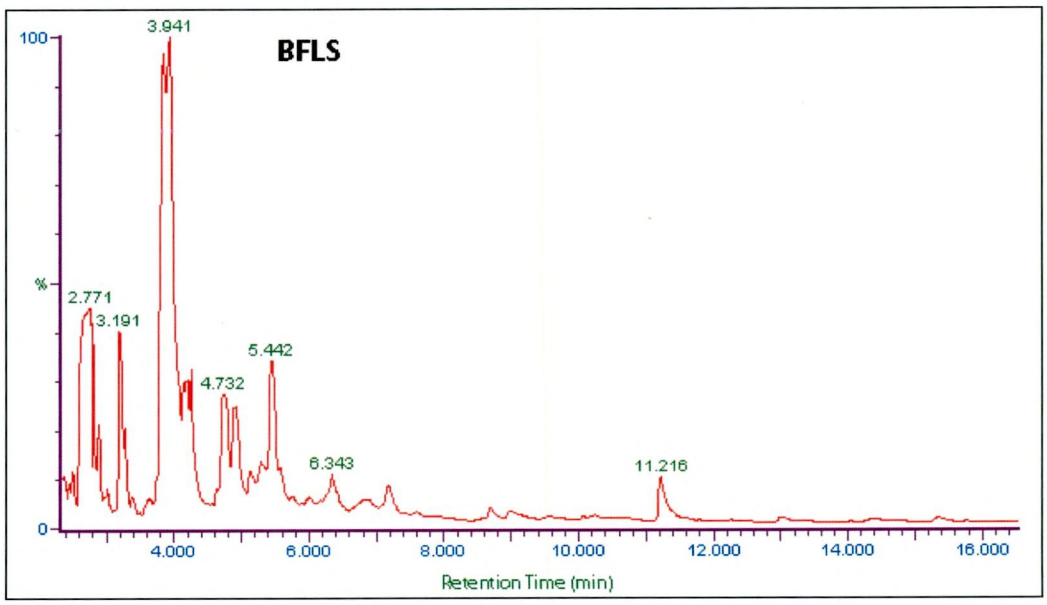

(b)

Figure - 21 Characterization of BFLS extract by (a) FT-IR and (b) GC-MS Techniques

Table – 8 Phytochemical constituents identified in the aqueous distillate of BFLS extract by GC - MS analysis

RETENTION TIME (min)	CHEMICAL COMPOUNDS	M.F	M.W
2.771	Bicyclo 2.2.1 Heptane-2-Carboxaldehyde,Exo	$C_8H_{12}O$	124
3.191	2-Methyl,2-Cyclopenten-1-one	C_6H_8O	96
3.941	Phenol	C_6H_6O	94
4.732	2-Methyl Phenol	C_7H_8O	108
5.442	2-Methoxy Phenol	$C_7H_8O_2$	124
6.343	Cis-D-Dihydrocarveol	$C_{10}H_{18}O$	154
11.216	2,6-Dimethoxy Phenol	$C_8H_{10}O_3$	154

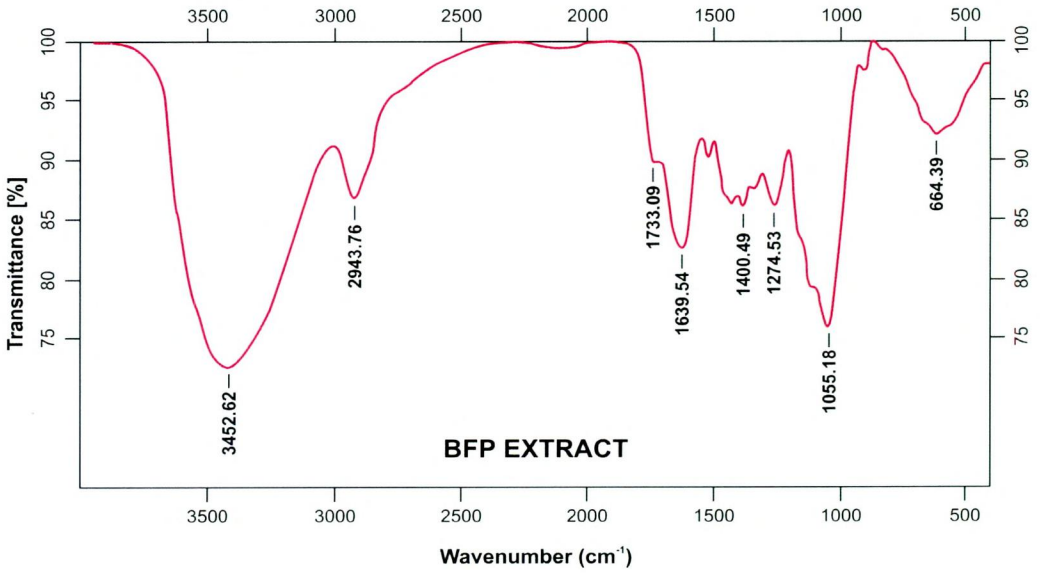

(a)

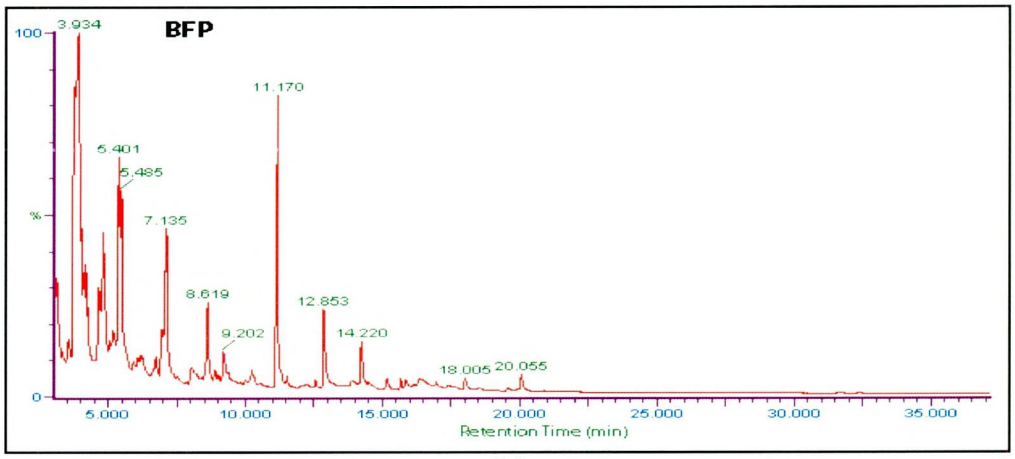

(b)

Figure- 22 Characterization of BFP extract by (a) FT-IR and (b) GC-MS Techniques

Table - 9 Phytochemical constituents identified in the aqueous distillate of BFP extract by GC - MS analysis

RETENTION TIME (min)	CHEMICAL COMPOUNDS	M.F	M.W
3.934	Phenol	C_6H_60	94
5.401	4-Methyl Phenol,	C_7H_8O	108
5.485	2-Methoxy Phenol	$C_7H_8O_2$	124
7.135	2-Methoxy-4-methyl-phenol	$C_8H_{10}O_2$	138
8.619	4-Ethyl-2-Methoxy Phenol	$C_9H_{12}O_2$	152
9.202	1-(5-Hydroxymethyl-2-Furanyl)-1-Ethanone	$C_7H_8O_3$	140
11.170	2,6-Dimethoxy Phenol	$C_8H_{10}O_3$	154
12.853	Benzoic acid, 4-Hydroxy-3-Methoxy	$C_8H_8O_4$	168
14.220	Benzene,1,2,3-Trimethoxy-5-Methyl	$C_{10}H_{14}O_3$	182
18.005	1-(6,6-Dimethyl-2-Methylene-3-Cyclohexenyl)-Buten-3-one	$C_{13}H_{18}O$	190
20.055	2-Pentanone,1-(2,4,6-Trihydroxyphenyl)	$C_{11}H_{14}O_4$	210

4.1.12 GC-MS study of BFP extract

The GC retention data of the BFP correspond to structural assignation performed after NIST (library search) with a database and by mass spectra interpretation is presented in Table-9. From the GC-MS analysis (Figure-22.b), it is observed that BFP extract consists of 11 major components **(Chauhan and Gunasekaran, 2007).**

Table - 10 FT-IR spectral data of BFS, BFLS and BFP extracts

Observed IR frequency, (cm^{-1})			Frequency range, (cm^{-1})	Assignment	Reference
BFS	BFLS	BFP			
3408.94	3409.38	3452.62	3500-3000	O-H stretch	Vinod Kumar, *et al.*, **2011**
2931.69	2929.85	2943.76	3000 - 2800	C-H stretch	Ebenso, *et al.*, **2008**
1708.43	1713.10	1733.09	1780 - 1650	C=O stretch	Nnabuk Okaon Eddy. **2009**
1596.36	1642.86	1639.54	1680 - 1580	C=C stretch	Silverstein, *et al.*, **1967**
1401.23	1399.40	1400.49	1465 - 1350	C-H bend	Eddy, *et al.*, **2009e**
1253.46	1250.24	1274.53	1235-1280	C-O-C	Pandian Bothi Raja, *et al.*, **2008**
1053.45	1053.22	1055.18	1300-950	C-O stretch	Eddy, *et al.*, **2009e**
616.94	623.15	664.39	900 - 650	C-H "oop"	Eddy, *et al.*, **2009e**

4.2 MASS LOSS METHOD

The mass loss method of monitoring corrosion rate is useful because of its simple application and reliability. Although there are many experimental techniques which can be used to evaluate the percentage inhibition efficiency of studied inhibitors, mass loss is probably the most widely and frequently used method **(Ekpe *et al.*, 1995; Okafor *et al.*, 2005)**.

4.2.1 EFFECT OF CONCENTRATION OF CN AND BF EXTRACTS ON MS CORROSION

Mass loss measurements were conducted using 100 mL capacity beakers containing 100 mL test solution at room temperature. The mild steel coupons were weighed and suspended in the beaker with the help of hook. The coupons were scrubbed with bristle brush under running water, dried in acetone and reweighed. The mass loss, in grams, was taken as the difference in the mass of the mild steel coupons before and after immersion in different test solutions. Tests were performed for the free acid solution, solution containing various concentrations of shell, leaf stalk and peduncle of CN and BF (0.5%v/v, 1.0%v/v, 1.5%v/v, 2.0%v/v, 2.5%v/v, 3%v/v, 3.5%v/v and 4.0%v/v) at room temperature. The experiments were performed in triplicate to ensure good result. From the mass loss values, corrosion rates were computed using the equation (3.1) and inhibition efficiency (IE%) was computed using equation (3.2).

4.2.1.1 CNS extract in 0.5 M H_2SO_4 and 1 M HCl

Values of the corrosion rates of mild steel in the absence and presence of extract of CNS and their corresponding percentage inhibition efficiencies were recorded in Table-11. Values of inhibition efficiency obtained from gravimetric method reveal that the corrosion rate of mild steel in the presence of extract of CNS have been found to decrease with increase in the concentration of the extract, indicating that these extract retarded the corrosion of mild steel in both 0.5 M H_2SO_4 and 1 M HCl and proportionately that the inhibition efficiencies of extract of CNS increased with increase in the concentration of the extracts. At room temperature, maximum inhibition efficiencies of 98.6% and 98.1% have been obtained in 0.5 M H_2SO_4 and 1 M HCl solution containing 4.0%v/v CNS extract at 24 h respectively. The effect of concentration of CNS extract at various time intervals with respective inhibition efficiencies are represented in Figure – 23 (a and b).

Table – 11 Inhibition efficiency as a function of immersion time and concentration of CNS extract on MS in 0.5 M H_2SO_4 and 1 M HCl

Conc. (%v/v)	½ h		1 h		3 h		6 h		12 h		24 h	
	CR mpy	IE (%)	CR mpy	IE (%)	CR mpy	IE (%)	CR mpy	IE (%)	CR mpy	IE (%)	CR mpy	IE (%)
0.5 M H_2SO_4												
Blank	1234	-	1312	-	1558	-	1808	-	1481	-	1158	-
0.5	271	77.9	139	90.1	153	90.5	171	92.3	120	89.3	89	91.9
1.0	170	86.1	95	92.7	91	94.1	94	94.7	72	95.1	49	95.7
1.5	139	88.7	79	93.9	59	96.1	67	96.2	45	96.9	33	97.0
2.0	109	91.1	61	95.3	46	97.0	49	97.2	36	97.5	22	98.0
2.5	102	91.6	61	95.3	45	97.1	38	97.8	31	97.8	18	98.4
3.0	90	92.6	43	96.7	35	97.7	34	98.0	21	98.5	16	**98.6**
3.5	89	92.7	43	96.7	35	97.7	33	98.1	21	98.5	16	**98.6**
4.0	89	92.7	43	96.7	34	97.8	33	98.1	21	98.5	16	**98.6**
1 M HCl												
Blank	1060	-	1105	-	1268	-	1504	-	1131	-	916	-
0.5	303	71.3	261	76.3	138	89.0	135	91.0	107	90.5	61	93.2
1.0	236	77.7	201	81.7	117	90.7	87	93.9	69	94.1	37	95.8
1.5	184	82.5	136	87.6	85	93.2	65	95.2	54	95.6	31	96.5
2.0	132	87.5	112	89.8	68	94.6	51	96.5	42	96.2	25	97.2
2.5	120	88.6	88	92.0	63	95.0	42	97.1	37	96.7	20	97.7
3.0	115	89.1	85	92.3	42	96.6	38	97.4	34	96.9	17	**98.1**
3.5	114	89.2	85	92.3	41	96.7	38	97.4	33	97.0	17	**98.1**
4.0	114	89.2	85	92.3	41	96.7	38	97.4	33	97.0	17	**98.1**

4.2.1.2 CNLS extract in 0.5 M H_2SO_4 and 1 M HCl on MS corrosion

Results of the present investigations on the corrosion behaviour of mild steel

Table – 12 Inhibition efficiency as a function of immersion time and concentration of CNLS extract on MS in 0.5 M H_2SO_4 and 1 M HCl

Conc. (%v/v)	½ h		1 h		3 h		6 h		12 h		24 h	
	CR mpy	IE (%)	CR mpy	IE (%)	CR mpy	IE (%)	CR mpy	IE (%)	CR mpy	IE (%)	CR mpy	IE (%)
0.5 M H_2SO_4												
Blank	1234	-	1312	-	1558	-	1808	-	1481	-	1158	-
0.5	439	64.3	350	73.3	235	84.9	204	88.7	220	85.1	169	85.3
1.0	248	79.8	214	83.6	140	90.9	110	93.9	115	92.2	86	92.5
1.5	192	84.3	197	84.9	109	93.0	67	96.2	70	95.2	60	94.7
2.0	189	84.6	184	85.9	85	94.5	56	96.8	55	96.2	29	97.4
2.5	146	88.1	146	88.8	71	95.3	40	97.7	37	97.4	23	97.9
3.0	127	89.7	107	91.8	64	95.8	31	98.2	33	97.7	18	**98.4**
3.5	126	89.7	107	91.8	63	95.9	31	98.2	33	97.7	18	**98.4**
4.0	126	89.7	107	91.8	63	95.9	31	98.2	33	97.7	18	**98.4**
1 M HCl												
Blank	1060	-	1105	-	1268	-	1504	-	1131	-	916	-
0.5	300	71.6	250	77.3	195	84.6	188	87.5	175	84.4	111	87.8
1.0	271	74.3	230	79.1	122	90.3	97	93.5	103	90.8	63	93.0
1.5	181	83.8	178	82.9	94	92.5	76	94.9	66	94.1	46	94.9
2.0	156	85.2	141	87.1	86	93.2	83	94.4	63	94.4	42	95.3
2.5	133	87.3	125	88.6	75	94.0	66	95.5	55	95.0	38	95.8
3.0	109	89.7	111	89.9	61	95.1	63	95.7	50	95.5	33	**96.3**
3.5	108	89.8	110	90.0	61	95.1	63	95.8	50	95.5	33	**96.3**
4.0	108	89.8	110	90.0	61	95.1	63	95.8	50	95.5	33	**96.3**

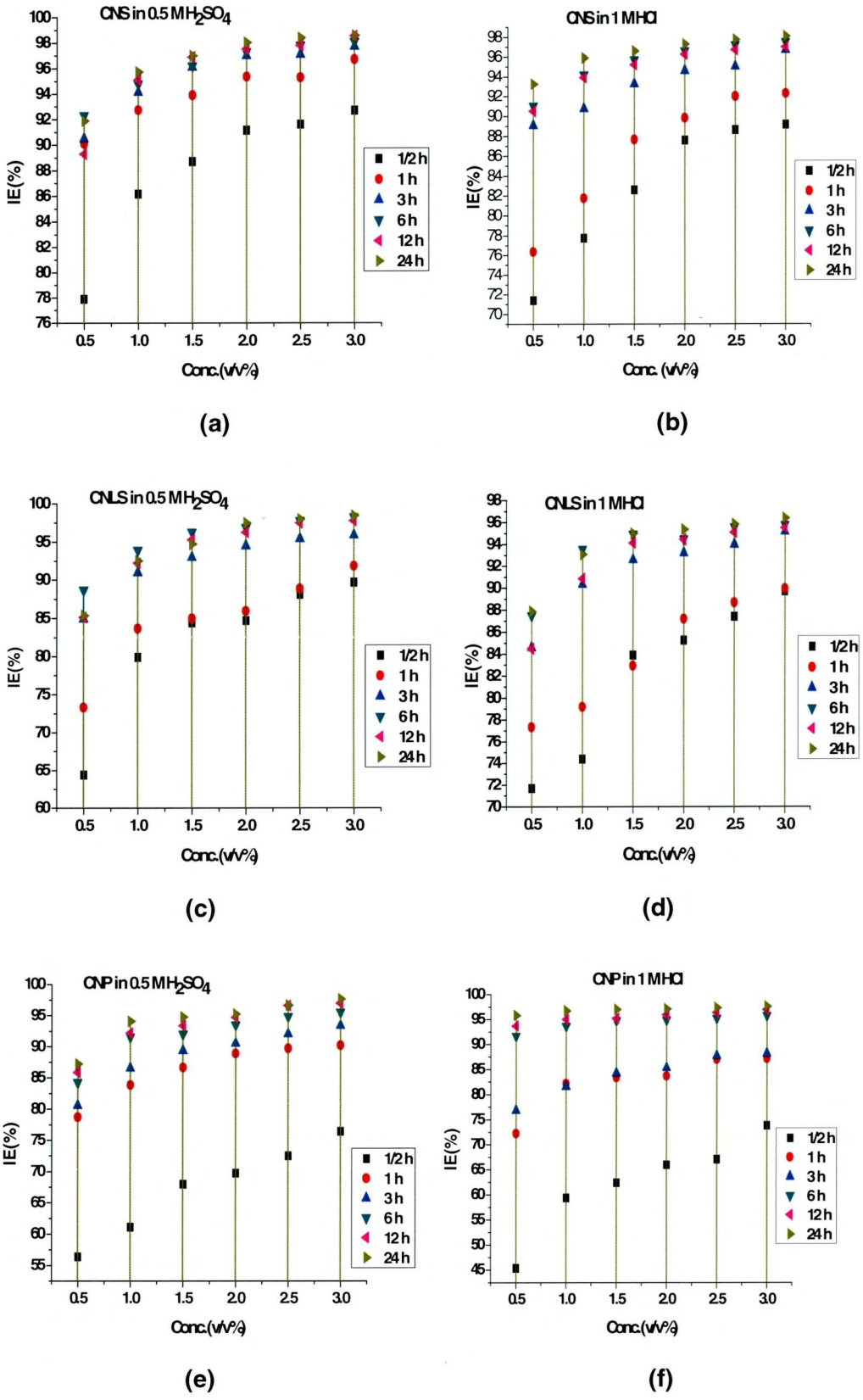

Figure - 23 The relationship between IE (%) and Concentration of CN extracts in 0.5 M H_2SO_4 and 1 M HCl

in the presence of various concentrations of CNLS extract at different time of immersion from the Table - 12 indicates that the corrosion rate of mild steel gradually decreased between the concentration range from 0.5%v/v to 4.0%v/v of CNLS extract in 0.5 M H_2SO_4 and 1 M HCl, respectively indicate that the inhibition efficiency increases with increase in extract concentration at all studied immersion time and the maximum inhibition efficiency of 98.4% and 96.3% have been obtained at 24 h with 4.0%v/v concentration within the range of concentrations studied (Figure - 23(c and d). Further increase in concentration of CNLS extract produced similar inhibition efficiency. The inhibitive action of CNLS extract towards the acid corrosion of mild steel can be attributed to the adsorption of extract components onto the steel surface. Corrosion inhibition is initiated by the displacement of adsorbed water molecules by the inhibitor species leading to specific adsorption on the metal surface **(Solmaz *et al.*, 2008a).**

4.2.1.3 CNP extract in 0.5 M H_2SO_4 and 1 M HCl on MS corrosion

The analysis of the result from the Table-13 and Figure-23 (e and f) shows clearly that the corrosion rate decreases while the percentage inhibition efficiency

Table - 13 Inhibition efficiency as a function of immersion time and concentration of CNP extract on MS in 0.5 M H_2SO_4 and 1 M HCl

Conc. (%v/v)	½ h		1 h		3 h		6 h		12 h		24 h	
	CR mpy	IE (%)	CR mpy	IE (%)	CR mpy	IE (%)	CR mpy	IE (%)	CR mpy	IE (%)	CR mpy	IE (%)
0.5 M H_2SO_4												
Blank	1234	-	1312	-	1558	-	1808	-	1481	-	1158	-
0.5	538	56.3	279	78.6	303	80.5	285	84.2	210	85.8	164	87.1
1.0	480	61.1	212	83.8	209	86.5	153	91.5	116	92.1	68	94.0
1.5	395	67.9	175	86.6	165	89.3	144	92.0	99	93.3	60	94.7
2.0	373	69.7	146	88.8	148	90.4	119	93.4	79	94.6	55	95.2
2.5	339	72.4	135	89.6	124	92.0	94	94.8	51	96.5	38	96.6
3.0	291	76.4	129	90.1	103	93.3	55	96.9	66	95.5	27	**97.6**
3.5	290	76.4	128	90.2	102	93.4	55	96.9	66	95.5	27	**97.6**
4.0	290	76.4	128	90.2	102	93.4	55	96.9	66	95.5	27	**97.6**
1 M HCl												
Blank	1060	-	1105	-	1268	-	1504	-	1131	-	916	-
0.5	579	45.3	307	72.1	294	76.8	126	91.6	72	93.6	38	95.8
1.0	431	59.3	198	82.0	234	81.5	95	93.6	57	94.9	30	96.7
1.5	398	62.3	184	83.2	200	84.2	79	94.7	54	95.1	27	96.9
2.0	361	65.9	181	83.6	186	85.2	77	94.8	46	95.8	26	97.0
2.5	349	67.0	144	86.9	156	87.6	72	95.1	41	96.3	25	97.2
3.0	278	73.7	142	87.1	150	88.1	64	95.7	35	96.9	22	**97.5**
3.5	277	73.8	141	87.2	150	88.1	64	95.7	35	96.9	22	**97.5**
4.0	277	73.8	141	87.2	150	88.1	64	95.7	35	96.9	22	**97.5**

increases with increasing inhibitor concentration reaching a maximum value of 97.6% and 97.5% at a concentration of 4.0%v/v CNP extract at 24 h in 0.5 M H_2SO_4 and

1 M HCl solution respectively. This behaviour can be attributed due to the adsorption of natural compounds on the surface of the metal.

4.2.1.4 BFS extract in 0.5 M H_2SO_4 and 1 M HCl on MS corrosion

The material loss expressed as the corrosion rate (mpy) for the mild steel coupons in 0.5 M H_2SO_4 and 1 M HCl solutions containing different concentrations of BFS as a function of inhibitor concentration is enlisted in Table - 14. It has been observed that the corrosion rate decreased with the increase in concentration of BFS extract, indicating that the extent of inhibition is dependent on the amount of extract present. The examination of results obtained indicates that the plant extracts show a significant inhibitive effect on mild steel in 0.5 M H_2SO_4 and 1 M HCl solutions at various time intervals.

Table – 14 Inhibition efficiency as a function of immersion time and concentration of BFS extract on MS in 0.5 M H_2SO_4 and 1 M HCl

Conc. (%v/v)	½ h		1 h		3 h		6 h		12 h		24 h	
	CR mpy	IE (%)	CR mpy	IE (%)	CR mpy	IE (%)	CR mpy	IE (%)	CR mpy	IE (%)	CR mpy	IE (%)
0.5 M H_2SO_4												
Blank	1234	-	1312	-	1558	-	1808	-	1481	-	1158	-
0.5	335	72.8	276	78.9	228	85.3	220	87.8	229	84.5	170	85.2
1.0	321	73.9	176	86.5	188	87.8	131	92.7	128	91.3	84	92.6
1.5	295	76.0	144	88.9	168	89.1	84	95.3	107	92.7	66	94.2
2.0	261	78.8	132	89.9	124	92.0	82	95.2	88	94.0	57	95.0
2.5	248	79.8	114	91.2	115	92.6	76	95.7	77	94.7	37	96.7
3.0	186	84.9	91	93.0	101	93.5	66	96.3	64	95.6	27	**97.6**
3.5	185	85.0	90	93.1	101	93.5	66	96.3	64	95.6	27	**97.6**
4.0	185	85.0	90	93.1	101	93.5	66	96.3	64	95.6	27	**97.6**
1 M HCl												
Blank	1060	-	1105	-	1268	-	1504	-	1131	-	916	-
0.5	229	78.3	256	76.7	318	74.9	297	80.2	143	87.3	37	95.9
1.0	140	86.7	211	80.8	302	76.1	252	83.2	134	88.1	30	96.7
1.5	129	87.7	183	83.4	220	82.6	232	84.5	116	89.7	27	97.0
2.0	116	88.9	129	88.3	224	82.3	199	86.7	82	92.6	21	97.6
2.5	94	91.0	106	90.4	202	84.0	192	87.1	76	93.2	20	97.7
3.0	71	93.3	95	91.3	199	84.2	192	87.1	61	94.5	17	**98.1**
3.5	70	93.3	95	91.3	199	84.2	192	87.1	61	94.5	17	**98.1**
4.0	70	93.3	95	91.3	199	84.2	192	87.1	61	94.5	17	**98.1**

From the Figure 24(a and b), it has been observed that the inhibition efficiencies increase with increase in BFS extract concentration and the maximum inhibition efficiency of 97.6% and 98.1% were obtained with 4.0%v/v concentration at 24 h within the range of concentrations studied. This indicates that the phytochemical components of the extracts were adsorbed onto the mild steel surface resulting in the blocking of the reaction sites, and protection of the mild steel surface from the attack of the corrosive active ions in the acid medium **(Okafor and Ebenso, 2007; Abiola *et al.*, 2009)**.

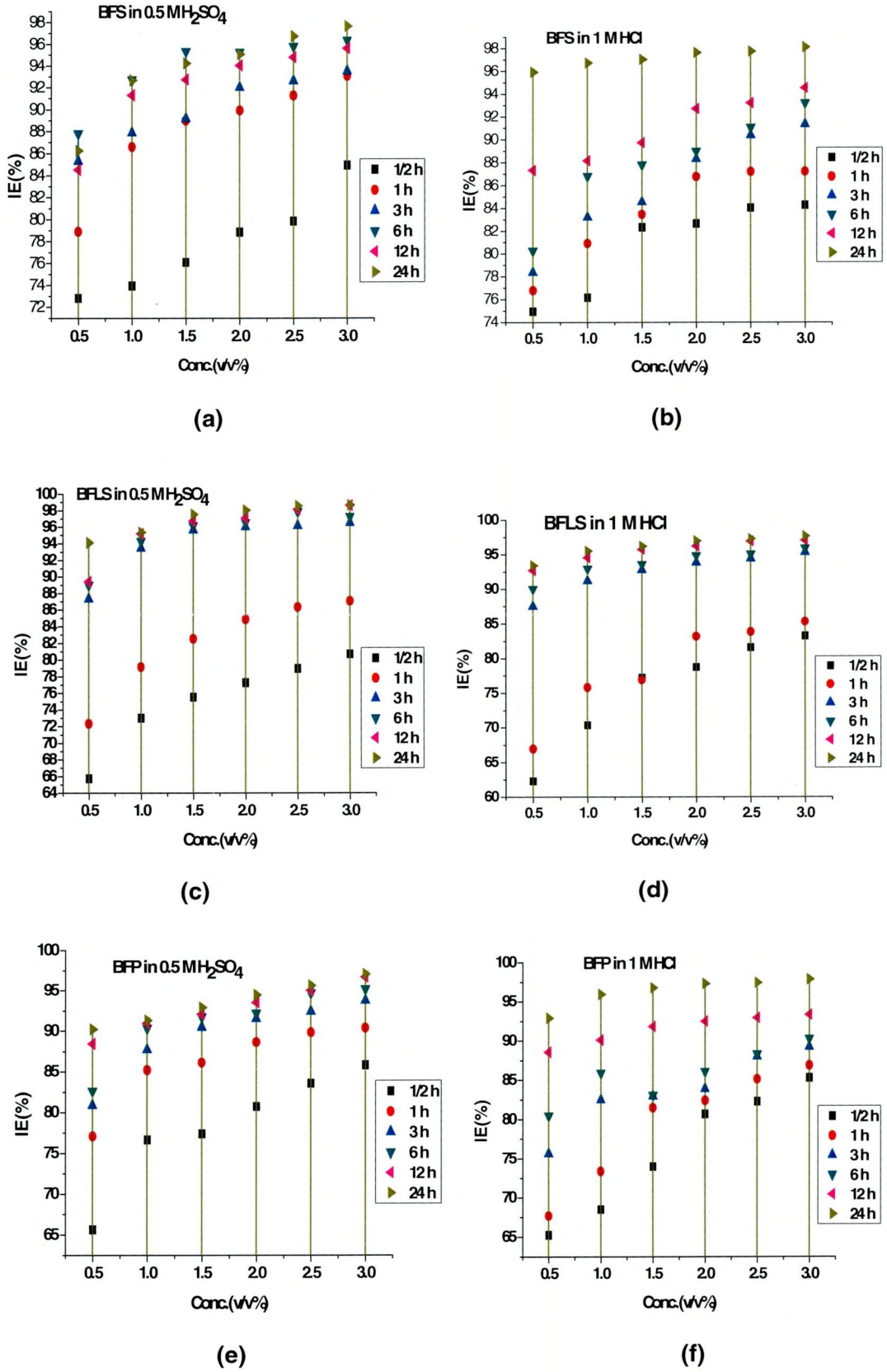

Figure – 24 The relationship between IE(%) and Concentration of BF extracts in 0.5 M H_2SO_4 and 1 M HCl

4.2.1.5 BFLS extract in 0.5 M H_2SO_4 and 1 M HCl on MS corrosion

The percentage inhibition efficiency of BFLS on mild steel acid corrosion has obtained from mass loss measurements at different concentrations of inhibitor at room temperature. The variation in percentage inhibition efficiency with concentration of the studied green inhibitor is shown in Table-15. It has been observed that the corrosion rate decreased with the increase in concentration of BFLS extract and percentage inhibition efficiency was found to increase with the concentration of inhibitor. The maximum inhibition efficiencies of 98.7% and 97.0% were obtained in 0.5 M H_2SO_4 and 1 M HCl solutions containing 4.0%v/v CNLS extract at 24 h. The increase in inhibition efficiency was due to the increase in the number of constituent molecules of BFLS extract adsorbed on the metal surface at 4.0%v/v concentrations **(Zhang and Hua, 2009)**, so that the active sites of the metal were protected by the inhibitor molecules. (Figure - 24 (c and d)).

Table - 15 Inhibition efficiency as a function of immersion time and concentration of BFLS extract on MS in 0.5 M H_2SO_4 and 1 M HCl

Conc. (%v/v)	½ h		1 h		3 h		6 h		12 h		24 h	
	CR mpy	IE (%)	CR mpy	IE (%)	CR mpy	IE (%)	CR mpy	IE (%)	CR mpy	IE (%)	CR mpy	IE (%)
0.5 M H_2SO_4												
Blank	1234	-	1312	-	1558	-	1808	-	1481	-	1158	-
0.5	423	65.7	363	72.3	197	87.3	198	89.0	156	89.4	68	94.1
1.0	333	73.0	273	79.1	101	93.4	103	94.2	70	95.2	53	95.3
1.5	301	75.5	229	82.5	67	95.6	69	96.1	48	96.7	28	97.5
2.0	280	77.2	198	84.8	61	96.0	62	96.5	42	97.1	22	98.1
2.5	259	78.9	179	86.3	59	96.1	49	97.2	27	98.1	16	98.6
3.0	238	80.7	169	87.1	53	96.5	38	97.8	20	98.6	15	**98.7**
3.5	237	80.7	169	87.1	52	96.6	38	97.8	20	98.6	15	**98.7**
4.0	237	80.7	169	87.1	52	96.6	38	97.8	20	98.6	15	**98.7**
1 M HCl												
Blank	1060	-	1105	-	1268	-	1504	-	1131	-	916	-
0.5	433	59.1	365	66.9	158	87.5	150	90.0	74	93.4	67	92.6
1.0	314	70.3	267	75.7	111	91.2	106	92.9	51	95.4	50	94.5
1.5	241	77.2	255	76.8	92	92.7	96	93.5	43	96.1	39	95.7
2.0	225	78.7	186	83.1	78	93.8	77	94.8	34	96.9	34	96.2
2.5	195	81.6	178	83.8	70	94.4	74	95.0	30	97.2	28	96.9
3.0	177	83.3	162	85.3	59	95.3	60	96.0	30	97.6	23	**97.0**
3.5	176	83.3	162	85.3	58	95.4	60	96.0	30	97.6	23	**97.0**
4.0	176	83.3	162	85.3	58	95.4	60	96.0	30	96.7	23	**97.0**

4.2.1.6 BFP extract in 0.5 M H_2SO_4 and 1 M HCl on MS corrosion

Table - 16 summaries the gravimetric trends of the MS immersed in 0.5 M H_2SO_4 and 1 M HCl, respectively in the absence and the presence of the inhibitor at various concentrations at room temperature. The addition of BFP extract in both acid medium decreases the corrosion rate of mild steel. The decrease of corrosion rate

may be interpreted by the simultaneous action of inhibitor on cathodic and anodic reactions. Analyzing the Table-16, it has been noted that the inhibition efficiencies increase with increase in BFP extract concentration and the maximum inhibition efficiency of 97.0% and 97.8 % were obtained with 4.0%v/v concentration within the range of concentrations studied (Figure - 24(e and f)). This high inhibitory effect may be interpreted by the presence of phytochemical constituents present in the BFP extract.

Values of the corrosion rate (CR) of mild steel in 0.5 M H_2SO_4 and 1 M HCl in the presence of various concentration of BF extract at different time intervals are presented in Table (14-16). The results obtained indicate that the corrosion rates of mild steel decrease with increase in the concentration of BFS, BFLS and BFP extracts. Hence, the studied inhibitors retarded the rate of corrosion of mild steel in both acid media. Accordingly the values of inhibition efficiencies obtained for various concentrations of BFS, BFLS and BFP, increase with increasing concentration of BFS, BFLS and BFP extracts.

Table - 16 Inhibition efficiency as a function of immersion time and concentration of BFP extract on MS in 0.5 M H_2SO_4 and 1 M HCl

Conc. (%v/v)	½ h		1 h		3 h		6 h		12 h		24 h	
	CR mpy	IE (%)	CR mpy	IE (%)	CR mpy	IE (%)	CR mpy	IE (%)	CR mpy	IE (%)	CR mpy	IE (%)
0.5 M H_2SO_4												
Blank	1234	-	1312	-	1558	-	1808	-	1481	-	1158	-
0.5	424	65.6	300	77.0	297	80.8	314	82.6	171	88.4	113	90.2
1.0	288	76.6	194	85.1	190	87.7	174	90.3	133	90.9	100	91.3
1.5	278	77.4	182	86.1	148	90.4	149	91.7	117	92.0	81	92.9
2.0	237	80.7	148	88.6	132	91.5	141	92.1	95	93.5	64	94.4
2.5	202	83.5	133	89.8	118	92.4	95	94.7	73	95.0	50	95.6
3.0	175	85.7	126	90.3	97	93.7	87	95.1	49	96.6	34	**97.0**
3.5	174	85.7	126	90.3	97	93.7	87	95.1	49	96.6	34	**97.0**
4.0	174	85.7	126	90.3	97	93.7	87	95.1	49	96.6	34	**97.0**
1 M HCl												
Blank	1060	-	1105	-	1268	-	1504	-	1131	-	916	-
0.5	368	65.2	357	67.6	247	75.6	366	80.4	130	88.5	64	92.9
1.0	333	68.5	294	73.3	178	82.9	256	85.8	112	90.0	37	95.9
1.5	275	73.9	205	81.4	214	83.0	263	82.5	92	91.8	29	96.7
2.0	204	80.6	194	82.3	176	86.0	242	83.8	85	92.4	24	97.3
2.5	187	82.3	164	85.1	148	88.3	180	88.0	79	92.9	23	97.4
3.0	155	85.3	144	86.8	123	90.2	161	89.2	75	93.3	19	**97.8**
3.5	154	85.3	144	86.6	123	90.2	161	89.2	75	93.3	19	**97.8**
4.0	154	85.3	144	86.6	123	90.2	161	89.2	75	93.3	19	**97.8**

Assessing the inhibition efficiencies of extract of shell, leaf stalk and peduncle of CN and BF with 4.0%v/v concentration in both 0.5 M H_2SO_4 and 1 M HCl

Figure-25 shows a histogram, depicting the comparison of the inhibition efficiencies of extract of shell, leaf stalk and peduncle of CN and BF with 4.0%v/v at 24 h immersion in both acid media.

The order of percentage inhibition efficiency of CN and BF extracts:

In 0.5 M H_2SO_4 at 24 h immersion with 4.0%v/v concentration

CNP (97.6%) < CNLS (98.4%) < CNS (98.6%)

BFP (97.0%) < BFS (97.6%) < BFLS (98.7%)

In 1M HCl at 24 h immersion with 4.0%v/v concentration

CNLS (96.3%) < CNP (97.5%) < CNS (98.1%)

BFLS (97.0 %) < BFP (97.8%) < BFS (98.1%)

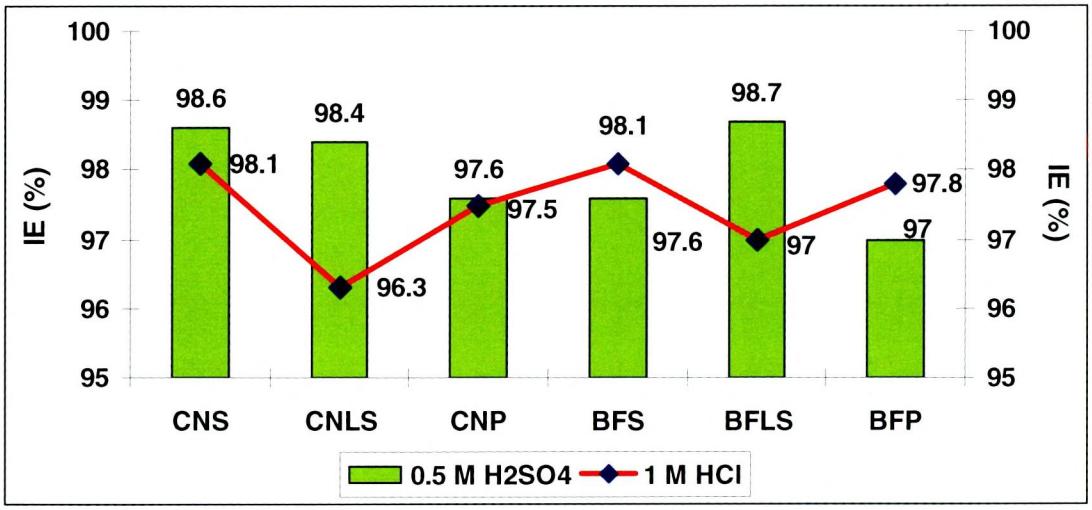

Figure - 25 Variation of inhibition efficiencies of extracts of shell, leaf stalk and peduncle of CN and BF with 4.0 %v/v concentrations at 24 h immersion on MS corrosion.

From the values of Figure-25, it is clear that the CN and BF extracts effectively inhibit the corrosion rate of MS in both 0.5 M H_2SO_4 and 1 M HCl media. Values of IE in 0.5 M H_2SO_4 were found to be slightly higher than in 1 M HCl. This was due to the availability of more sites on metal surface for adsorption in H_2SO_4 medium because of lesser adsorption of the sulphate ions on the metal surface **(Ahamad and Quraishi, 2009)**.

All the investigated CN extracts and BF extracts afforded a maximum of 97% IE in both acid media. Enhanced inhibition efficiencies of the studied extracts might be due to the presence of their phytochemical constituents. **Eddy and Ebenso, 2008**, noted that the phytochemical constituents of extracts were the major factors that determined the inhibition efficiency of the plant extracts.

4.2.2 EFFECT OF IMMERSION TIME OF CN AND BF EXTRACTS ON MS CORROSION

Mass loss is a non-electrochemical technique for the determination of corrosion rates and inhibitor efficiency which provided more reliable results than electrochemical techniques because the experimental conditions were approached in

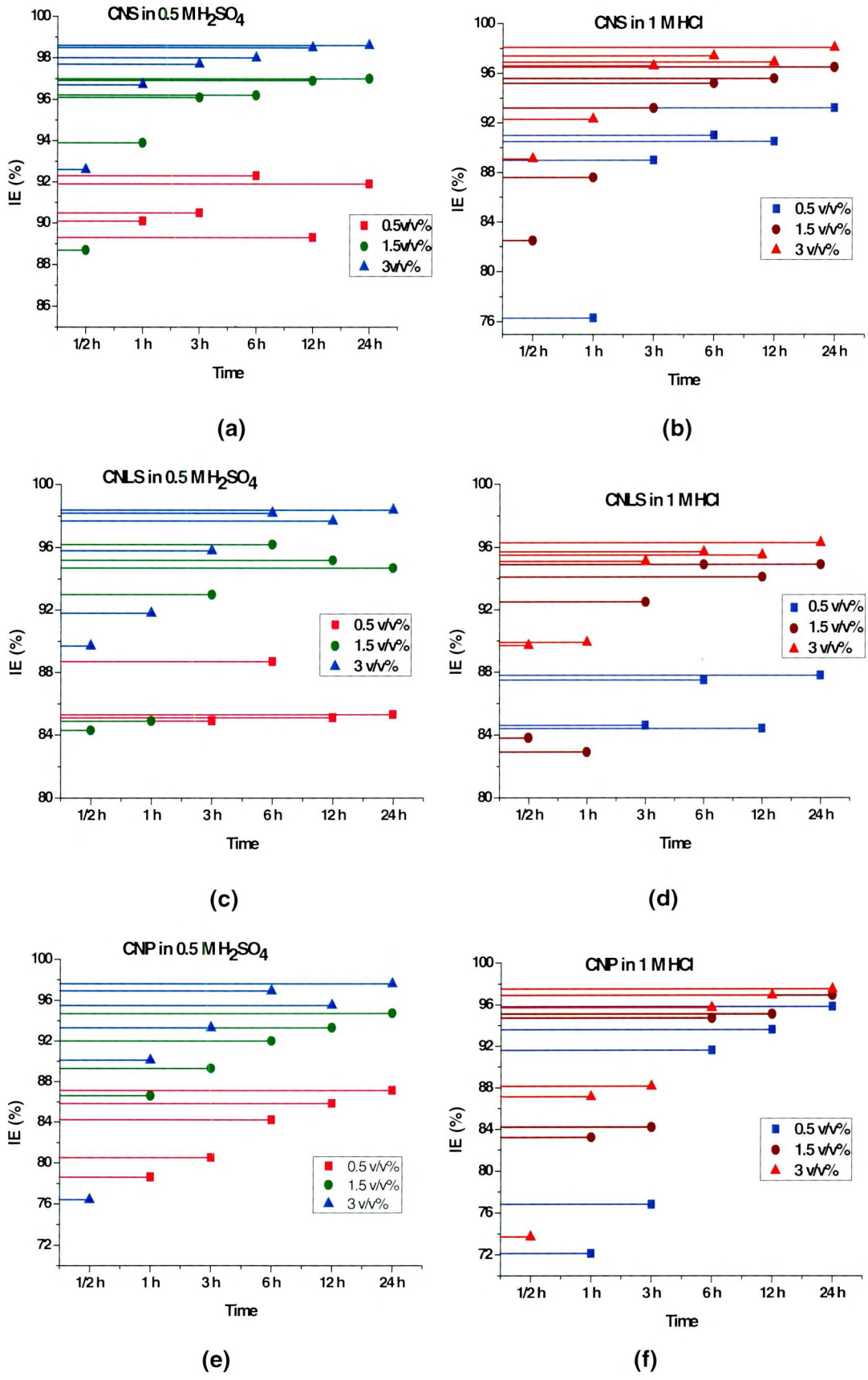

Figure - 26 The relationship between IE(%) and Time of CN extracts in 0.5 M H_2SO_4 and 1 M HCl on MS corrosion

a more realistic manner. However, immersion tests were time-consuming. The mass loss of mild steel coupons have been evaluated for a periods of ½ h, 1 h 3 h, 6 h, 12 h and 24 h of immersion in 0.5 M H_2SO_4 and 1 M HCl solutions in the absence and presence of inhibitor. Further inspection of Table (11-16) revealed that the inhibitor efficiency of studied inhibitors increased markedly with an increase of the exposure time. The mass loss for the mild steel in 0.5 M H_2SO_4 and 1 M HCl containing different concentrations of the studied inhibitor as a function of time are presented in Figure-(26 and 27), respectively. The results show that mass loss increases with increase in time, concentration of studied inhibitors. The decrease in mass loss is due to the inhibitive effects of studied inhibitor and these effects increase with increase in studied inhibitor concentrations. This trend may result from the fact that adsorption and surface coverage increases with the increases in concentration. Thus the surface has been efficiently separated from the medium **(Al-Andis *et al.*, 1995)**.

4.2.2.1 Impact of immersion time of CNS, CNLS and CNP on MS corrosion in 0.5 M H_2SO_4

Figure 26.(a.c.e) illustrate that the percentage inhibition efficiencies of the inhibitor at different concentrations in 0.5 M H_2SO_4. The results have revealed that the percentage inhibition efficiency increases with increases in the concentration of the inhibitor. In the case of higher concentration (4.0%v/v) the inhibition efficiency experienced an exponential increase over the period of time in CNS and CNP and it implicates that the current inhibitors show the highest inhibition efficiency 98.6 and 97.6%, at 24 h respectively. In 4.0%v/v concentration of CNLS efficiency range of 89.7% (1/2 h) to 98.2% (6 h) and then slightly declined to 97.7% (12 h) and marginally increased to 98.4% (24 h).

4.2.2.2 Impact of immersion time of CNS, CNLS and CNP on MS corrosion in 1 M HCl

To investigate the effect of inhibition with exposure time, experiments have been carried out at various time intervals. It is clear from Figure-26 (b.d.f) and that , as the time of immersion increases from ½ h to 6 h, the protection efficiency for CNS and CNLS in 1 M HCl increased from 89.2% and 89.8% (4.0%v/v concentration at ½ h) to 97.4% and 95.8% respectively (4.0%v/v concentration at 6 h). After 6 h there was a slight decline in IE to 97.0% and 95.5% at 12 h and then an increase in IE at 24 h (98.1 and 96.3%) was observed **(Subhashini *et al.*, 2010)**. In 4.0%v/v concentration of CNP, the inhibition efficiency experienced an exponential increase over the period of time and furnish 97.6% and 97.5% IE at 24 h in both investigated media.

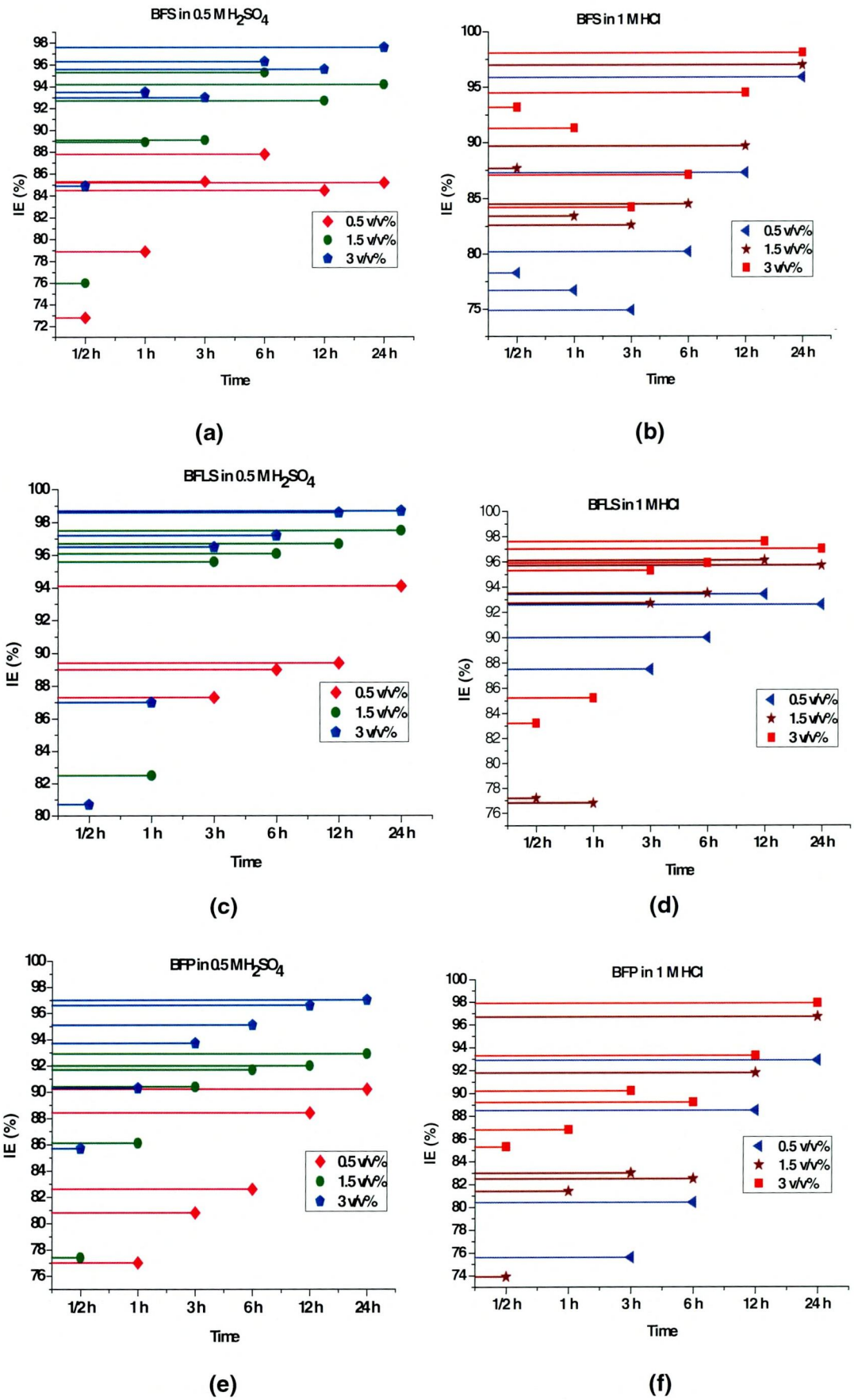

Figure-27 The relationship between IE (%) and Time of BF extracts in 0.5 M H_2SO_4 and 1 M HCl on MS corrosion

4.2.2.3 Impact of immersion time of BFS, BFLS and BFP on MS corrosion in 0.5 M H_2SO_4

Data on percentage inhibition efficiency of shell, leaf stalk and peduncle of BF extract in 0.5 M H_2SO_4 during immersion of MS with the current inhibitors are presented in the Figure-27(a.c.e). Increase in IE with concentration of the extract might be due to the increase in the surface coverage of the adsorbed molecules on mild steel surface. In BFLS and BFP, as the immersion time increased from ½ h to 24 h, the IE also increased from 80.7% (1/2 h) to 98.7% (24 h) and 85.7% (1/2 h) to 97.0 % (24 h) with 4.0%v/v concentration irrespectively (Table14-16). The increase in IE with an increase in immersion time indicated the stability and persistence of the inhibitor layer on the MS surface. The protection efficiency for BFS increased from 85.0% (1/2 h) to 96.3% (4.0%v/v concentration at 6 h). After 6 h there was a marginal decrease upto 95.6% (12 h) and then an increase in IE at 24 h (97.6%).

4.2.2.4 Impact of immersion time of BFS, BFLS and BFP on MS corrosion in 1 M HCl

The effect of immersion time on BFS, BFLS and BFP in 1 M HCl have been studied and depicted in Figure- 27 (b.d.f). From the Figure, it can be inferred that as the time of immersion increased from ½ h to 24 h, the protection efficiency also increased from 84.2% (3 h) to 98.1 % (24 h) for BFS, 83.3 % (1/2 h) to 97.0% (24 h) for BFLS and 85.3% (1/2 h) to 97.8% (24 h) for BFP, thereby indicated the enhanced stability of the adsorbed constituents of the extract on MS surface, at longer periods of immersion **(Mohammed Ajmal, 2000)**.

For a given time of immersion, inhibition efficiency increased with the increase in concentration. For a particular concentration, the inhibition efficiency increased with an increase in immersion time. This might be due to the formation of barrier film which prevented the attack of acid on metal surface.

Analysis of the results, furnished in Table (14-16), reveal that inhibition efficiencies of BFS, BFLS and BFP in both medium functioned excellently at all periods of immersion. At earlier periods of immersion, all the BF extracts furnished inhibition efficiencies in the range of 85% to 90% at the maximum concentration in 1 M HCl and 85% to 94% in 0.5 M H_2SO_4 and at longer periods of immersion, all the investigated inhibitors afford a maximum IE in the range of 93% to 95% in both acid medium. Those results inferred that inhibitor efficiencies of BF extract increased continuously with time of immersion. It is obvious from the table that studied inhibitors were promising inhibitors in 0.5 M H_2SO_4 and1 M HCl at various time of immersion.

It is of interest to mention that after several hours from the beginning of the mass loss experiments, the IE% reaches almost to 98% in all the studied inhibitors. Visual observation and the results revealed that with increased period of exposure,

the corrosion rates were decreasing. This could be due to increased viscosity of solution as a result of dissolved corrosion products thereby diluting the extract.

The inhibitive action of shell, leaf stalk and peduncle of CN and BF extracts toward the acid corrosion of MS can be attributed to the adsorption of the shell, leaf stalk and peduncle of CN and BF extracts components onto the steel surface. Corrosion inhibition was initiated by the displacement of adsorbed water molecules by the inhibitor species leading to specific adsorption on the metal surface **(Solmaz *et al.*, 2008b)**. Studies conducted by **Edeoga *et al.*, 2005; Akaneme, 2007** have shown that the plant extracts are a complex mixture of various phytochemical components. The phytochemical components present in the studied inhibitors have phenyl, methyl, methoxy groups and heteroatoms, such as O in their molecules. Thus, the corrosion of MS might be attributed to the adsorption of shell, leaf stalk and peduncle of CN and BF components, through these atoms that are regarded as centers of adsorption, onto the metal surface thereby creating a barrier for mass and charge transfer and thus isolating the metal from further attack of the corrosive anions.

It is evident from the study that longer period of immersion results indicates a strong stable layer of adsorbed phytochemical constituents present in shell, leaf and peduncle of CN and BF extract on the MS surface. Most of the compounds contained in studied inhibitors can be easily adsorbed on the metal surface giving rise to such enhanced inhibition.

4.2.3 EFFECT OF TEMPERATURE OF CN AND BF EXTRACTS ON MS

Temperature is an important parameter in studies on metal dissolution **(de Souza, *et al.*, 2008)**. The corrosion rate in acid solution, for example, increases exponentially with a temperature increase because the hydrogen evolution over potential decreases **(Popova *et al.*, 2003)**. The MS specimens in triplicate were immersed in 100ml of electrolyte (0.5 M H_2SO_4 and 1 M HCl) with and without the addition of different concentrations of studied inhibitors at 303 – 343 K (as per chemical cleaning industries). The time duration of experiments were optimized and conducted for ½ h in the temperature range of 303 – 343 K in stationary condition. At the end of exposure period, specimens were cleaned according to ASTM G31-72 **(ANONIMO, 1999)** and their mass has been recorded.

Naturally occurring substance were found to be promising inhibitors and they proved to be temperature resistant, they can be suitably recommended for boiler systems. Our present results represented in Table (17-22) revealed significant relationship between the temperature, concentration and inhibition efficiency.

Inhibition efficiencies calculated in the presence of shell, leaf stalk and peduncle of CN and BF extracts on mild steel corrosion in 0.5 M H_2SO_4 and 1 M HCl at each experimental temperature viz., 303 K, 313 K, 323 K, 333 K and 343 K are listed in Table17-22. Analysis of the Table and Figure indicate.

- ✶ As the concentration of shell, leaf stalk and peduncle of CN and BF increased, the IE also increased at all studied temperature.
- ✶ The maximum inhibition has obtained at the studied plant extracts concentration of 4.0%v/v for all the testing temperatures.

4.2.3.1 Role of temperature on MS in the presence of CNS extract in 0.5 M H_2SO_4 and 1M HCl

The data of corrosion rates and corresponding efficiency collected are presented in Table-17.

Table - 17 Influence of temperature on the inhibition efficiency of CNS extract on MS corrosion in 0.5 M H_2SO_4 and 1 M HCl medium

Conc. (%v/v)	303 K		313 K		323 K		333 K		343 K	
	CR (mpy)	IE (%)	CR (mpy)	IE (%)	CR (mpy)	IE (%)	CR (mpy)	IE (%)	CR (mpy)	IE (%)
0.5 M H_2SO_4										
Blank	1234	-	3417	-	7114	-	12222	-	19046	-
0.5	271	77.9	505	85.2	1206	83.0	2278	81.3	4199	77.9
1.0	170	86.1	314	90.8	777	89.0	1593	86.9	2584	86.4
1.5	139	88.7	248	92.7	537	92.7	1057	91.3	2184	88.5
2.0	109	91.1	179	94.7	384	94.6	887	92.7	1655	91.3
2.5	102	91.6	137	95.9	294	95.8	734	93.9	1335	92.9
3.0	90	92.6	119	**96.5**	292	95.8	652	94.6	1295	**93.2**
3.5	90	92.6	119	**96.5**	292	95.8	652	94.6	1295	**93.2**
4.0	90	92.6	119	**96.5**	292	95.8	652	94.6	1295	**93.2**
1 M HCl										
Blank	1060	-	2349	-	4307	-	10061	-	17245	-
0.5	303	71.3	612	73.9	1204	72.0	3942	60.8	7886	54.2
1.0	236	77.7	448	80.9	857	80.1	2404	76.1	5442	68.4
1.5	184	82.5	336	85.6	643	85.0	2055	79.5	4716	72.6
2.0	132	87.5	275	88.2	584	86.4	1593	84.1	3994	76.8
2.5	120	88.6	241	89.7	446	89.6	1339	86.6	3121	81.9
3.0	115	89.1	214	**90.8**	412	90.4	1123	88.8	2757	**84.0**
3.5	115	89.1	214	**90.8**	412	90.4	1123	88.8	2757	**84.0**
4.0	115	89.1	214	**90.8**	412	90.4	1123	88.8	2757	**84.0**

Examination of Table-17 and Figure-28 reveal that the presence of inhibitor leads to decrease of the corrosion rate at all studied temperature and at all concentration respectively. As the temperature increased from 303 K to 313 K, the IE also increased. CNS extract (4.0%v/v concentration) in 0.5 M H_2SO_4 and 1 M HCl could afford a maximum IE(%) of 96.5% and 90.8% at 313 K. However, the values of IE(%) at 323 K, 333 K and 343 K were stabilized and ultimately the investigated CNS extract could furnish around 93.2 % and 84.0% respectively, at 343 K in 0.5 M H_2SO_4

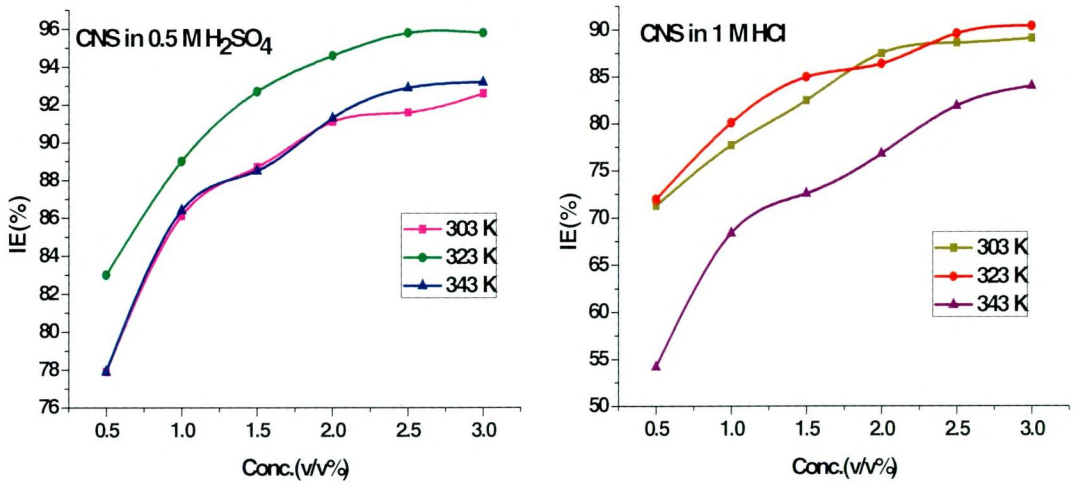

(a) (b)

Figure - 28 Effect of temperature on IE of the CNS extracts in (a) 0.5 M H_2SO_4 and (b) 1 M HCl at various concentrations.

and 1 M HCl respectively. This enhanced inhibition efficiency at elevated temperature inferred the stability of the adsorbed layer of CNS extract on MS surface.The strength of the adsorbed insoluble film on the MS surface confirmed the effective inhibition of CNS extract at high temperature.

4.2.3.2 Role of temperature on MS corrosion in the presence of CNLS extract in 0.5 M H_2SO_4 and 1M HCl

Inspection of the Table-18 and Figure-29 reveal that IE(%) at 4.0%v/v concentration of CNLS in 0.5 M H_2SO_4 and 1 M HCl bath increased from 89.6% to 95.2% and 89.9% to 90.3% with increase in temperature upto 313 K after 313 K, IE was found to be stabilized at 343 K, affording a maximum of 91.6% and 86.5% at 343 K. The high protective ability of CNS extract at high temperature in both examined media is well documented from temperature studies results.

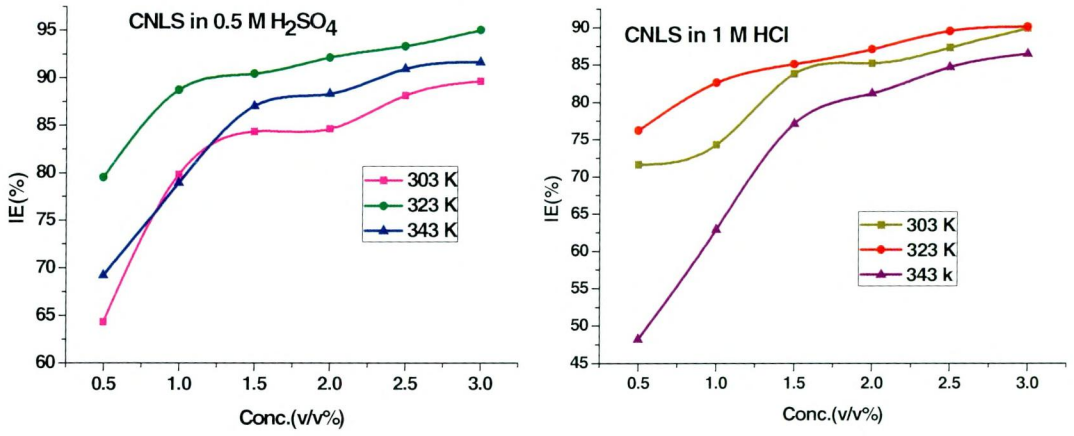

(a) (b)

Figure-29 Effect of temperature on IE of the CNLS extracts in (a) 0.5 M H_2SO_4 and (b) 1 M HCl at various concentrations

Table-18 Influence of temperature on the inhibition efficiency of CNLS extract on MS corrosion in 0.5 M H_2SO_4 and 1 M HCl medium

Conc. (%v/v)	303 K		313 K		323 K		333 K		343 K	
	CR (mpy)	IE (%)	CR (mpy)	IE (%)	CR (mpy)	IE (%)	CR (mpy)	IE (%)	CR (mpy)	IE (%)
0.5 M H_2SO_4										
Blank	1234	-	3417	-	7114	-	12222	-	19046	-
0.5	439	64.3	691	79.7	1454	79.5	3494	71.4	5862	69.2
1.0	248	79.8	370	89.1	799	88.7	2335	80.8	4015	78.9
1.5	192	84.3	303	91.1	677	90.4	1509	87.6	2468	87.0
2.0	189	84.6	220	93.5	558	92.1	1318	89.2	2224	88.3
2.5	146	88.1	195	94.2	471	93.3	1035	91.5	1727	90.9
3.0	127	89.6	162	**95.2**	353	95.0	855	93.0	1598	**91.6**
3.5	127	89.6	162	**95.2**	353	95.0	855	93.0	1598	**91.6**
4.0	127	89.6	162	**95.2**	353	95.0	855	93.0	1598	**91.6**
1 M HCl										
Blank	1060	-	2349	-	4307	-	10061	-	17245	-
0.5	300	71.6	595	74.6	1021	76.2	4944	50.8	8922	48.2
1.0	271	74.3	477	79.6	746	82.6	2377	76.3	6387	62.9
1.5	171	83.8	391	83.3	640	85.1	1782	82.2	3942	77.1
2.0	156	85.2	315	86.5	554	87.1	1497	85.1	3235	81.2
2.5	133	87.3	261	88.8	450	89.5	1276	87.3	2623	84.7
3.0	106	89.9	232	**90.3**	415	90.1	1049	89.5	2314	**86.5**
3.5	106	89.9	232	**90.3**	415	90.1	1049	89.5	2314	**86.5**
4.0	106	89.9	232	**90.3**	415	90.1	1049	89.5	2314	**86.5**

4.2.3.3 Role of temperature on MS in the presence of CNP extract in 0.5 M H_2SO_4 and 1 M HCl

The variation in percentage inhibition efficiency is shown in Table-19 and Figure-30 (a and b). From the values of Table-19, it is clear that the CNP extract effectively inhibits the corrosion rate of mild steel in both 0.5 M H_2SO_4 and 1 M HCl media at all studied temperature. Inhibition efficiency in both acid media was found to increases from 76.4% (303 K) to 92.4% (313 K) and 73.7% (303 K) to 92.3% (313 K) respectively. After 313 K, IE was found to be stabilized at 343 K, affording a maximum of 88.2% and 83.6%, respectively with 4.0%v/v concentration of inhibitor in both 0.5 M H_2SO_4 and 1 M HCl. Analysis of the Table-19, concluded that CNP extract functions effectively upto 343 K furnishing a maximum of 90% IE in both studied media. The results of the current study using CNP extract ascertained the effectiveness and strength of adsorbed layer on mild steel surface at high temperatures.

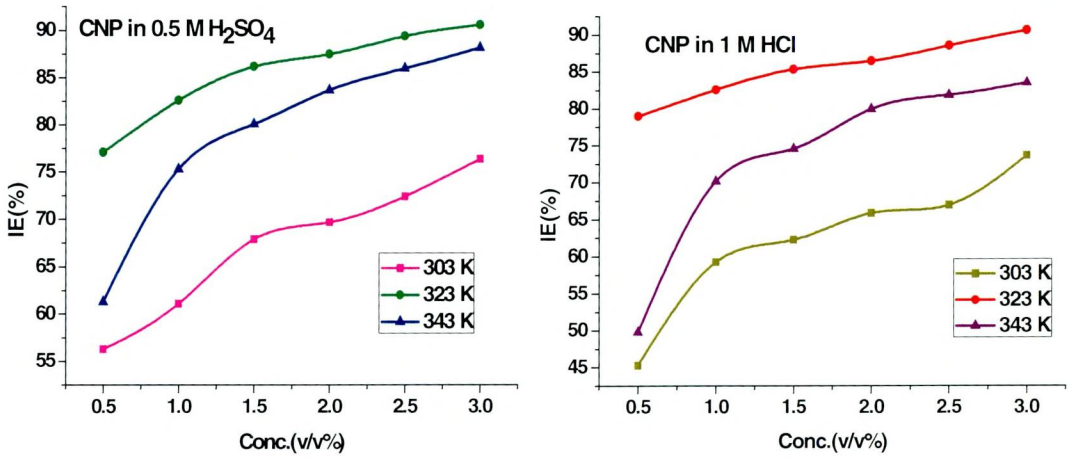

(a) (b)

Figure - 30 Effect of temperatures on IE of the CNP extracts in (a) 0.5 M H_2SO_4 and (b) 1 M HCl at various concentrations

Table-19 Influence of temperature on the inhibition efficiency of CNP extract on MS corrosion in 0.5 M H_2SO_4 and 1 M HCl medium

Conc. (%v/v)	303 K		313 K		323 K		333 K		343 K	
	CR (mpy)	IE (%)	CR (mpy)	IE (%)	CR (mpy)	IE (%)	CR (mpy)	IE (%)	CR (mpy)	IE (%)
0.5 M H_2SO_4										
Blank	1234	-	3417	-	7114	-	12222	-	19046	-
0.5	538	56.3	650	80.9	1624	77.1	3478	71.5	7369	61.3
1.0	480	61.1	389	88.6	1232	82.6	2209	81.9	4693	75.3
1.5	395	67.9	353	89.6	976	86.2	1695	86.1	3778	80.1
2.0	373	69.7	324	90.5	888	87.5	1454	88.1	3091	83.7
2.5	339	72.4	282	91.7	747	89.4	1357	88.8	2657	86.0
3.0	291	76.4	256	**92.4**	663	90.6	1175	90.3	2232	**88.2**
3.5	291	76.4	256	**92.4**	663	90.6	1175	90.3	2232	**88.2**
4.0	291	76.4	256	**92.4**	663	90.6	1175	90.3	2232	**88.2**
1 M HCl										
Blank	1060	-	2349	-	4307	-	10061	-	17245	-
0.5	579	45.3	442	81.1	901	79.0	2741	72.7	8645	49.8
1.0	431	59.3	329	85.9	748	82.6	1818	81.9	5127	70.2
1.5	398	62.3	303	87.0	626	85.4	1557	84.5	4376	74.6
2.0	361	65.9	252	89.2	580	86.5	1425	85.8	3443	80.0
2.5	349	67.0	213	90.9	488	88.6	1186	88.2	3109	81.9
3.0	278	73.7	180	**92.3**	399	90.7	991	90.1	2828	**83.6**
3.5	278	73.7	180	**92.3**	399	90.7	991	90.1	2828	**83.6**
4.0	278	73.7	180	**92.3**	399	90.7	991	90.1	2828	**83.6**

4.2.3.4 Role of temperature on MS in the presence of BFS extract in 0.5 M H_2SO_4 and 1M HCl

The influence of temperature on the corrosion behaviour of MS in 0.5 M H_2SO_4 and 1M HCl in the presence and absence of BFS extract of varying concentrations were investigated by mass loss method in the temperature range 303 K to 343 K.

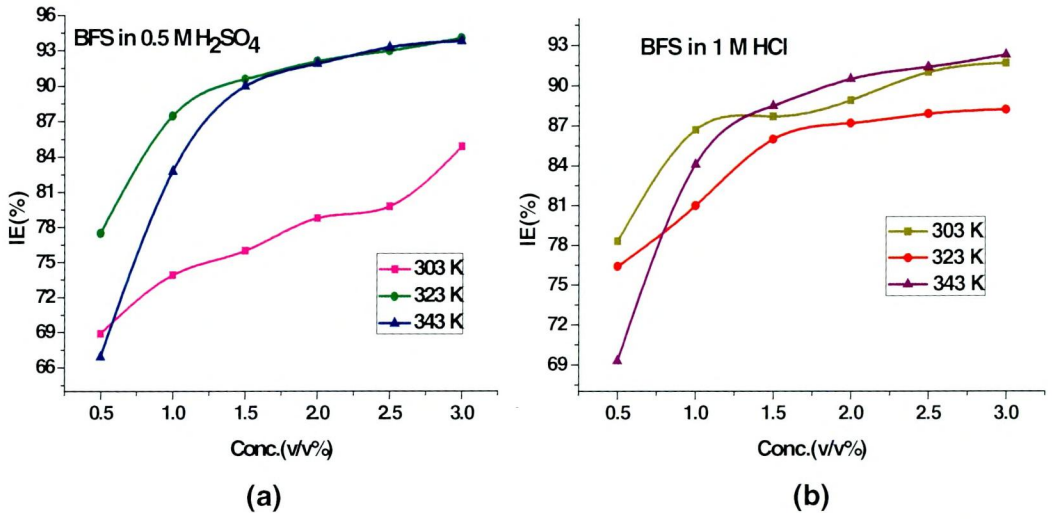

Figure – 31 Effect of temperature on IE of the BFS extracts in (a) 0.5 M H_2SO_4 and (b) 1 M HCl at various concentrations

Table – 20 Influence of temperature on the inhibition efficiency of BFS extract on MS corrosion in 0.5 M H_2SO_4 and 1 M HCl medium

Conc. (%v/v)	303 K		313 K		323 K		333 K		343 K	
	CR (mpy)	IE (%)	CR (mpy)	IE (%)	CR (mpy)	IE (%)	CR (mpy)	IE (%)	CR (mpy)	IE (%)
0.5 M H_2SO_4										
Blank	1234	-	3417	-	7114	-	12222	-	19046	-
0.5	383	68.9	929	72.8	1598	77.5	2271	81.4	6302	66.9
1.0	321	73.9	814	76.1	884	87.5	1504	87.6	3268	82.8
1.5	295	76.0	682	80.0	665	90.6	1120	90.8	1898	90.0
2.0	261	78.8	643	81.1	560	92.1	880	92.8	1533	91.9
2.5	248	79.8	557	80.1	497	93.0	730	94.0	1266	93.3
3.0	186	84.9	488	85.7	413	94.1	673	**94.4**	1177	**93.8**
3.5	186	84.9	488	85.7	413	94.1	673	**94.4**	1177	**93.8**
4.0	186	84.9	488	85.7	413	94.1	673	**94.4**	1177	**93.8**
1 M HCl										
Blank	1060	-	2349	-	4307	-	10061	-	17245	-
0.5	229	78.3	442	81.1	1015	76.4	1710	83.0	5278	69.3
1.0	140	86.7	293	87.5	814	81.0	1175	88.3	2740	84.1
1.5	129	87.7	228	90.2	600	86.0	1041	89.6	1971	88.5
2.0	116	88.9	201	91.4	550	87.2	818	91.8	1629	90.5
2.5	94	91.0	186	92.0	517	87.9	729	92.7	1479	91.4
3.0	87	91.7	159	93.2	504	88.2	671	**93.3**	1319	**92.3**
3.5	87	91.7	159	93.2	504	88.2	671	**93.3**	1319	**92.3**
4.0	87	91.7	159	93.2	504	88.2	671	**93.3**	1319	**92.3**

Inspection of Table-20 reveals that the BFS extract exhibited a maximum IE of 94.4% (333 K) in 0.5 M H_2SO_4 and 93.3% (333 K) in 1 M HCl. Further analysis of Figure-31(a and b) infers that IE of BFS extract increased with the increase in concentration at the studied temperatures and at various concentrations.

4.2.3.5 Role of temperature on MS in the presence of BFLS extract in 0.5 M H_2SO_4 and 1M HCl

Table-21 represents the corrosion rates and IE(%) of MS specimen in 0.5 M H_2SO_4 and 1M HCl in the absence and presence of different concentrations of BFLS extract at different temperatures.

Table – 21 Influence of temperature on the inhibition efficiency of BFLS extract on mild steel corrosion in 0.5 M H_2SO_4 and 1 M HCl medium

Conc. (%v/v)	303 K		313 K		323 K		333 K		343 K	
	CR (mpy)	IE (%)	CR (mpy)	IE (%)	CR (mpy)	IE (%)	CR (mpy)	IE (%)	CR (mpy)	IE (%)
0.5 M H_2SO_4										
Blank	1234	-	3417	-	7114	-	12222	-	19046	-
0.5	423	65.7	661	80.6	1482	79.1	3164	74.1	5148	72.9
1.0	333	73.0	470	86.2	1031	85.5	1912	84.3	3331	82.5
1.5	301	75.5	348	89.8	799	88.7	1497	87.7	2451	87.1
2.0	280	77.2	285	91.6	623	91.2	1166	90.4	2026	89.3
2.5	259	78.9	248	92.7	616	91.3	1124	90.8	1885	90.1
3.0	238	80.7	211	**93.8**	493	93.0	937	**92.3**	1537	**91.9**
3.5	238	80.7	211	**93.8**	493	93.0	937	**92.3**	1537	**91.9**
4.0	238	80.7	211	**93.8**	493	93.0	937	**92.3**	1537	**91.9**
1 M HCl										
Blank	1060	-	2349	-	4307	-	10061	-	17245	-
0.5	350	66.9	539	77.0	1180	72.5	3551	64.7	7500	56.5
1.0	256	75.7	387	83.5	835	80.6	2161	78.5	5108	70.3
1.5	245	76.8	341	85.4	681	84.1	1677	83.3	3588	79.1
2.0	178	83.1	288	87.7	553	87.1	1345	86.6	2909	83.1
2.5	171	83.8	251	89.3	479	88.8	1206	88.0	2197	87.2
3.0	155	85.2	211	**91.0**	436	89.8	1049	**89.5**	1838	**89.3**
3.5	155	85.2	211	**91.0**	436	89.8	1049	**89.5**	1838	**89.3**
4.0	155	85.2	211	**91.0**	436	89.8	1049	**89.5**	1838	**89.3**

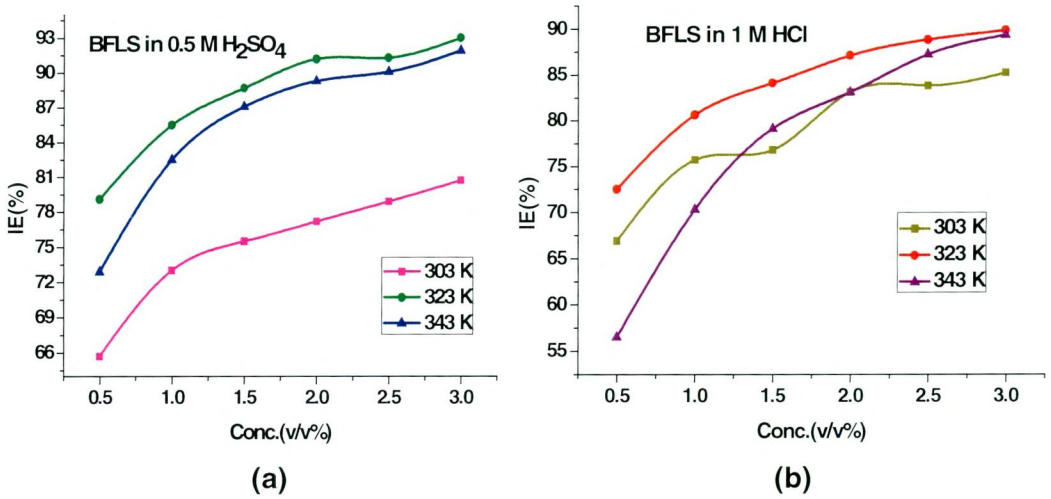

Figure - 32 Effect of temperature on IE of the BFLS extracts (a) 0.5 M H_2SO_4 and (b) 1 M HCl at various concentrations

Figure-32 illustrates that IE(%) at 4.0%v/v concentration of BFLS in 0.5 M H_2SO_4 bath increased from 80.7% (303 K) to 93.8% (313 K) and it was stabilized to 91.9% (343 K). In 1 M HCl medium, BFLS affords an IE(%) of 85.2% (303 K), 91.0 % (313 K) and stabilized to 89.3% (343 K). Efficient inhibitive actions were afforded by BFLS extract and it confirmed the stability and strength of adsorbed insoluble film on mild steel surface. **(Ita and Offiong, 2001; Ehteram A. Noor, 2007)**.

4.2.3.6 Role of temperature on MS in the presence of BFP extract in 0.5 M H_2SO_4 and 1M HCl

The influence of temperature on percentage inhibition efficiency was studied by conducting mass loss measurements at 303 - 343 K containing different concentration of BFP (Table-22).

Table - 22 Influence of temperature on the inhibition efficiency of BFP extract on MS corrosion in 0.5 M H_2SO_4 and 1 M HCl medium

Conc. (%v/v)	303 K		313 K		323 K		333 K		343 K	
	CR (mpy)	IE (%)	CR (mpy)	IE (%)	CR (mpy)	IE (%)	CR (mpy)	IE (%)	CR (mpy)	IE (%)
0.5 M H_2SO_4										
Blank	1234	-	3417	-	7114	-	12222	-	19046	-
0.5	424	65.6	787	76.9	1478	79.2	2361	80.6	5654	70.3
1.0	288	76.6	574	83.1	1070	84.9	1681	86.2	2887	84.8
1.5	278	77.4	400	88.2	755	89.3	1211	90.0	2039	89.2
2.0	237	80.7	326	91.1	629	91.1	997	91.8	1725	90.9
2.5	202	83.5	303	90.4	562	92.0	795	93.4	1342	92.9
3.0	175	85.7	288	91.5	432	93.9	705	**94.2**	1211	**93.6**
3.5	175	85.7	288	91.5	432	93.9	705	**94.2**	1211	**93.6**
4.0	175	85.7	288	91.5	432	93.9	705	**94.2**	1211	**93.6**
1 M HCl										
Blank	1060	-	2349	-	4307	-	10061	-	17245	-
0.5	368	65.2	746	68.2	1073	75.0	2389	76.2	4982	71.1
1.0	333	68.5	630	73.1	884	79.4	1724	82.8	3331	80.6
1.5	275	73.9	546	76.7	684	84.1	1118	88.8	1940	88.7
2.0	204	80.6	509	78.3	600	86.0	1002	90.0	1724	90.0
2.5	187	82.3	502	78.6	450	89.5	899	91.0	1655	90.4
3.0	155	85.3	412	**82.4**	407	90.5	751	**92.5**	1362	**92.1**
3.5	155	85.3	412	**82.4**	407	90.5	751	**92.5**	1362	**92.1**
4.0	155	85.3	412	**82.4**	407	90.5	751	**92.5**	1362	**92.1**

Figure 33 (a and b) shows the variation of percentage inhibition efficiency with temperature. It is clear from the figure that IE(%) at 4.0%v/v concentration of BFP in 0.5 M H_2SO_4 bath increased from 85.7% (303 K) to 94.2% with increase in temperature upto 333 K after 333 K, IE has been found to be stabilized at 343 K, affording a maximum of 93.6% at 343 K. and the IE at 4.0%v/v concentration of BFP in 1 M HCl bath decreased from 85.3% to 82.4% with increase in temperature upto 313 K after 313 K, IE has been found to be stabilized at 343 K, affording a maximum

of 92.5% at 333 K. In both examined media, a maximum inhibition efficiencies of 94% in 0.5 M H_2SO_4 and 92% in 1 M HCl were furnished.

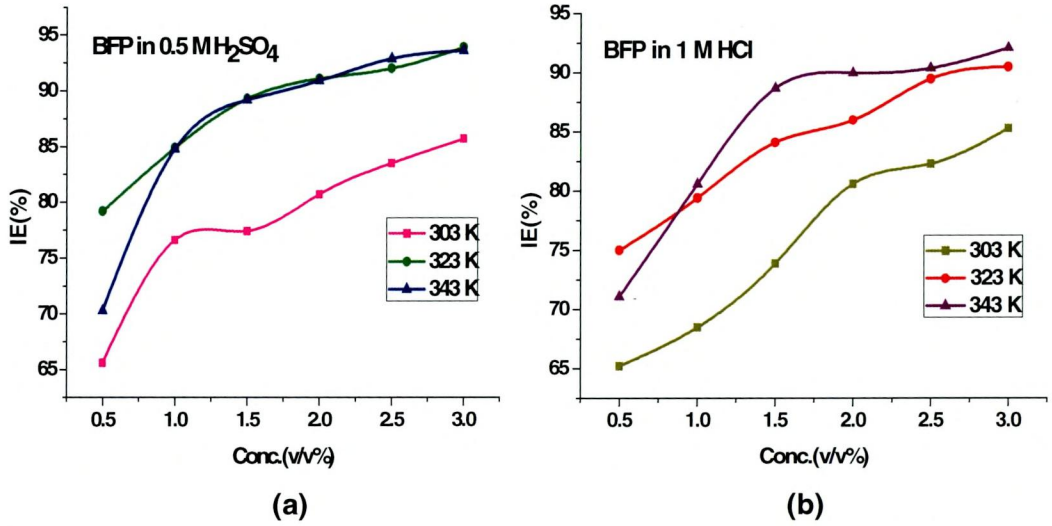

(a) (b)

Figure - 33 Effect of temperature on IE of the BFP extracts in (a) 0.5 M H_2SO_4 and (b) 1 M HCl at various concentrations

Effect of temperature of CN extracts on inhibition efficiency in 0.5 M H_2SO_4 and 1 M HCl

Figure-34 shows the variation of inhibition efficiency versus 4.0%v/v concentration of different parts of CN extracts at 303 – 343 K in 0.5 M H_2SO_4 and 1 M HCl obtained from mass loss measurements. The significant difference between the values of percentage inhibition efficiency of CN obtained at 303 – 343 K suggests that the mechanism of adsorption of the inhibitor on the MS steel surface might be due to physical adsorption at low temperature and at higher temperature, chemical adsorption predominates.

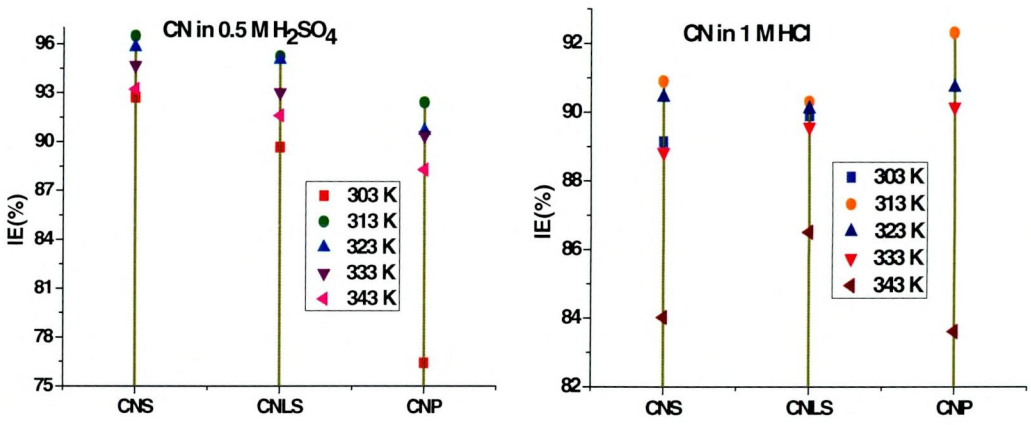

(a) (b)

Figure - 34 Graph representing the effect of temperature on MS corrosion in (a) 0.5 M H_2SO_4 and (b) 1 M HCl in the presence of CN extracts

For a physical adsorption mechanism, inhibition efficiency of an inhibitor decreases with temperature while for a chemical adsorption mechanism, values of inhibition

efficiency increase with temperature **(Ebenso *et al.*, 2004)**. Pictorial representation of IE(%)of CN extracts in 0.5 M H_2SO_4 and 1 M HCl on mild steel corrosion at different temperatures in Figure-34.

Effect of temperature of BF extracts on inhibition efficiency in 0.5 M H_2SO_4 and 1 M HCl

Figure-35 shows the plot of inhibition efficiency as a function of concentration (4.0%v/v) for shell, leaf stalk and peduncle of BF extracts in 0.5 M H_2SO_4 and 1 M HCl. The percentage inhibition efficiency of the BF extracts increased and decreased with increasing temperature, which might be attributed to a possible shift of the adsorption-desorption equilibrium toward desorption of the adsorbed inhibitor due to increase thermal agitation.

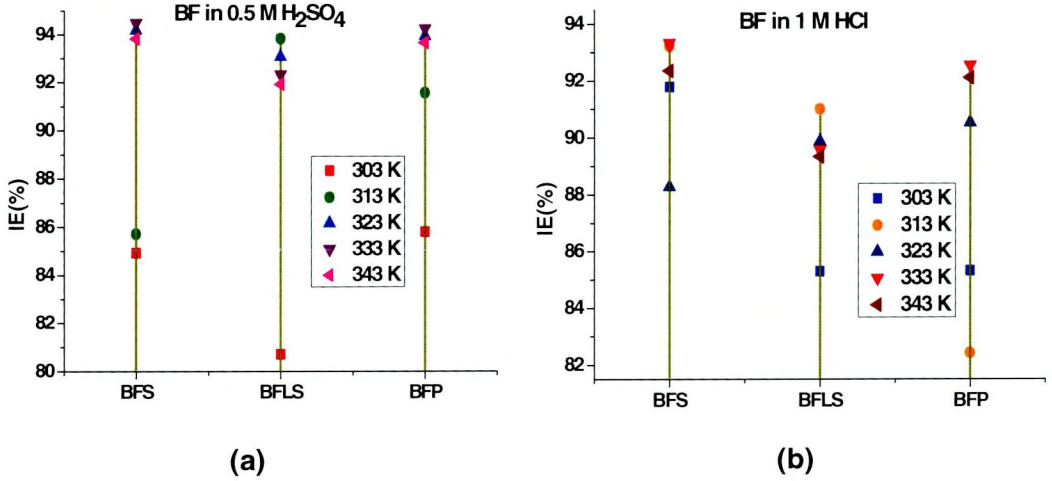

Figure - 35 Graph representing the effect of temperature on mild steel corrosion in (a) 0.5 M H_2SO_4 and (b) 1 M HCl in the presence of BF extracts

Also from Figure-35, percentage inhibition efficiencies were found to decrease with increase in experimental temperature. This is an indication that at higher temperatures there might be a desorption of BF extracts from the mild steel surface. According to **Obot *et al.*, (2009)** and confirmed by **Umoren et al., (2008)** in percentage inhibition efficiency with increase in temperature is an indication that the adsorption of BF extracts on MS is physical adsorption takes place at low temperature and at higher temperatures, chemical adsorption predominates.

Maximum percentage inhibition efficiency of the studied CN and BF extracts were found to be around 92% at all tested temperatures. This enhancement in IE(%) might be due to the stability of the adsorbed layer on MS surface at higher temperatures. It is clear that the percentage inhibition efficiencies in presence of CN and BF extracts increase with increasing the concentration of extract up to 4.0%v/v. Above that level, increasing the concentration from 3.0%v/v to 4.0%v/v has a little or on effect on the inhibition efficiency of MS corrosion by CN and BF extracts. This

behaviour could be attributed to the synergistic effect of the major chemical constituents of CN and BF extract (Figure-34 and 35) leading to cover anodic and cathodic sites through their oxygen functional group (OH).

Figures (34 and 35) illustrate the variation of percentage inhibition efficiency with concentration for the studied extracts. Inspection of the plots suggested that the inhibition processes were heterogeneous and involved several steps. The plots indicated that an increase or decrease in the inhibitor efficiency depending on its concentration were detected with increasing temperature indicating that adsorption of inhibitor species on mild steel surface at these conditions was not merely physical or chemical adsorption but they obeyed a mixed type adsorption (physical and chemical adsorption).

Physical (electrostatic) adsorption takes place when inhibition efficiency decreases with increase in temperature (whereas chemical adsorption takes place when inhibition efficiency increases with increase in temperature **(Umoren *et al.*, 2006)**. The inhibitive action of the extracts was due mainly to the presence of phytochemicals present in the palm tree extracts. These compounds contain heteroatoms such as oxygen, nitrogen and aromatic rings with π-bonds in their molecules, which serve as centers of adsorption onto the metal surface. Owing to the complex chemical composition of palm tree extract, the presence of other phytochemical components of the extracts may not be ruled out in the adsorption process. The corrosion inhibition efficiency trend in different acid media was in the decreasing order 0.5 M H_2SO_4 > 1 M HCl. The slightly higher IE (%) in H_2SO_4 than HCl may be due to the availability of more sites on the metal surface in H_2SO_4 solution because of the lesser adsorption of the sulphate ion on the MS surface **(Bentiss *et al.*, 2006)**.

Table-(17-22) illustrate the variation of IE (%) with shell, leaf stalk and peduncle of CN and BF concentration at different temperatures in 0.5 M H_2SO_4 than 1 M HCl. The obtained data's reveal that in 0.5 M H_2SO_4 and 1 M HCl, the percentage inhibition efficiency increased with an increase in the inhibitor concentration. This suggests that the inhibitor species are adsorbed on the mild steel/solution interface where the adsorbed species mechanically screen the coated part of the metal surface from the action of the corrosive medium.

As observed from Tables (17-22), the effect of temperature on the inhibition efficiency of the studied inhibitor at all concentrations and temperatures shows that for BFS, BFLS and BFP, the data suggested in both 0.5 M H_2SO_4 and 1 M HCl solutions, an increase or decrease in the inhibitor efficiency depending on its concentration was detected with increasing temperature, between 303 and 343K

indicating that adsorption of inhibitor species on mild steel surface at these conditions is not merely physical or chemical adsorption but obeying a mixed adsorption (physical and chemical adsorption) **(Oguzie, 2005)**.

The effect of temperature on the inhibited acid-metal reaction is highly complex, because many changes occur on the metal surface such as rapid etching and desorption of inhibitor and the inhibitor itself may undergo decomposition and/or rearrangement. However, it was found that few inhibitors with acid-metal systems have specific reactions which are effective at high temperature as (or more) they are at low temperature **(Oguzie *et al.*, 2004)**. Analysis of the results of temperature studies indicate that physical adsorption takes place at low temperature and at higher temperatures, chemical adsorption predominates.

Shelf life performance of CN and BF extracts at room temperature and in refrigerated condition

For industrial purpose the extracts can be prepared in large scale and can be stored for a period of 6 months. This process may help to minimize the labour of the workers. Bearing this in mind efforts have been taken to prepare the extracts in large scale and portion of it is kept in the refrigerator condition and rest of the portion is kept at room temperature. Mass loss method is best suited method to analyze the inhibitive action of these extracts. Experiments were conducted by selecting an optimum concentration, in the present case 4.0%v/v concentration of CN and BF extracts by mass loss measurements for a period of 3 h immersion using the extracts kept at refrigerated. Simultaneously the extracts kept at room temperature were also tested for 3 h immersion by the same method. Results pertaining to these studies present in Table-(23 a and b) and pictorially represented in graphs (Figure 36). Analysis of data reveals that in IE(%) was found to be the maximum in both cases. The extracts can be stored in the fridge otherwise the extracts may be prepared freshly that can be stored at room temperature for the industrial purpose. This test conducted to confirm the long lasting capacity of the investigated inhibitors. Results obtained also inferred the strong inhibitive action of the inhibitors kept at room temperature for the 6 months as well as in the refrigerator for the same period. It is upto the interest of industrialist to utilize the inhibitors at room temperature or refrigerated condition.

During storage the extract showed resistant towards fungal and bacterial attack **(El-Etre, *et al.*, 2005)**. There was no unpleasant odour or evolution of gas during storage. The strongly polar phenol group induces the antioxidant characteristics as reflected by very little change of viscosity after six months when

stored in room temperature **(Das, *et al.*, 2004).** Thus these extracts have been proved as good performers for 6 months. Thus they have appreciable shelf life.

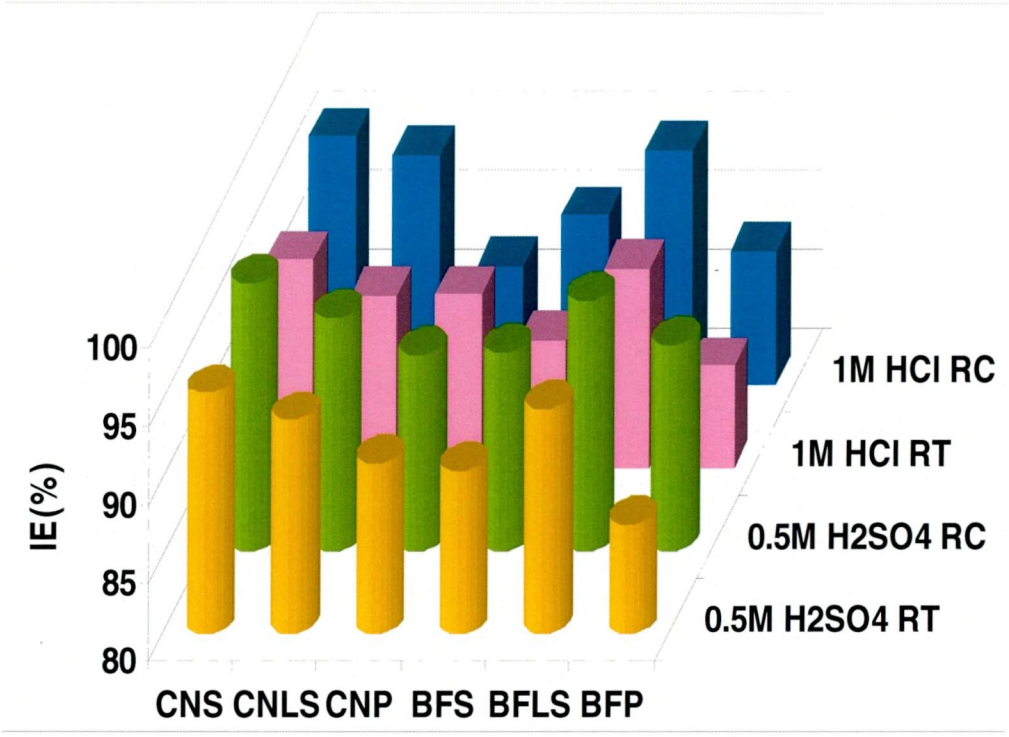

RC - Refrigerated Conditions.
RT - Room Temperature.

Figure-36 Strength of the inhibitive action at 6th month of CN and BF extracts in 3 h immersion period in 0.5 M H_2SO_4 and 1 M HCl at RC and at RT

Table – 23.a Strength of the inhibitive action of 4.0%v/v concentration of CN extracts in 3 h immersion period in 0.5 M H_2SO_4 and 1 M HCl at room temperature and at refrigerator condition

Time of immersion (in month)	Inhibition efficiency (%)											
	CNS				CNLS				CNP			
	Room		Refrigerator		Room		Refrigerator		Room		Refrigerator	
	0.5 M H_2SO_4	1 M HCl	0.5 M H_2SO_4	1 M HCl	0.5 M H_2SO_4	1 M HCl	0.5 M H_2SO_4	1 M HCl	0.5 M H_2SO_4	1 M HCl	0.5 M H_2SO_4	1 M HCl
1	96.9	95.1	97.7	96.4	94.6	93.9	95.6	95.0	92.7	87.6	93.1	88.2
2	96.3	94.7	97.8	96.3	94.5	92.7	95.4	94.9	92.5	87.4	93.0	88.0
3	95.6	94.1	97.6	96.1	94.3	92.5	95.3	94.9	92.2	87.0	92.9	87.9
4	95.4	93.9	97.4	96.0	94.5	92.3	95.1	94.7	91.9	86.8	92.7	87.7
5	95.4	93.4	97.4	95.9	94.7	91.8	94.9	94.5	91.5	86.3	92.5	87.7
6	95.4	93.2	97.0	95.7	93.7	90.9	94.9	94.5	91.0	86.3	92.5	87.5

Table – 23.b Strength of the inhibitive action of 4.0%v/v concentration of BF extracts in 3 h immersion period in 0.5 M H_2SO_4 and 1 M HCl at room temperature and at refrigerator condition

Time of immersion (in month)	Inhibition efficiency (%)											
	BFS				BFLS				BFP			
	Room		Refrigerator		Room		Refrigerator		Room		Refrigerator	
	0.5 M H_2SO_4	1 M HCl	0.5 M H_2SO_4	1 M HCl	0.5 M H_2SO_4	1 M HCl	0.5 M H_2SO_4	1 M HCl	0.5 M H_2SO_4	1 M HCl	0.5 M H_2SO_4	1 M HCl
1	92.3	90.5	93.3	91.3	96.4	94.1	96.5	95.3	89.4	88.6	93.5	89.1
2	91.8	90.3	93.2	91.2	96.0	93.8	96.4	95.2	89.2	88.3	93.4	89.0
3	91.6	89.8	93.0	91.0	95.8	93.6	96.3	95.1	88.8	88.0	93.4	88.8
4	91.3	89.4	92.9	90.9	95.6	93.2	96.3	95.1	88.5	87.8	93.3	88.8
5	91.0	88.7	92.7	90.9	95.2	92.8	96.1	94.9	87.9	87.6	93.2	88.6
6	90.5	88.1	92.7	90.7	94.4	92.7	96.0	94.8	87.0	86.5	93.1	88.4

4.3 ADSORPTION PHENOMENA

4.3.1 Structure and Properties of Surface Layers

Macroscopically, the region of contact between an electrode and an electrolyte is a two-dimensional surface (an interface) separating the two phases. Microscopically, the same region is structured in a complex way. When two condensed phases are brought in contact, the surface-layer properties of each phase will change under the effect of the other phase. Close to the boundary in both phases, surface layers of a certain thickness develop which differ from the principal phases in their properties. In a surface layer, particles are surrounded by other particles in an asymmetric fashion, and the forces acting on them do not balance. This gives rise to concentration changes relative to the values found in the bulk phase; it also leads to changes in the energy state of the individual particles and of the layer as a whole. The set of two surface layers existing at the junction of two condensed phases is called the *interphase* (in contrast to the macroscopic interface) **(Bagotsky, 2006)**.

The interphase between an electrode and an electrolyte solution has a very complex electrical structure. In this interphase various adsorption processes take place:

1. ***Adsorption of ions from the solution***. There are two types of ionic adsorption from solutions onto electrode surfaces:
   - ✶ **Physisorption,** involves electrostatic forces between ionic charges or dipoles on the adsorbed species and the electric charge at the metal/solution interface. The heat of adsorption is low and therefore this type of adsorption is stable only at relatively low temperatures.
   - ✶ **Chemisorption,** involves charge sharing or charge transfer from the inhibitor molecules to the metal surface to form a coordinate type bond. In fact, electron transfer is typically for transition metals having vacant low-energy electron orbital. Chemisorption is typified by much stronger adsorption energy than physical adsorption. Such a bond is therefore more stable at higher temperatures.

   Specifically adsorbing ions are called *surface active*. Specific adsorption is more pronounced with anions.

2. ***Solvent adsorption.*** The adsorption of solvent molecules is manifested in their orientation and ordered arrangement at the interface.

3. ***Adsorption of other components of the system***. This includes components taking part in the electrode reaction as well as "inert" components not taking part.

Both the electrical structure of the interphase and the occurrence of adsorption processes have a great influence on electrochemical reactions on an electrode's surface and on various electrochemical phenomena.

4.3.2 Types of Adsorption

The amount of species of the adsorbed substance *j* (adsorbate) per unit area of the true surface area of the electrode or of any other adsorbent will be labeled A_j and will be called *real adsorption*. In the limiting case, all adsorbed particles are packed right again the adsorbent's surface. This limiting case is called *monolayer adsorption*. In other cases, several layers of the adsorbate can form on the adsorbent's surface (*multilayer adsorption*)

When the component *j* can exist in both phases (e.g., the electrolyte and the electrode) it will undergo redistribution after the phases have come into contact, and in particular, some of it will be transferred into the interior of the phase, where none of it had existed previously. In this case the term *absorption* (or bulk uptake) is used for the component.

When the two phases in contact are condensed phases and the entire volume is taken up by incompressible substances, positive adsorption of one component must be attended by negative adsorption (desorption) of other components. This phenomenon is called *adsorptive displacement*. **(Bagotsky, 2006).**

$$\text{Adsorbate} + \text{Adsorbent} \underset{\text{desorption}}{\overset{\text{Adsorption}}{\rightleftharpoons}} \text{Adsorption} \qquad (4.1)$$

In the case of monolayer adsorption, a limiting adsorption value exists that is attained when the surface is covered completely by particles of a given substance (i.e., at full monolayer coverage). The limiting adsorption value A°_j depends on the effective surface area S_j taken up by one particle: $1/S$. This parameter characterizes the number of sites that can be occupied by adsorbed particles on a given surface.

A convenient parameter for quantitative estimates of adsorption which is of the monolayer type is the degree of surface coverage defined by the relation

$$\theta \equiv \frac{A_j}{A^{o}_{\ j}} \quad (1 \geq \theta \geq 0) \qquad (4.2)$$

In any particular case, the adsorption value depends on the properties of both the adsorbate (its *adsorbability*) and the adsorbent (its *adsorptive power*). Substances with enhanced adsorbability are called *surface active*. By convention, adsorption is regarded as insignificant when $\theta < 0.1$, and as significant when $\theta > 0.5$.

4.3.3 Adsorption Isotherm

Adsorption isotherms provide information about the interaction among the adsorbed molecules themselves and also their interactions with the electrode surface. It is well known that the effect of temperature on the inhibited acid–metal reaction is highly complex, because many changes occur on the metal surface such as rapid etching and desorption of inhibitor and the inhibitor itself may undergo decomposition and/or rearrangement. It was found that few inhibitors with acid–metal systems have specific reactions which are effective at high temperature as (or more) they are at low temperature **(Ehteram A. Noor and Aisha H. Al-Moubaraki, 2008).**

Recently, plant extract have been investigated and found to have potential as corrosion inhibitors for various metals and alloys in acid media. These substances generally become effective by adsorption on metal surfaces. The adsorption species help to protect metals from aggressive medium which causes decomposition of the metal. **Behpour *et al.*, (2009)** also stated that the adsorption may depend not only on the nature and charge of the metal but also on the chemical structure of the inhibitor. Inhibitors naturally react physically or chemically with metals by adsorbing on its surface. The adsorption may form a layer on the metal and function as a barrier protecting the metal.

The adsorption phenomenon could take place via:

- Electrostatic attraction between the charged metal and charged inhibitors molecules.
- Dipole type interaction between unshared electron pairs in the inhibitor with the metal.
- electron interaction with the metal.
- Combination of all of the above **(Abdel-Gaber *et al.*, 2006b)**.

They also suggest that the inhibiting action occurred by simple blocking of the available cathodic sites on the metal surface, which lead to a decrease in the exposed area necessary for hydrogen evolution and lowered the dissolution rate with increasing inhibitor concentration. It is well recognized that the fist primary step in the action of inhibitors in acid solutions is generally agreed to be adsorption on to the metal surface, which is usually oxide free in acid solutions. In most inhibition studies, the formation of donor-acceptor surface complexes between π-electrons of inhibitor and the vacant d-orbital of metal was postulated **(Muralidharan, *et al.*, 1995)**.

Furthermore, the adsorption depends on the molecule's chemical composition, the temperature and the electrochemical potential at the metal/solution interface. So the adsorption of organic inhibitor molecules from the aqueous solution

can be regarded as a quasi-substitution process between the organic compounds in the aqueous phase [$Org_{(sol)}$] and water molecules at the electrode surface [$H_2O_{(ads)}$]

$$Org_{(sol)} + x\ H_2O_{(ads)} \leftrightarrow Org_{(ads)} + x\ H_2O_{(sol)} \quad (4.3)$$

where x is the size ratio, that is, the number of water molecules replaced by one organic inhibitor. Basic information on the interaction between the inhibitor of the mild steel surface can be provided by the adsorption isotherm.

The adsorption isotherms are used to investigate the mode of adsorption and the characteristic of adsorption of inhibitor on the metal surface and provide useful insights into the mechanism of corrosion inhibition. The surface coverage, θ, was calculated according to the following equation:

$$\theta = \frac{W_{Corr} - W_{Corr(inh)}}{W_{Corr}} \quad (4.4)$$

Surface coverage values (θ) for the inhibitor were obtained from the mass loss measurements for various concentrations at different temperatures (303–343 K). It is necessary to determine empirically which adsorption isotherm fits best to the surface coverage data in order to use the corrosion rate measurements to calculate the thermodynamic parameters pertaining to inhibitor adsorption. Adsorption isotherms are very important in understanding the mechanism of inhibition of corrosion reactions.

In this section of study, the changes in the surface coverage and thereby the change in the inhibition efficiency is measured using different models at the same level of temperature. These models include Langmuir, El-Awady kinetic thermodynamic, Temkin, Freundlich, Frumkin and Flory-Huggins adsorption isotherms.

Langmuir adsorption isotherm can be obtained according to equation (4.5) **(Eddy Nnabuk *et al.*, 2010)**.

$$\log (C/\theta) = \log C - \log K \quad (4.5)$$

where K is the equilibrium constant, C is the concentration of inhibitor and θ is the degree of surface coverage of the inhibitors. The plots of Langmuir adsorption isotherm is log (C/θ) Vs log C.

El-Awady kinetic thermodynamic adsorption isotherm can be described according to equation (4.6) **(Uwah *et al.*, 2010)**.

$$\log (\theta / 1- \theta) = \log K' + y \log C \quad (4.6)$$

where C is the concentration of the adsorbate θ is the degree of surface coverage and 1/y is the number of inhibitor molecules occupying one active sites. The plots of El Awady kinetic thermodynamic adsorption isotherm is log (θ/1- θ) Vs log C.

Temkin adsorption isotherm can be represented according to equation (4.7) **(Umoren *et al.*, 2007a)**.

$$\exp(-2a\theta) = KC \qquad (4.7)$$

where 'a' is molecular interaction parameters, θ is the degree of surface coverage, K is the equilibrium constant of adsorption process and C is the concentration of the inhibitors. The plots of Temkin adsorption isotherm is θ Vs ln C.

Freundlich adsorption isotherm can be written according to equation (4.8) **(Umoren *et al.*, 2007b)**.

$$\theta = K C^{1/n} \qquad (4.8)$$

where n is the adsorption intensity, C is the inhibitors concentration and K is the equilibrium constant of adsorption reaction. The plots of Freundlich adsorption isotherm is ln θ Vs ln C.

Frumkin adsorption isotherm can be deduced according to equation (4.9) **(Oguzie *et al.*, 2004)**.

$$\ln\frac{f(\theta,x)}{C} = \ln K + 2a\theta \qquad (4.9)$$

where 'a' is the lateral interaction term describing the molecular interaction in the adsorbed layer, θ is the degree of surface coverage, K is the equilibrium constant of adsorption process and C is the concentration of inhibitors. The plots of Frumkin adsorption isotherm is θ Vs log C

Flory-Huggins adsorption isotherm can be explained according to equation (4.10) **(Umoren *et al.*, 2007b)**.

$$\log(\theta/C) = \log K + x \log(1-\theta) \qquad (4.10)$$

where θ is the degree of surface coverage, C is the concentration of the system studied x is the number of water molecule replaced by one inhibitor molecule and K is the equilibrium constant for the adsorption process. The plot of Flory-Huggins adsorption isotherm is log (θ/C) Vs log (1-θ).

The model used takes the following form ln$y = \alpha + \beta x$, where 'y' is the surface coverage, α is the intercept, β is the slope and 'x' is the concentration. The same model has applied for the six adsorption isotherms to identify the most suitable model for the problem understudy using **Statistical Software Package SPSS 12.**

Goodness of Fit

Data were tested graphically by fitting to various isotherms. Statistical estimation of correlation for the curve fitting of isotherms have been used to investigate the goodness of fit of the isotherms. After estimating the regression line we need to know how good the fit of the line is to the sample observation of Y and X,

that is to say we need to measure the dispersion of observations around the regression line **(Schulthess and Dey, 1996)**. This knowledge is essential, because the closer the observations to the line, better the goodness of fit, that is the better is the explanation of the variations of Y by the changes in the explanatory variables. A measure of the goodness of fit is the square of correlation coefficient. R^2 which shows the % of the total variation of the dependent variables that can be explained by the independent variable X. Symbolically

$$R^2 = \frac{\sum Y_1^{\,2}}{\sum Y_1} = \frac{\exp lained\ \mathrm{var} iation}{Total\ \mathrm{var} iation} \qquad (4.11)$$

The value of R^2 generally lies between 0 and 1 ($0 \leq R^2 \leq 1$). The closer the value of R^2 lines to 1, the better is the regression line to data and vice versa. To test the overall significance of regression model, the technology of ANOVA is used, which is defined by the F value.

$$F = \frac{\exp lainedsumofsquare / \deg reesoffreedom}{\mathrm{Re} sidualsumofsquares / \deg reesoffreedom} \qquad (4.12)$$

A large F value will be evidenced against the null hypothesis the explanatory variable have no effect of Y. To investigate whether, the CN and BF extracts in 0.5 M H_2SO_4 and 1 M HCl are statistically significant, usually; F-tests are carried out **(Benita Sherine *et al.*, 2010)**. The result of these are given in Table-(24-29) . In table the influence on the percentage inhibition efficiencies of 0.5, 1, 1.5, 2.0, 2.5, 3.0, 3.5 and 4.0%v/v of CN and BF extracts in 0.5 M H_2SO_4 and 1 M HCl are investigated. Now F is a test statistic that is used in ANOVA. The Mean Squares are given by the Sums of Squares [SS] divided by the DF. The Sum of Squares is main concept of regression which is also called ordinary least squares regression. These are the squares that make the SS. The SS is short for Sums of Squared deviation from the regression. The first Sum of Squares is the total Sum of Squares. These are calculated by finding the residual difference between each value and the mean, squaring it, and then adding them up. The mean is like a regression equation with no predictor variable. To determine a value of the mean, the calculation can be performed as illustrated in Table (24-29). The obtained F-value for both acids in Langmuir, El-Awady kinetic thermodynamic, Temkin, Freundlich, Frumkin and Flory Huggins isotherm is statistically significant, since, it is greater than the critical F value 2.7587 for 4, 25 degree of freedom at 0.05 level of significance. Therefore it is concluded that the influence of inhibition efficiencies of various concentrations of CN and BF extracts in 0.5 M H_2SO_4 and 1 M HCl medium are statistically significant in these isotherm.

Table - 24 Adsorption parameters deduced from various adsorption isotherms - CNS in 0.5 M H_2SO_4 and 1 M HCl on MS corrosion

Adsorption Isotherm Model	Source of variation	0.5 M H_2SO_4					1 M HCl				
		Sum of Squares	df	Mean Square	F	Sig.	Sum of Squares	df	Mean Square	F	Sig.
Langmuir	Between	0.002	4	0.001	0.009	1.000 (p>0.05)	0.019	4	0.005	0.081	0.987 (p>0.05)
	Within	1.727	25	0.069			1.453	25	0.058		
	Total	1.729	29				1.472	29			
El-Awady kinetic Thermodynamic	Between	0.309	4	0.077	1.358	0.277 (p>0.05)	0.406	4	0.102	2.014	0.123 (p>0.05)
	Within	1.421	25	0.057			1.261	25	0.050		
	Total	1.730	29				1.667	29			
Temkin	Between	0.010	4	0.002	0.938	0.458 (p>0.05)	0.056	4	0.014	1.936	0.136 (p>0.05)
	Within	0.066	25	0.003			0.181	25	0.007		
	Total	0.076	29				0.237	29			
Freundlich	Between	0.002	4	0.001	0.903	0.477 (p>0.05)	0.019	4	0.005	1.902	0.141 (p>0.05)
	Within	0.016	25	0.001			0.062	25	0.002		
	Total	0.019	29				0.081	29			
Frumkin	Between	1.637	4	0.409	**20.001**	**(0.000)* (p<0.05)**	2.153	4	0.538	**18.954**	**(0.000)* (p<0.05)**
	Within	0.512	25	0.020			0.710	25	0.028		
	Total	2.149	29				2.863	29			
Flory Huggins	Between	0.002	4	0.001	0.009	1.000 (p>0.05)	0.019	4	0.005	0.081	0.987 (p>0.05)
	Within	1.727	25	0.069			1.453	25	0.058		
	Total	1.729	29				1.472	29			

p-value of 0.000, indicate that the prediction model is highly significant. p-value below 0.05, are significant(0.000 < 0.05)
Figure within ( ) give F ratio, * indicates 5% level of significance and df indicates degree of freedom.

Table - 25 Adsorption parameters deduced from various adsorption isotherms - CNLS in 0.5 M H_2SO_4 and 1 M HCl on MS corrosion

Adsorption Isotherm Model	Source of variation	0.5 M H_2SO_4					1 M HCl				
		Sum of Squares	df	Mean Square	F	Sig	Sum of Squares	df	Mean Square	F	Sig
Langmuir	Between	0.009	4	0.002	0.036	0.997	0.021	4	0.005	0.095	0.983
	Within	1.555	25	0.062			1.373	25	0.055		
	Total	1.564	29				1.394	29			
El-Awady kinetic thermodynamic	Between	0.510	4	0.127	1.962	0.131	0.317	4	0.079	1.219	0.328
	Within	1.624	25	0.065			1.627	25	0.065		
	Total	2.134	29				1.945	29			
Temkin	Between	0.033	4	0.008	1.419	0.257	0.053	4	0.013	1.216	0.329
	Within	0.145	25	0.006			0.273	25	0.011		
	Total	0.178	29				0.326	29			
Freundlich	Between	0.009	4	0.002	1.336	0.284	0.021	4	0.005	1.212	0.331
	Within	0.042	25	0.002			0.108	25	0.004		
	Total	0.051	29				0.128	29			
Frumkin	Between	2.703	4	0.676	**52.257**	**(0.000)* (p<0.05)**	1.683	4	0.421	**9.288**	**(0.000)* (p<0.05)**
	Within	0.323	25	0.013			1.132	25	0.045		
	Total	3.026	29				2.815	29			
Flory Huggins	Between	0.009	4	0.002	0.036	0.997	0.021	4	0.005	0.095	0.983
	Within	1.555	25	0.062			1.373	25	0.055		
	Total	1.564	29				1.394	29			

p-value of 0.000, indicate that the prediction model is highly significant. p-value below 0.05, are significant(0.000 < 0.05)
Figure within ( ) give F ratio, * indicates 5% level of significance and df indicates degree of freedom.

Table - 26 Adsorption parameters deduced from various adsorption isotherms - CNP in 0.5 M H_2SO_4 and 1 M HCl on MS corrosion

Adsorption Isotherm Model	Source of variation	0.5 M H_2SO_4					1 M HCl				
		Sum of Squares	df	Mean Square	F	Sig	Sum of Squares	df	Mean Square	F	Sig
Langmuir	Between	0.056	4	0.014	0.225	0.922	0.100	4	0.025	0.417	0.795
	Within	1.571	25	0.063			1.495	25	0.060		
	Total	1.627	29				1.594	29			
El-Awady kinetic thermodynamic	Between	1.295	4	0.324	**8.992**	**(0.000)* (p<0.05)**	1.718	4	0.430	**11.803**	**(0.000)* (p<0.05)**
	Within	0.900	25	0.036			0.910	25	0.036		
	Total	2.196	29				2.628	29			
Temkin	Between	0.173	4	0.043	**8.867**	**(0.000)* (p<0.05)**	0.272	4	0.068	**10.572**	**(0.000)* (p<0.05)**
	Within	0.122	25	0.005			0.161	25	0.006		
	Total	0.294	29				0.433	29			
Freundlich	Between	0.056	4	0.014	**8.482**	**(0.000)* (p<0.05)**	0.100	4	0.025	**8.724**	**(0.000)* (p<0.05)**
	Within	0.042	25	0.002			0.071	25	0.003		
	Total	0.098	29				0.171	29			
Frumkin	Between	6.868	4	1.717	**25.939**	**(0.000)* (p<0.05)**	9.109	4	2.277	**31.473**	**(0.000)* (p<0.05)**
	Within	1.655	25	0.066			1.809	25	0.072		
	Total	8.523	29				10.918	29			
Flory Huggins	Between	0.056	4	0.014	0.225	0.922	0.100	4	0.025	0.417	0.795
	Within	1.571	25	0.063			1.495	25	0.060		
	Total	1.627	29				1.594	29			

p-value of 0.000, indicate that the prediction model is highly significant. p-value below 0.05, are significant(0.000 < 0.05)
Figure within ( ) give F ratio, * indicates 5% level of significance and df indicates degree of freedom.

Table - 27 Adsorption parameters deduced from various adsorption isotherms - BFS in 0.5 M H_2SO_4 and 1 M HCl on MS corrosion

Adsorption Isotherm Model	Source of variation	0.5 M H_2SO_4					1 M HCl				
		Sum of Squares	df	Mean Square	F	Sig.	Sum of Squares	df	Mean Square	F	Sig.
Langmuir	Between	0.022	4	0.005	0.083	0.987	0.003	4	0.001	0.011	1.000
	Within	1.629	25	0.065			1.708	25	0.068		
	Total	1.650	29				1.711	29			
El-Awady kinetic thermodynamic	Between	1.090	4	0.273	**5.266**	**(0.003)* (p<0.05)**	0.181	4	0.045	1.208	0.332
	Within	1.294	25	0.052			0.935	25	0.037		
	Total	2.384	29				1.116	29			
Temkin	Between	0.080	4	0.020	**4.506**	**(0.007)* (p<0.05)**	0.012	4	0.003	0.939	0.458
	Within	0.112	25	0.004			0.078	25	0.003		
	Total	0.192	29				0.090	29			
Freundlich	Between	0.022	4	0.005	**4.178**	**(0.010)* (p<0.05)**	0.003	4	0.001	0.892	0.483
	Within	0.032	25	0.001			0.022	25	0.001		
	Total	0.054	29				0.025	29			
Frumkin	Between	5.779	4	1.445	**21.153**	**(0.000)* (p<0.05)**	0.958	4	0.240	**3.552**	**(0.020)* (p<0.05)**
	Within	1.708	25	0.068			1.686	25	0.067		
	Total	7.487	29				2.644	29			
Flory Huggins	Between	0.022	4	0.005	0.083	0.987	0.003	4	0.001	0.011	1.000
	Within	1.629	25	0.065			1.708	25	0.068		
	Total	1.650	29				1.711	29			

p-value of 0.000, indicate that the prediction model is highly significant. p-value below 0.05, are significant(0.000 < 0.05)
Figure within ( ) give F ratio, * indicates 5% level of significance and df indicates degree of freedom.

Table - 28 Adsorption parameters deduced from various adsorption isotherms - BFLS in 0.5 M H_2SO_4 and 1 M HCl on MS corrosion

Adsorption Isotherm Model	Source of variation	0.5 M H_2SO_4					1 M HCl				
		Sum of Squares	df	Mean Square	F	Sig.	Sum of Squares	df	Mean Square	F	Sig.
Langmuir	Between	0.022	4	0.005	0.082	0.987	0.009	4	0.002	0.038	0.997
	Within	1.655	25	0.066			1.483	25	0.059		
	Total	1.677	29				1.492	29			
El-Awady kinetic thermodynamic	Between	0.793	4	0.198	**4.917**	**(0.005)* (p<0.05)**	0.214	4	0.054	1.074	0.390
	Within	1.008	25	0.040			1.247	25	0.050		
	Total	1.801	29				1.461	29			
Temkin	Between	0.076	4	0.019	**5.450**	**(0.003)* (p<0.05)**	0.028	4	0.007	0.984	0.434
	Within	0.087	25	0.003			0.176	25	0.007		
	Total	0.163	29				0.204	29			
Freundlich	Between	0.022	4	0.005	**5.477**	**(0.003)* (p<0.05)**	0.009	4	0.002	0.965	0.444
	Within	0.025	25	0.001			0.059	25	0.002		
	Total	0.046	29				0.68	29			
Frumkin	Between	4.206	4	1.051	**19.275**	**(0.000)* (p<0.05)**	1.136	4	0.284	**6.579**	**(0.001)* (p<0.05)**
	Within	1.364	25	0.055			1.079	25	0.043		
	Total	5.569	29				2.216	29			
Flory Huggins	Between	0.022	4	0.005	0.082	0.987	0.009	4	0.002	0.038	0.997
	Within	1.655	25	0.066			1.483	25	0.059		
	Total	1.677	29				1.492	29			

p-value of 0.000, indicate that the prediction model is highly significant. p-value below 0.05, are significant(0.000 < 0.05)
Figure within ( ) give F ratio, * indicates 5% level of significance and df indicates degree of freedom.

Table –29 Adsorption parameters deduced from various adsorption isotherms - BFP in 0.5 M H_2SO_4 and 1 M HCl on MS corrosion

Adsorption Isotherm Model	Source of variation	0.5 M H_2SO_4					1 M HCl				
		Sum of Squares	df	Mean Square	F	Sig	Sum of Squares	df	Mean Square	F	Sig
Langmuir	Between	0.013	4	0.003	0.051	0.995	0.019	4	0.005	0.075	0.989
	Within	1.620	25	0.065			1.591	25	0.064		
	Total	1.634	29				1.610	29			
El-Awady kinetic thermodynamic	Between	0.576	4	0.144	**2.795**	**(0.048)* (p<0.05)**	0.650	4	0.163	**3.977**	**(0.012)* (p<0.05)**
	Within	1.288	25	0.052			1.022	25	0.041		
	Total	1.865	29				1.673	29			
Temkin	Between	0.047	4	0.012	2.728	0.052	0.066	4	0.017	**3.604**	**(0.019)* (p<0.05)**
	Within	0.109	25	0.004			0.115	25	0.005		
	Total	0.156	29				0.181	29			
Freundlich	Between	0.013	4	0.003	2.667	0.056	0.019	4	0.005	**3.477**	**(0.022)* (p<0.05)**
	Within	0.031	25	0.001			0.034	25	0.001		
	Total	0.044	29				0.054	29			
Frumkin	Between	3.055	4	0.764	**21.501**	**(0.000)* (p<0.05)**	3.448	4	0.862	**12.639**	**(0.000)* (p<0.05)**
	Within	0.888	25	0.036			1.705	25	0.068		
	Total	3.943	29				5.153	29			
Flory Huggins	Between	0.013	4	0.003	0.051	0.995	0.019	4	0.005	0.075	0.989
	Within	1.620	25	0.065			1.591	25	0.064		
	Total	1.634	29				1.610	29			

p-value of 0.000, indicate that the prediction model is highly significant. p-value below 0.05, are significant(0.000 < 0.05)
Figure within ( ) give F ratio, * indicates 5% level of significance and df indicates degree of freedom.

4.3.4 Results of SPSS 12 package on adsorption behaviour of investigated inhibitors in acidic media

Values of adsorption parameters deduced from various adsorption isotherm and the estimated coefficients of studied inhibitors in 0.5 M H_2SO_4 and1M HCl are enlisted in Table-(24-29).

Analyzing the values of F, the table was arrived at and the adsorption models which were followed by studied inhibitors are presented. The highest values of F were highlighted in the Tables-30. The obeyed adsorption isotherms for the investigated inhibitors are further explained.

Table - 30 The results of Statistical SPSS 12 package on adsorption isotherms and the various adsorption models obeyed by the investigated inhibitors and their highest F values

Inhibitor	0.5 M H_2SO_4		1 M HCl	
	Models	Highest value of F	Models	Highest value of F
CNS	Frumkin	20.001	Frumkin	18.954
CNLS	Frumkin	52.257	Frumkin	9.288
CNP	El-Awady kinetic thermodynamic	8.992	El-Awady kinetic thermodynamic	11.803
	Frumkin	25.939	Frumkin	31.473
BFS	El-Awady kinetic thermodynamic	5.266	-	-
	Frumkin	21.253	Frumkin	3.552
BFLS	El-Awady kinetic thermodynamic	4.917	-	-
	Frumkin	19.275	Frumkin	6.579
BFP	El-Awady kinetic thermodynamic	2.795	El-Awady kinetic thermodynamic	3.977
	Frumkin	21.501	Frumkin	12.639

El-Awady kinetic thermodynamic Model for CN and BF extracts

The adsorption isotherm relationship of El-Awady kinetic thermodynamic model which is given by the following equation:

$$\log [\theta/(1-\theta)] = \log K' + y \log C. \qquad (4.13)$$

where θ is the degree of coverage, x is the number of active sites.

Surface coverage (θ) data are very useful while discussing adsorption characteristics. For an inhibitor to have a high surface coverage on the surface, a chemical bond between the inhibitor and the metal atom stronger than the one for water molecules should be formed. The adsorption therefore of corrosion inhibitors at the metal/solution interface may be due to the formation of either electrostatic or covalent bonding between the adsorbates and the metal surface atoms.

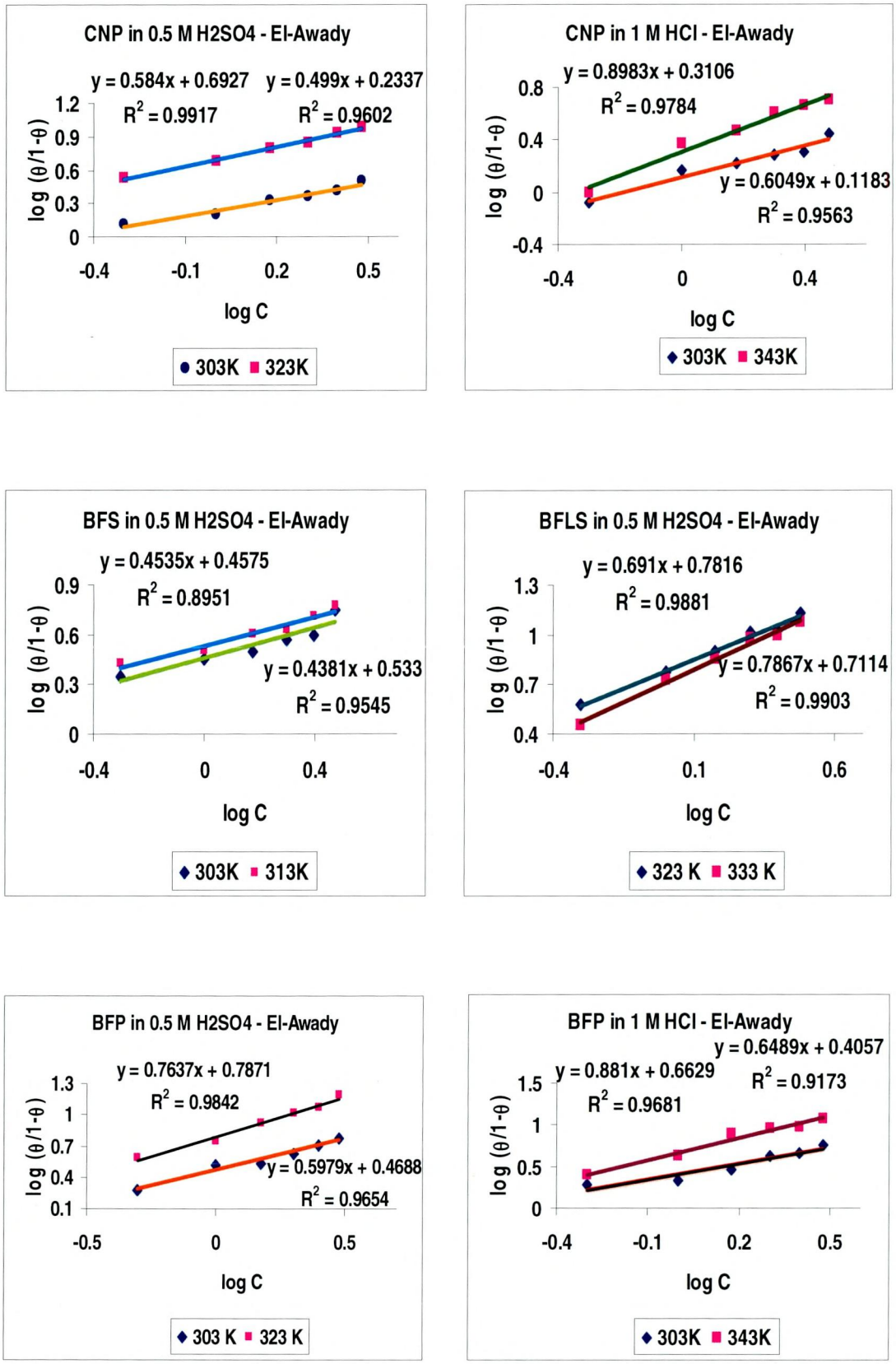

Figure - 37 El-Awady kinetic thermodynamic isotherm for adsorption of obeyed inhibitor on the MS surface in 0.5 M H_2SO_4 and 1 M HCl

'x' is the number of inhibitor molecules occupying one active site (or the number of water molecules replaced by one molecule (1/y = x). The calculated values of 'x' for all the obeyed inhibitors are given in Table-31. Inspection of the data shows that the values 'x' are less than one and are approximately equal to one mean that the studied inhibitor molecule will occupy more than one active site. Values indicate that the phytochemical constituents present in the obeyed inhibitor molecules occupy more than one active site (Figure-37).

Table – 31 Deduced adsorption parameters using El-Awady kinetic thermodynamic adsorption isotherm - CN and BF extract on the MS surface in 0.5 M H_2SO_4 and 1 M HCl

Inhibitor	Acid Medium	Temp. (K)	R^2	Slope	Intercept	y
CNP	0.5 M H_2SO_4	303	0.960	0.499	0.233	2.003
		323	0.991	0.583	0.692	1.712
	1 M HCl	303	0.956	0.604	0.118	1.653
		343	0.978	0.898	0.310	0.113
BFS	0.5 M H_2SO_4	303	0.895	0.453	0.457	2.204
		313	0.954	0.438	0.533	2.282
BFLS	0.5 M H_2SO_4	323	0.988	0.691	0.781	1.447
		333	0.990	0.786	0.711	1.274
BFP	0.5 M H_2SO_4	303	0.965	0.597	0.468	1.672
		323	0.984	0.763	0.787	1.309
	1 M HCl	303	0.917	0.648	0.405	1.540
		343	0.968	0.881	0.662	1.135

Frumkin Adsorption Model for CN and BF extracts

Adsorption behaviour of CN and BF extracts are best explained by Frumkin adsorption isotherms. The plots of θ (where θ = I/100) versus log C are depicted in Figure-38 and 39. for various concentrations of shell, leaf stalk and peduncle of CN and BF extracts, respectively at different temperature (303 K - 343 K) for 0.5 M H_2SO_4 and 1 M HCl respectively. The values of θ and C were taken from mass loss measurements. From these plots, it is found that the Frumkin's isotherm is the most suitable for the adsorption process of the investigated CN and BF extracts onto the MS. The relation between θ and log C gives S-shape curve. The Frumkin's isotherm can be expressed by the following equation:

$$\frac{\theta}{1-\theta} \exp(-f\theta) = KC \qquad (4.14)$$

where θ is the surface coverage, *K* is the equilibrium constant of the adsorption process, and C is the inhibitor concentration. The value of *K* indicates that CN and BF shell, leaf stalk and peduncle extracts is strongly adsorbed on the steel surface. Values of adsorption parameters deduced from various adsorption isotherm and the estimated coefficients of studied inhibitors in both acidic media are presented in Table-(32 a and b).

The variations of surface coverage with concentration of different plant extracts are shown in Figure-38 and 39. These curves have S-shaped **(Abdel-Gaber *et al.*, 2006a)** that are characterized by an initial steeply rising part indicating a formation of a mono-layer adsorbate film on the steel surface. At high concentration, the inhibitory effect remained constant suggesting complete saturation of the surface by the inhibitor molecules. The appearance of critical concentration after which the inhibitive effect of extract decreased is also observed. High surface coverage suggests that a chemical bond is formed between the metal atoms and the inhibitor.

Table – 32.a Deduced adsorption parameters using Frumkin adsorption isotherm for CN extract on the mild steel surface in 0.5 M H_2SO_4 and 1 M HCl

Inhibitor	Acid Medium	Temp. (K)	R^2	Slope	Intercept
CNS	0.5 M H_2SO_4	303	0.962	0.186	0.847
		343	0.970	0.197	0.849
	1 M HCl	303	0.981	0.244	0.785
		323	0.982	0.238	0.798
CNLS	0.5 M H_2SO_4	303	0.930	0.308	0.764
		343	0.970	0.297	0.791
	1 M HCl	303	0.938	0.247	0.777
		323	0.993	0.180	0.820
CNP	0.5 M H_2SO_4	303	0.972	0.253	0.628
		323	0.995	0.173	0.826
	1 M HCl	303	0.959	0.327	0.565
		343	0.948	0.424	0.659

Thus depending upon electron density on the functional atom of the organic inhibitor, the molecules may adsorb on the metal/solution interface by formation of either electrostatic or covalent bonds between the adsorbates and the metal surface atoms.

It is clear that the inhibition efficiency increase with increasing the concentration of extract which is proposed to be an insoluble complex adsorbed on mild steel surface, leading to more inhibition efficiency with increasing the

concentration of the extract under study, this complex lead to block most of the active centers on mild steel surface, thereby increasing the surface coverage.

Table – 32.b Deduced adsorption parameters using Frumkin adsorption isotherm for BF extracts on the MS surface in 0.5 M H_2SO_4 and 1 M HCl

Inhibitor	Acid Medium	Temp. (K)	R^2	Slope	Intercept
BFS	**0.5 M H_2SO_4**	303	0.940	0.184	0.738
		313	0.976	0.163	0.770
	1 M HCl	303	0.937	0.162	0.846
		323	0.959	0.161	0.816
BFLS	**0.5 M H_2SO_4**	323	0.982	0.176	0.850
		333	0.955	0.229	0.826
	1 M HCl	303	0.967	0.236	0.744
		333	0.962	0.315	0.762
BFP	**0.5 M H_2SO_4**	303	0.963	0.242	0.740
		323	0.990	0.188	0.851
	1 M HCl	303	0.940	0.271	0.712
		343	0.946	0.274	0.807

The plots of θ against log C are shown in Figure-38 and 39. The sigmoidal shape shows that the adsorption of the inhibitor on MS surface follows Frumkin isotherm. In Frumkin's adsorption isotherm, one adsorption molecules of CN and BF extracts displaces one of adsorption water. The slope of the lines given by equation

$$\ln \frac{f(\theta, x)}{C} = \ln K + 2a\theta \qquad (4.15)$$

The slope value for CN and BF at studied temperature in 0.5 M H_2SO_4 and 1 M HCl are positive (a>0), thus the electrostatic attraction between the adsorption molecules prevails. The plot of θ versus log C (Figure-38 and 39) straight lines were obtained with R^2> 0.9 for all the systems studied, indicating that the experimental data fit well into Frumkin adsorption isotherm.

Analyzing the results of SPSS 12 package on adsorption isotherms, from Table-30, it is understood that all the investigated CN and BF extracts in both acid media obey Frumkin and El-Awady kinetic thermodynamic models.

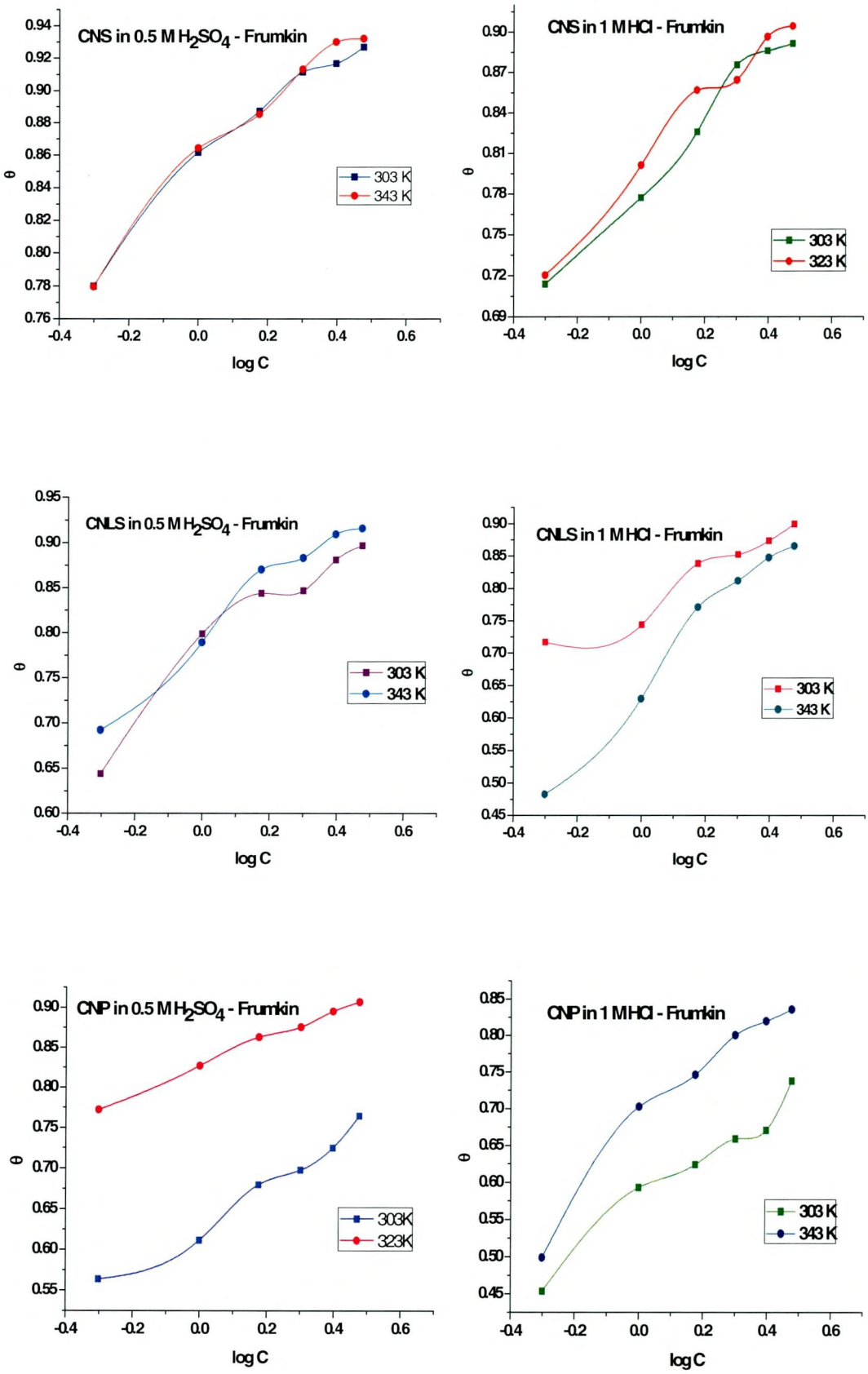

Figure - 38 Frumkin isotherm for adsorption of CN extracts on the MS surface in 0.5 M H_2SO_4 and 1 M HCl

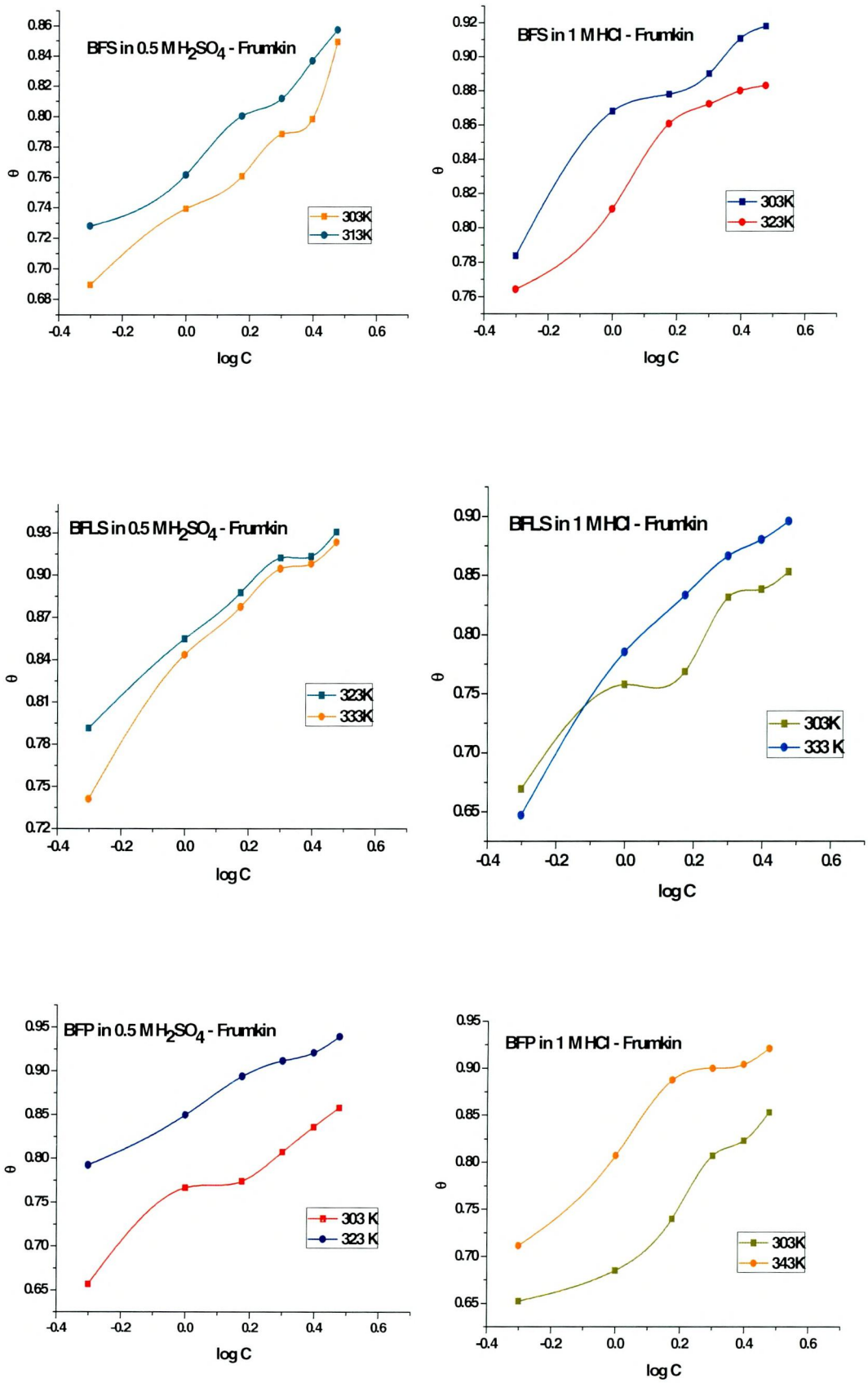

Figure-39 Frumkin isotherm for adsorption of BF extracts on the MS surface in 0.5 M H_2SO_4 and 1 M HCl

4.4 CORROSION KINETIC PARAMETERS:

The apparent activation for the corrosion process is calculated from Arrhenius type plot according to the following equation:

$$\log CR = k \exp(-E_a/RT) \quad (4.16)$$

where E_a is the apparent activation corrosion energy, *R* is the universal gas constant (R = 8.314 $Jmol^{-1}K^{-1}$), k is the Arrhenius pre-exponential constant and T is the absolute temperature.

Values of E_a for MS with the absence and presence of various concentrations of CN and BF extracts were determined from the slope of log CR Vs 1/T plots (Figure-40a and b) and presented in Tables – 33.a and b.

Table – 33(a and b) Activation energy for MS corrosion in 0.5 M H_2SO_4 and 1 M HCl in the absence and presence of different concentrations of CN/BF extracts

Table – 33.a

Inhibitor conc. (%v/v)	E_a (kJ/mol)					
	CNS		CNLS		CNP	
	0.5 M H_2SO_4	1 M HCl	0.5 M H_2SO_4	1 M HCl	0.5 M H_2SO_4	1 M HCl
Blank	58.55	60.74	58.55	60.74	58.55	60.74
0.5	60.28	72.14	58.59	76.56	59.33	61.52
1.0	60.99	68.42	63.75	67.91	53.95	56.73
1.5	59.94	71.25	57.78	67.09	52.11	54.71
2.0	60.55	73.80	57.76	65.54	49.07	53.15
2.5	58.44	70.66	56.79	64.85	48.68	51.71
3.0	60.38	68.85	57.69	65.99	47.96	53.88
Average	60.09	70.85	58.72	67.99	51.85	55.28

Table – 33.b

Inhibitor conc. (%v/v)	E_a (kJ/mol)					
	BFS		BFLS		BFP	
	0.5 M H_2SO_4	1 M HCl	0.5 M H_2SO_4	1 M HCl	0.5 M H_2SO_4	1 M HCl
Blank	58.55	60.74	58.55	60.74	58.55	60.74
0.5	56.01	65.61	56.60	68.84	54.07	54.83
1.0	45.27	63.39	51.75	66.12	49.15	48.27
1.5	36.42	60.11	48.56	59.72	43.83	39.84
2.0	33.28	57.65	46.00	61.20	43.73	42.70
2.5	30.41	59.35	47.01	57.32	40.94	42.58
3.0	34.66	59.46	44.74	56.20	41.00	42.63
Average	39.34	60.92	49.11	61.56	45.45	45.14

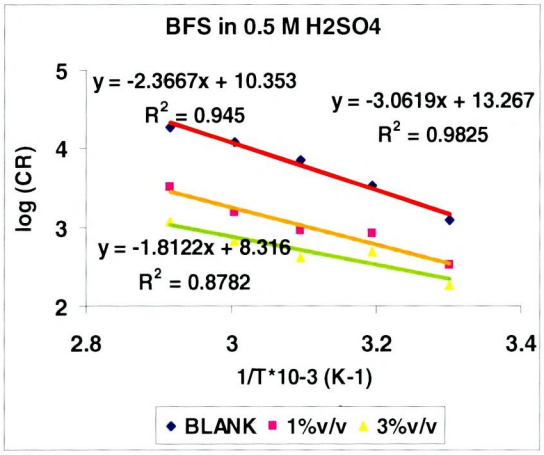

(a)

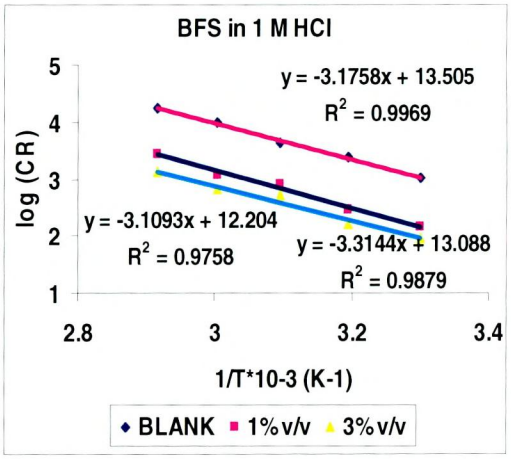

(b)

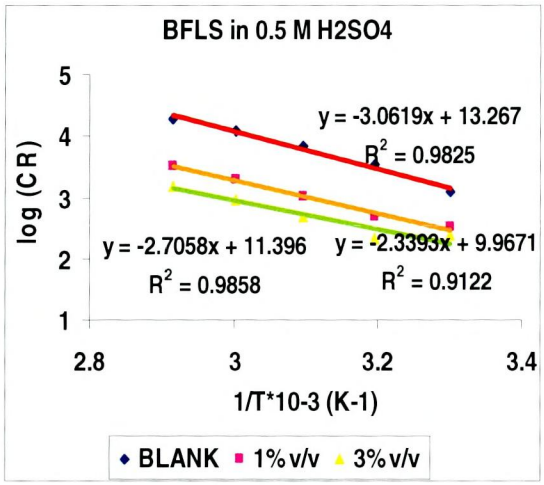

(c)

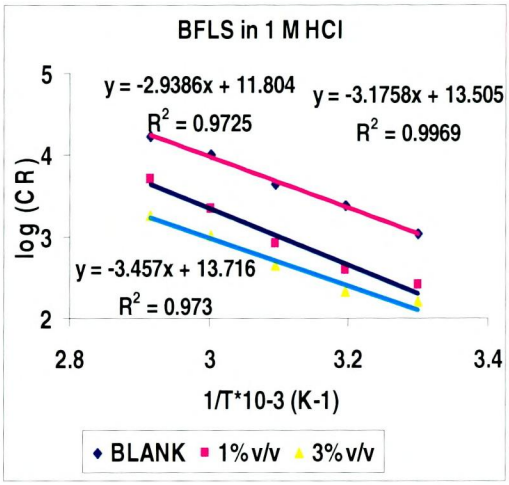

(d)

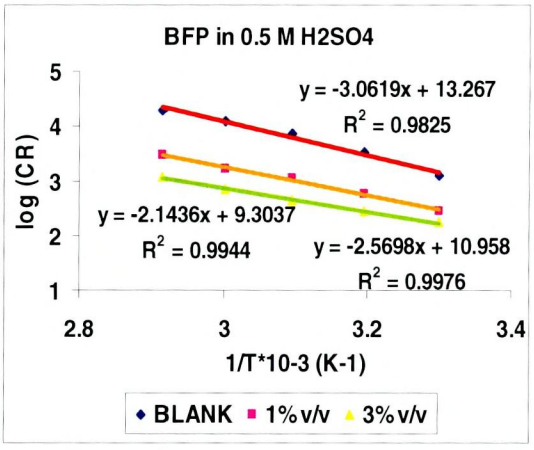

(e)

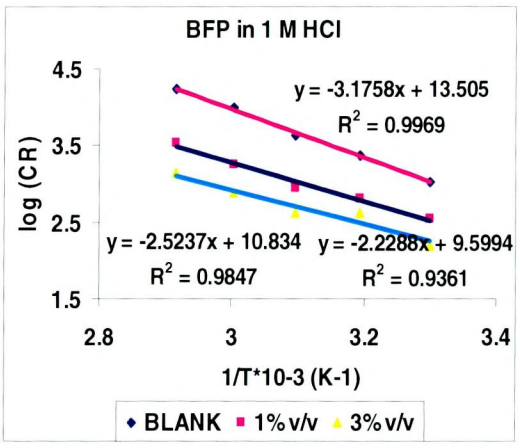

(f)

Figure – 40.b Arrhenius plot for mild steel corrosion in 0.5 M H_2SO_4 and 1 M HCl in the absence and presence of different concentration of BF extracts

Linear plots were obtained, from the slope ($-E_a/2.303R$), activation energy (E_a) values are deduced and listed in Table 33 (a and b). The temperature dependence of the inhibiting effect and the comparison of the values of the apparent activation energy of the corrosion process in the absence and presence of inhibitors can provide further evidence concerning the mechanism of the inhibiting action. The decrease of the inhibitor efficiency with temperature rise, which refers to a higher value of E_a, when compared to that in an acid with no inhibitor, is interpreted as an indication for an electrostatic character of the inhibitor's adsorption. Unchanged or lower values of E_a in inhibited systems compared to the blank have been reported to be indicative of chemisorption mechanism, whereas higher values of E_a suggest a physical adsorption mechanism.

Investigation of the result presented in the Table-33.a. infer, CNS in both acidic media, CNLS in 1 M HCl furnish high E_a values compared to the blank. CNLS in 0.5 M H_2SO_4 could afford unchanged E_a values compared to the blank. CNP in both acidic media render low E_a values compared to the blank. Analyzing Table-33.b BFS, BFLS and BFP in 0.5 M H_2SO_4 and BFP in 1 M HCl furnish low E_a values compared to the blank. BFS in 1 M HCl render unchanged E_a value with reference to the blank. BFLS in 1 M HCl could give high E_a values compared to the blank.

Experiments conducted by **Bag *et al.*, (1996)** also reflected lower E_a values for the inhibited systems. The presence of inhibitors, decreased the E_a of the reaction to an extent depending on the nature of inhibitor. The lower value of E_a in an inhibited solution when compared to that of an uninhibited one shows that strong chemisorption bond between the inhibitor and the metal is highly probable. E_a values were higher than that in its absence (blank).

The higher values of E_a in the inhibited solution can be correlated with the increased thickness of the double layer, which enhances the activation energy of the corrosion process. The higher E_a values in the presence of inhibitor compared to the blank solution indicates that the inhibitor will be effective at low temperatures, but efficiencies will be diminished at higher temperatures **(Umoren *et al.*, 2006)**. The increase in activation energy after the addition of inhibitor to acid solution can indicate that physical adsorption (electrostatic interaction) occurs in the first stage. Indeed CN/BF extracts molecule which contains mostly oxygen atom in its structure can be protonated to form cation forms in acid medium. It is logical to assume that in this case the electrostatic cation adsorption is responsible for the good protective properties of this compound. However, the adsorption phenomenon of CN/BF extracts are not considered only as a physical or as chemical adsorption phenomenon, but a wide spectrum of conditions, ranging from the dominance of

chemisorption or electrostatic effects may arise due to the complex nature of the corrosion inhibiting process. Physical adsorption in inhibition of corrosion of carbon steel in acidic solution is small but important because it is preceding stage of chemisorption of CN/BF extracts on MS **(Obi-Egbedi *et al.*, 2011).**

4.4.1 Activation parameters – Entropy of Activation and Enthalpy of Activation

The relationship between log (CR/T) versus 1/T for MS corrosion in 0.5 M H_2SO_4 and 1M HCl in the absence and presence of different concentrations of CN/BF extracts were shown in Figure-41(a and b). Straight lines were obtained with slope of ($-\Delta H^\circ_a/2.303R$) and an intercept of ($\log R/Nh + \Delta S^\circ_a/2.303R$) from which the values of ΔH°_a and ΔS°_a respectively were computed and listed in Table-34. The enthalpy of activation, ΔH°_a and entropy of activation, ΔS°_a were obtained from Eyring transition state equations (3.12) and (3.13) mentioned in methods and materials (Chapter III).

Table-34 Average value of activation parameters for MS/ inhibitors in 0.5 M H_2SO_4 and 1 M HCl systems at different temperatures

Inhibitor	ΔH°_{ads} (kJ/mol)		ΔS°_{ads} (J/mol K^{-1})	
	0.5 M H_2SO_4	1 M HCl	0.5 M H_2SO_4	1 M HCl
Blank	61.30	63.48	55.34	59.91
CNS	62.84	73.61	39.75	76.79
CNLS	61.47	70.74	38.06	67.85
CNP	62.84	58.01	39.75	28.95
BFS	42.06	63.67	-21.10	42.61
BFLS	51.84	64.31	9.290	47.72
BFP	48.18	47.87	-2.712	-3.481

CN/BF extracts in both acidic media, the positive value of the enthalpies (ΔH°_{ads}) reflects the endothermic nature of the mild steel dissolution process meaning that dissolution of steel is difficult **(Sudhish k. Shukla, *et al.*, 2011; Ebenso *et al.*, 2008).** The positive values of entropies (ΔS°_a) in the presence of CNS, CNLS, CNP and BFLS in both acidic media and BFS in 1 M HCl implies that the activation complex in the rate determining step represents as association rather than a dissociation step, meaning that an increase in disordering takes place on going from reactants to the activation complex **(Elachouri *et al.*, 1996).** The negative values of entropies (ΔS°_a) in the presence of BFP in both acidic media and BFS in 0.5 M H_2SO_4 implies the inhibitor molecules, freely moving in the bulk solution were adsorbed in an orderly fashion onto the mild steel surface. This implies that the activation complex in the rate determining step represents as association rather than a dissolution step, meaning that a decrease in disordering takes place on going from reactants to the activated complex **(Obi-Egbedi *et al.*, 2011).**

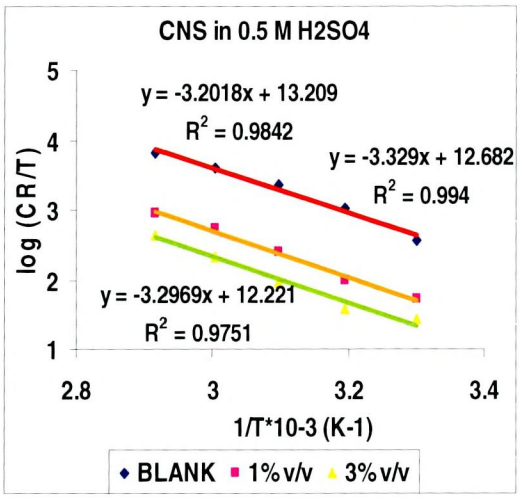

(a)

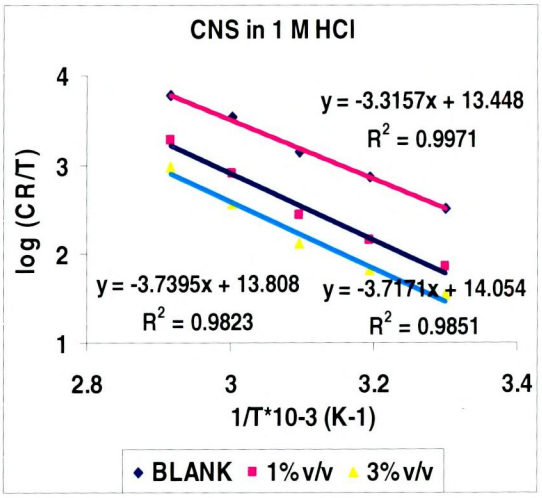

(b)

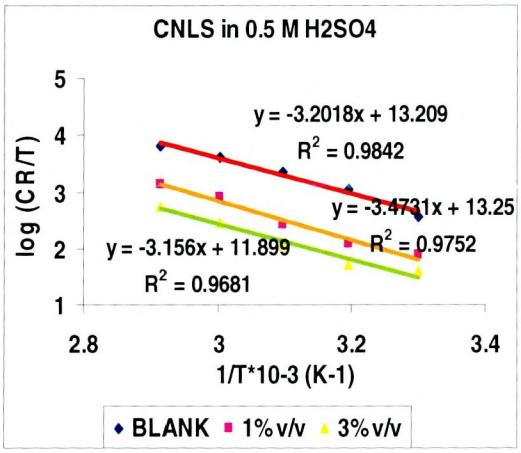

(c)

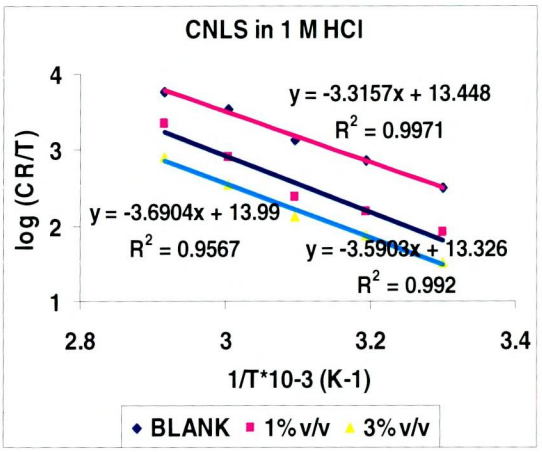

(d)

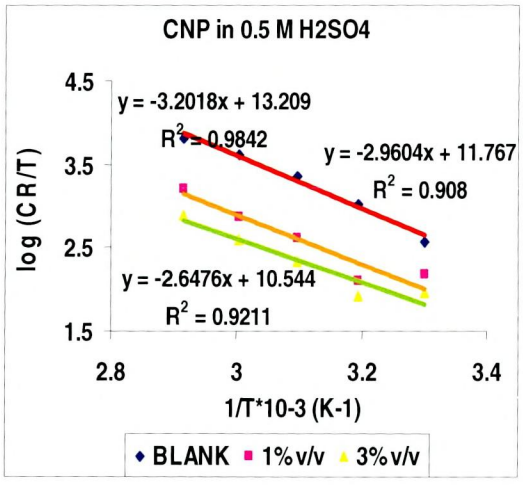

(e)

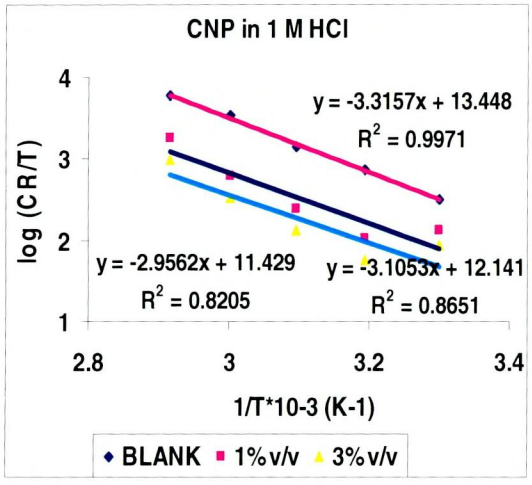

(f)

Figure- 41.a Transition state plot for MS corrosion in 0.5 M H_2SO_4 and 1 M HCl in the absence and presence of different concentrations of CN extracts

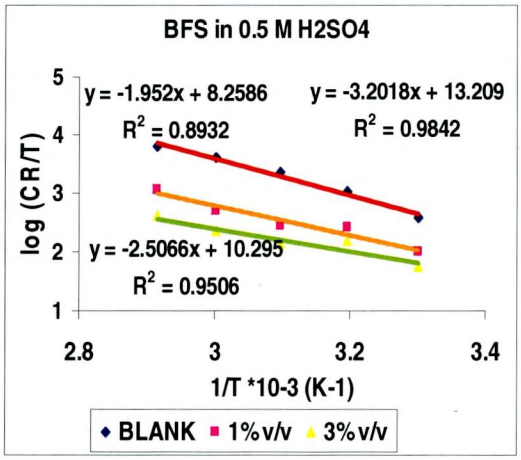

(a)

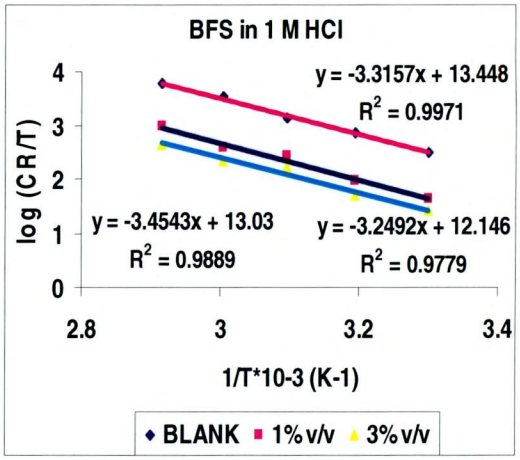

(b)

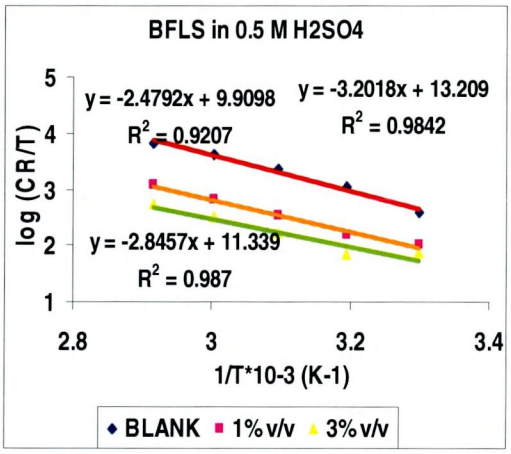

(c)

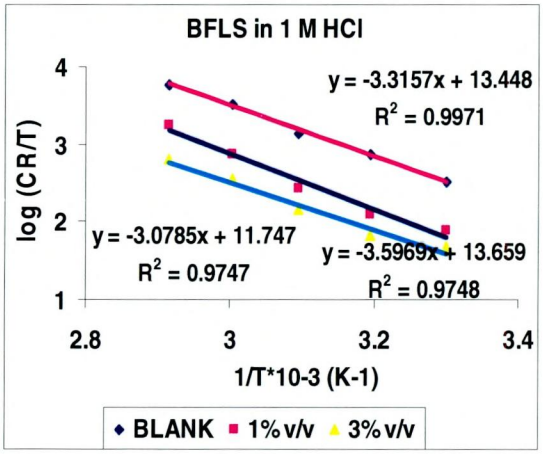

(d)

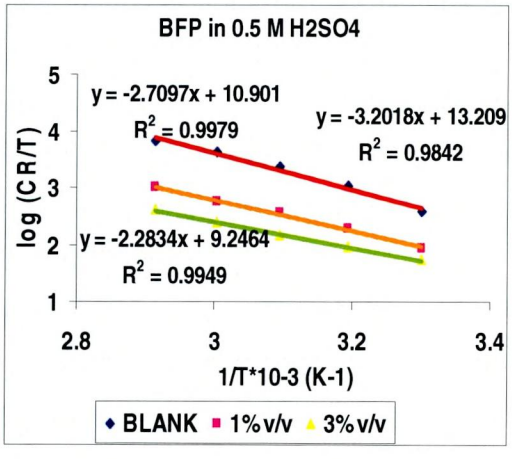

(e)

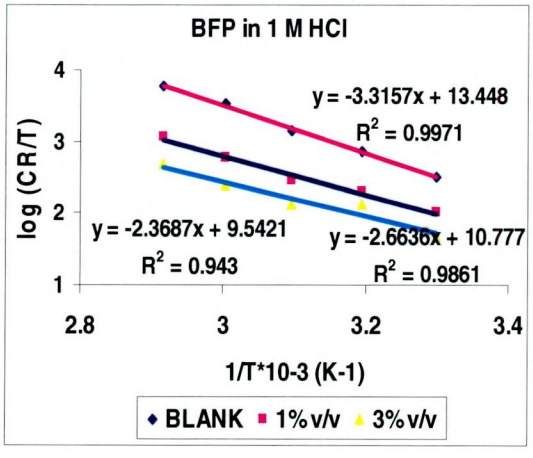

(f)

Figure- 41.b Transition state plot for MS corrosion in 0.5 M H_2SO_4 and 1 M HCl in the absence and presence of different concentrations of BF extracts

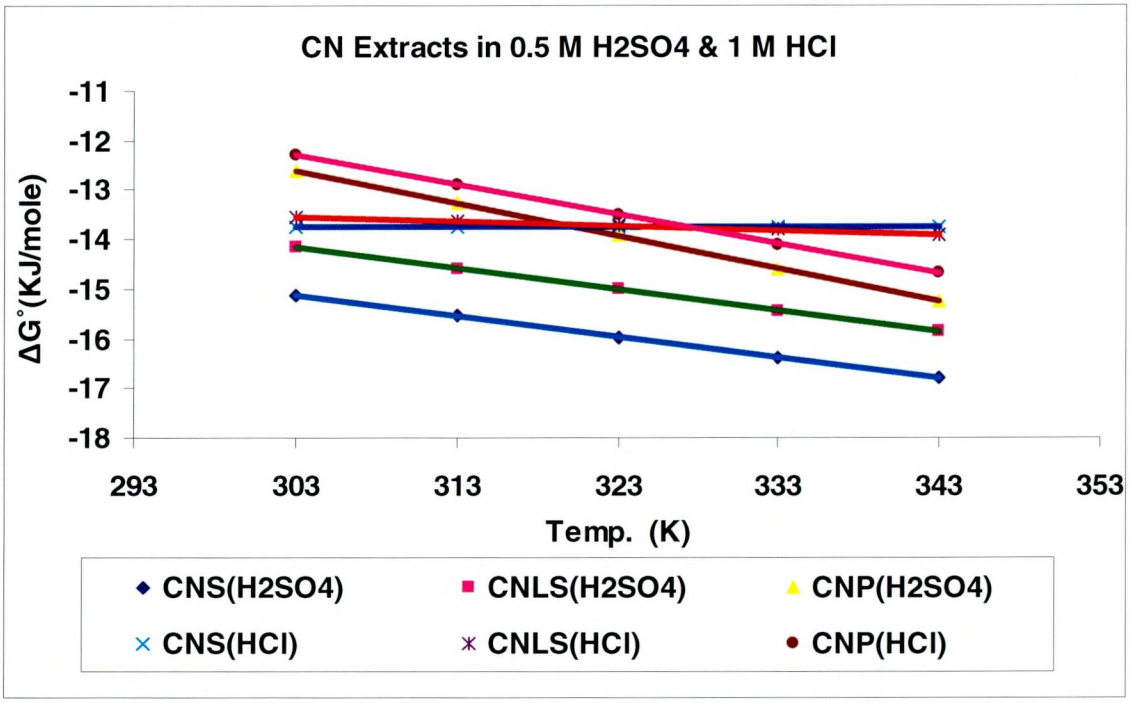

(a)

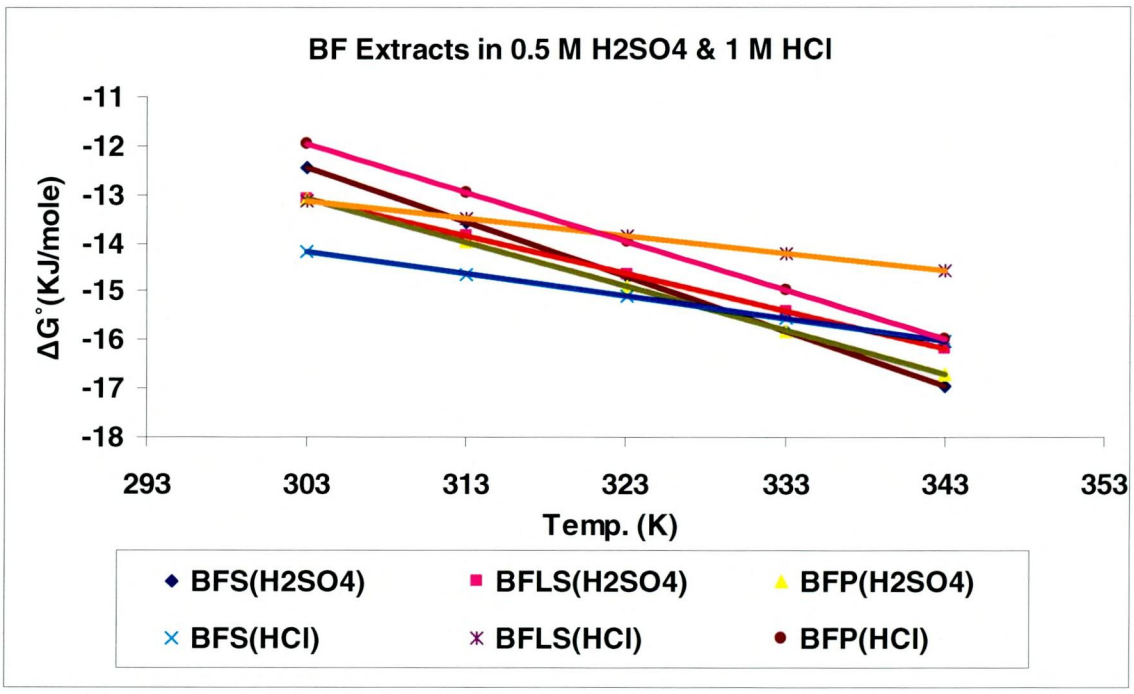

(b)

Figure- 42 Best fit curves of -ΔG Vs T for (a) CN and (b) BF in 0.5 M H_2SO_4 and 1M HCl

Table – 35.a Thermodynamic adsorption parameters for mild steel/inhibitors at different temperatures in 0.5 M H_2SO_4 and 1 M HCl of CN extracts

Inhibitor	$-\Delta G^\circ_{ads}$ (kJ/mol)					ΔH°_{ads}	ΔS°_{ads}
	303 K	313 K	323 K	333 K	343 K	kJ/mol	J/mol K^{-1}
0.5 M H_2SO_4							
CNS	14.28	16.28	16.55	16.38	16.31	-2.523	-41.6
CNLS	13.07	15.56	15.82	15.23	15.38	-1.155	-42.9
CNP	10.93	14.94	14.62	14.85	14.29	7.488	-66.3
1 M HCl							
CNS	13.20	14.01	14.32	13.93	13.26	-13.614	-0.4
CNLS	13.07	13.84	14.27	13.93	13.47	-10.841	-8.9
CNP	10.38	14.62	14.45	14.69	13.35	5.914	-60.1

Table – 35.b Thermodynamic adsorption parameters for mild steel/ inhibitors at different temperatures in 0.5 M H_2SO_4 and 1 M HCl of BF extracts

Inhibitor	$-\Delta G^\circ_{ads}$ (kJ/mol)					ΔH°_{ads}	ΔS°_{ads}
	303 K	313 K	323 K	333 K	343 K	kJ/mol	J/mol K^{-1}
0.5 M H_2SO_4							
BFS	12.27	12.95	15.73	16.27	16.29	21.990	-113.6
BFLS	11.90	15.06	15.26	15.39	15.61	10.388	-77.5
BFP	12.4	14.49	15.37	16.14	16.11	14.394	-90.7
1 M HCl							
BFS	14.19	14.96	14.32	16.15	15.88	-0.338	-45.7
BFLS	12.44	14.15	14.26	14.37	14.13	-2.242	-36
BFP	12.09	12.46	14.31	15.45	15.64	18.600	-100.9

components to the empty d orbitals of the metal. Similar explanation was offered by **Ehteram A. Noor, (2007)**. ΔG°_{ads} values tabulated in Table-(35 a and b) reveal that the studies CN/BF extracts are adsorbed spontaneously on mild steel surface. In the present investigation, the calculated ΔG°_{ads} values are negative and less than 20 kJ/mole, at the same time ΔG°_{ads} values increase upto a particular temperature and then the ΔG°_{ads} values are stabilized. Generally, values of ΔG°_{ads} around -20 $kJmol^{-1}$ or lower are consistent with the electrostatic interaction between the charged molecules and the charged metal (physisorption); those around -40 $kJmol^{-1}$ or higher involve charge sharing or transfer from organic molecules to the metal surface to form a coordinate type of bond (chemisorption) **(Donahue *et al.*, 1965).** Hence it may be assumed that the adsorption of the inhibitor molecules is not merely physical or chemisorption but obeying a mixed adsorption.

4.5.2 ΔH°_{ads} and ΔS°_{ads}

The positive sign of ΔH°_{ads} for the systems – CNP, BFS, BFLS and BFP in 0.5 M H_2SO_4 and CNP and BFP in 1 M HCl reflects the endothermic nature of dissolution. The negative sign of ΔH°_{ads} for the systems – CNS and CNLS in 0.5 M H_2SO_4 and CNS, CNLS, BFS and BFLS in 1 M HCl indicates that the adsorption of inhibitor molecules is an exothermic process. The entropy of adsorption for the system – CN and BF in both acid media obtained from equation (3.16) were negative because inhibitors molecule freely moving in the bulk solution, where adsorption in an orderly fashion onto the mild steel, resulting in a decrease in entropy **(Obi-Egbedi *et al.*, 2010).** The negative values of entropy of adsorption, (ΔS°_{ads}) in the presence of all the studied inhibitors, are attributed to the adsorption process which is accompanied by an increase in order of the system due to the adsorption of the studied inhibitor on the metal surface **(Gomma and Wahdan, 1994).** Inspection of Table –(35 a and b) revealed that decrease in enthalpy and entropy is the driving force for the adsorption of CN and BF in both acid media on the MS surface **(Umoren *et al.*, 2007b).**

4.6 ELECTROCHEMICAL MEASUREMENTS

Electrochemical testing provides a method for determining the corrosion rate of a metal. Electrochemical testing is even more valuable since mass loss would take significant time to detect. When evaluating corrosion inhibitors, this feature allows for quick assessment of inhibitor performance, including general corrosion rate and film durability. The tests are performed by applying a potential to an electrode in an electrolyte and measuring the electrical current produced.

4.6.1 POTENTIODYNAMIC POLARIZATION STUDIES

The potentiodynamic polarization curves of mild steel in 0.5 M H_2SO_4 and 1 M HCl with the addition of various concentrations of shell, leaf stalk and peduncle of CN and BF extract is shown in Figure-(43-48). The corrosion kinetic parameters such as corrosion potential (E_{corr}), corrosion current density (I_{corr}), anodic Tafel slope (b_a) and cathodic Tafel slope (b_c) deduced from the curves are given in Table-(36-41). Both anodic and cathodic polarization curves for mild steel in both acids at various concentrations shell, leaf stalk and peduncle of CN and BF are shown in Figures (43-48).

4.6.1.1 Potentiodynamic polarization studies of MS in the presence of shell, leafstalk and peduncle of CN in 0.5 M H_2SO_4 and 1 M HCl

a. Polarization studies of mild steel with the addition of CNS extract

Both the anodic and cathodic polarization behaviour of mild steel in 0.5 M H_2SO_4 and 1 M HCl in the absence and presence of CNS extract are shown in Figure-43(a and b). The corrosion current density values of mild steel corrosion decreases.

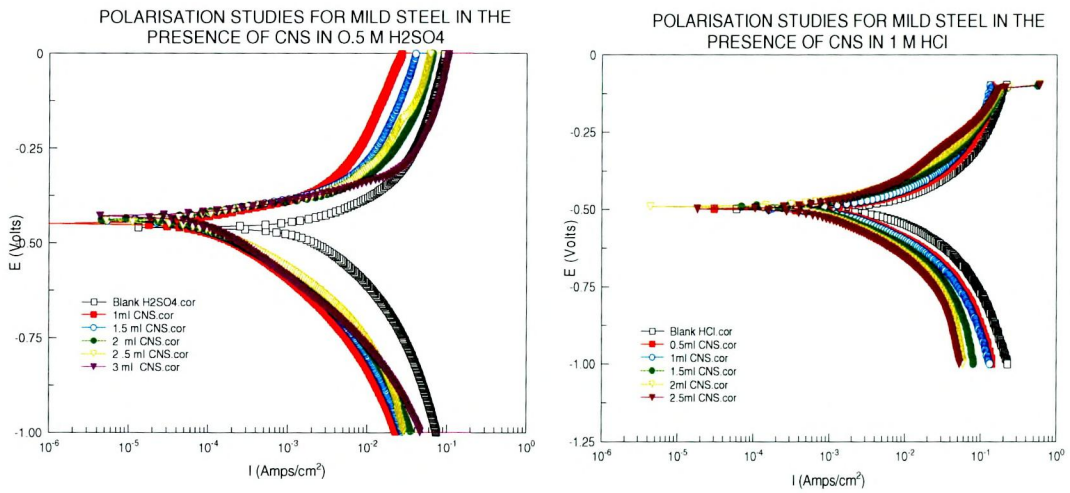

(a) **(b)**

Figure - 43 Potentiodynamic polarization of MS in (a) 0.5 M H_2SO_4 and (b) 1 M HCl in presence or absence of CNS extract

Table – 36 Electrochemical parameters for the corrosion of MS in the presence of CNS in 0.5 M H_2SO_4 and 1 M HCl

Conc. (%v/v)	CNS in 0.5 M H_2SO_4					CNS in 1 M HCl				
	I_{corr} (μA/ cm^2)	$-E_{corr}$ (mV/ SCE)	b_a (mV/ dec)	b_c (mV/ dec)	IE (%)	I_{corr} (μA /cm^2)	$-E_{corr}$ (mV/ SCE)	b_a (mV/ dec	b_c (mV/ dec)	IE (%)
Blank	620	443	227	176	-	692	498	214	170	-
0.5	301	440	184	134	86	332	499	191	121	69
1.0	243	449	180	110	94	272	499	176	120	84
1.5	115	442	169	108	95	134	489	158	100	90
2.0	88	441	157	97	96	102	491	134	99	91
2.5	73	443	135	71	96	88	499	131	93	92
3.0	53	432	121	73	**97**	72	498	126	90	**92**

from 620 μA/cm^2 of the blank in 0.5 M H_2SO_4 acid to 53 μA/cm^2 for the addition of 3.0%v/v of CNS extract and, from 692 μA/cm^2 of the blank in 1 M HCl to 72 μA/cm^2 for the addition of 3.0%v/v of CNS extract resulting in 97 and 92 % of inhibition efficiencies. The E_{corr} value has not been shifted to any particular direction from the blank value, which also indicates that the inhibitor acts through mixed mode of inhibition. Tafel slopes b_a and b_c changes with increasing concentration of CNS extract in both investigated acid media (Table-36).

Tafel slopes b_a and b_c obtained in the presence and absence of the CNS extract in both media revealed that the inhibition of corrosion of mild steel was under mixed control indicating that both anodic dissolution and cathodic hydrogen evolution mechanism were affected in presence of the inhibitor.

b. Polarization studies of MS with the addition of CNLS extract

Figure-44 (a and b) shows typical anodic and cathodic potentiodynamic polarization curves for mild steel in 0.5 M H_2SO_4 and 1 M HCl in the absence and presence of various concentration of CNLS extract at room temperature. Corrosion current density of mild steel corrosion in the presence of CNLS extract in 0.5 M H_2SO_4 established a maximum decrease in I_{corr} value from 604 μA/cm^2 of the blank to 48 μA/cm^2 (Table-37).These results yielded maximum inhibition efficiency of 92%. As the concentration of CNLS extract in 1 M HCl increased, the corrosion current density reduced from 615 μA/cm^2 of the blank to 57 μA/cm^2 for 3.0%v/v concentration and afforded an inhibition efficiency of 90%. The E_{corr} values were slightly shifted in the presence of CNLS extract suggesting that these inhibitor inhibits the corrosion of mild steel in both acidic media by controlling the anodic and cathodic reactions. Inhibitors of this type are known as mixed type inhibitors. The change in the values of b_a and b_c in the presence of CNLS extract also infer that the inhibitor behaves as mixed type inhibitor.

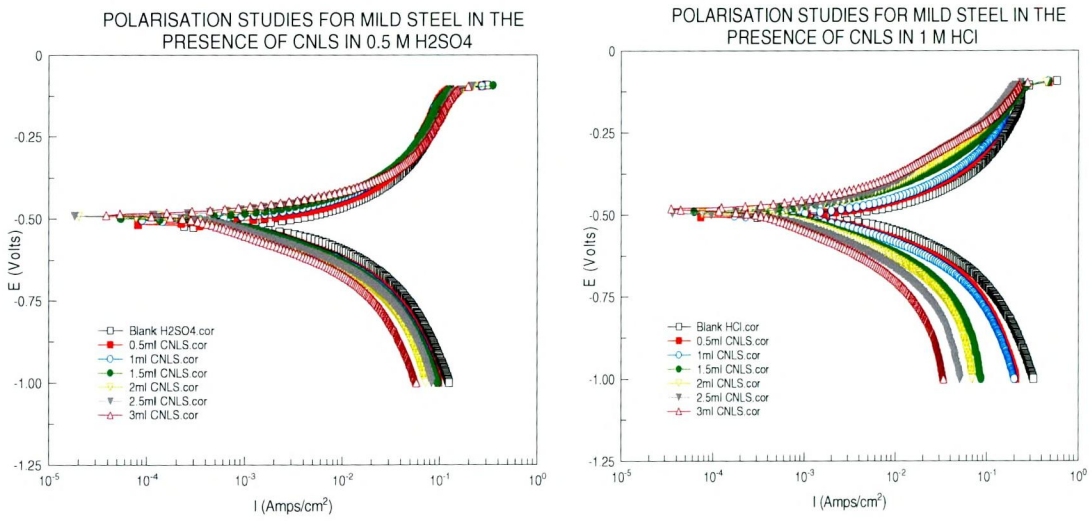

(a) **(b)**

Figure - 44 Potentiodynamic polarization of mild steel in (a) 0.5 M H_2SO_4 and (b) 1 M HCl in presence or absence of CNLS extract

Table – 37 Electrochemical parameters for the corrosion of MS in the presence of CNLS in 0.5 M H_2SO_4 and 1 M HCl

Conc. (%v/v)	CNLS in 0.5 M H_2SO_4					CNLS in 1 M HCl				
	I_{corr} (µA/ cm^2)	$-E_{corr}$ (mV/ SCE)	b_a (mV/ dec)	b_c (mV/ dec)	IE (%)	I_{corr} (µA/ cm^2)	$-E_{corr}$ (mV/ SCE)	b_a (mV/ dec)	b_c (mV/ dec)	IE (%)
Blank	604	513	226	182	-	615	508	185	122	-
0.5	257	510	197	125	57	382	507	182	121	37
1.0	186	507	177	111	69	307	505	156	114	49
1.5	137	501	161	100	77	124	498	151	110	79
2.0	58	495	157	74	90	118	495	150	104	80
2.5	50	492	126	72	91	105	491	146	95	82
3.0	48	491	124	70	**92**	57	484	144	89	**90**

c. Polarization studies of MS with the addition of CNP extract

Potentiodynamic polarization curves for mild steel in 0.5 M H_2SO_4 and 1 M HCl with various concentration of CNP extract at room temperature are shown in Figure 45 (a and b). Investigation of Tables-38 revealed that the corrosion current density of MS remarkably decreased from 728 µA/cm^2 to 36 µA/cm^2 between the concentration range from 0.5%v/v to 3.0%v/v of CNP extract in 0.5 M H_2SO_4. Maximum protection ability of CNP extract in 0.5 M H_2SO_4 was found to be 95% for 3.0%v/v concentration. The influence of CNP in 1 M HCl furnished a maximum inhibition efficiency of 83%v/v for 3.0%v/v concentration of CNP extract. This value was obtained due to decrease in I_{corr} from 540 µA/cm^2 to 91 µA/cm^2 for the concentration range 0.5 %v/v to 3.0%v/v concentration. E_{corr}, b_a and b_c values do not change appreciably with the addition of the CNP indicating that the inhibitor is not

interfering with the anodic dissolution or cathodic hydrogen evolution reactions independently but acts as a mixed type of inhibitor.

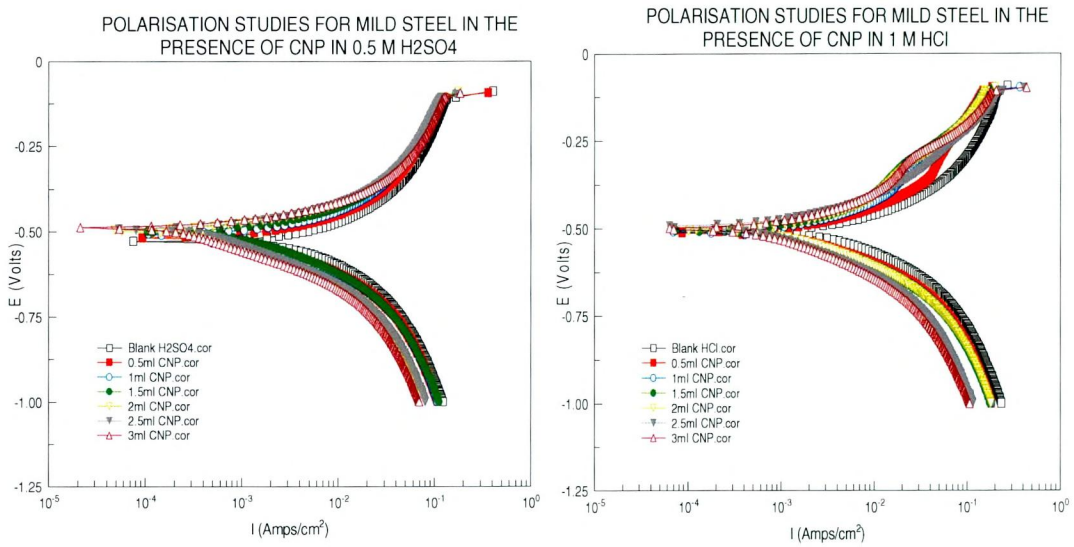

(a) (b)

Figure - 45 Potentiodynamic polarization of MS in (a) 0.5 M H_2SO_4 and (b) 1 M HCl in presence or absence of CNP extract

Table – 38 Electrochemical parameters for the corrosion of MS in the presence of CNP in 0.5 M H_2SO_4 and 1 M HCl

Conc. (%v/v)	CNP in 0.5 M H_2SO_4					CNP in 1 M HCl				
	I_{corr} (µA/ cm^2)	$-E_{corr}$ (mV/ SCE)	b_a (mV/ dec)	b_c (mV/ dec)	IE (%)	I_{corr} (µA/ cm^2)	$-E_{corr}$ (mV/ SCE)	b_a (mV/ dec)	b_c (mV/ dec)	IE (%)
Blank	728	518	257	197	-	540	511	169	136	-
0.5	278	517	194	128	61	236	508	138	118	56
1.0	203	509	175	115	72	207	507	128	124	61
1.5	173	510	167	108	76	171	503	139	142	68
2.0	82	514	151	79	88	159	505	149	152	70
2.5	57	512	174	86	92	108	502	141	94	79
3.0	36	511	131	69	**95**	91	500	156	114	**83**

4.6.1.2 Potentiodynamic polarization studies of MS in the presence of shell, leaf stalk and peduncle of BF in 0.5 M H_2SO_4 and 1 M HCl

a. Polarization studies of MS with the addition of BFS extract

Figure 46 (a and b) represents the anodic and cathodic Tafel polarization curves of mild steel in different concentrations of 0.5 M H_2SO_4 and 1 M HCl solutions of BFS extract. Analysis of the results depicted in Tables-39 indicate that the corrosion current density of mild steel markedly decreased from 634 µA/cm^2 to 74 µA/cm^2 yielded a maximum protection ability of 88% for 3.0%v/v concentration and the reduction in I_{corr} from 696 µA/cm^2 to 121 µA/cm^2 afforded a maximum protection ability of 82% in the presence of BFS in 0.5 M H_2SO_4 and 1 M HCl respectively. The

E_{corr} values do not show reasonable change in the presence of inhibitors, therefore, BFS can be classified as mixed type inhibitor. The values of the Tafel slopes b_a and b_c clearly indicates that both the cathodic and anodic reactions are inhibited thus reducing the corrosion on mild steel surface.

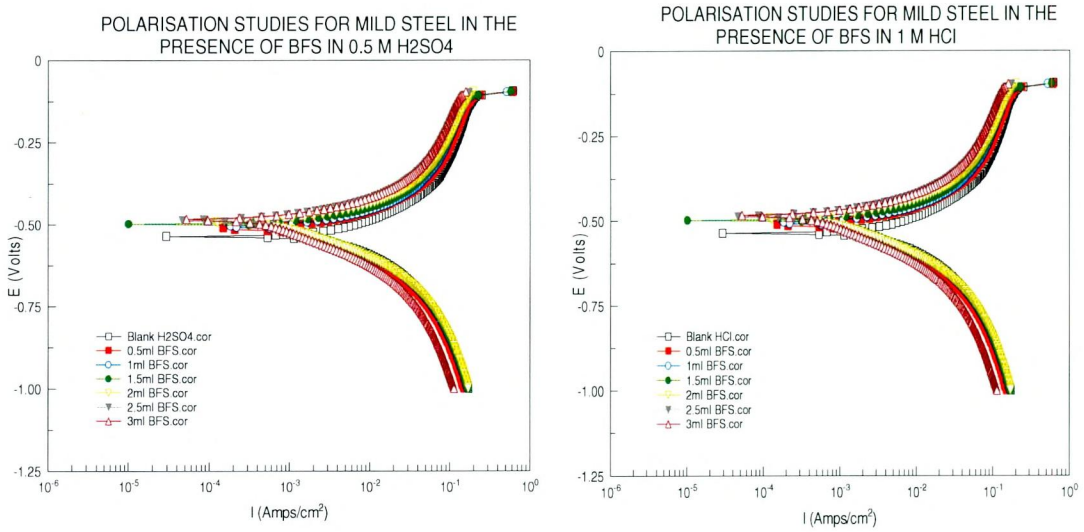

(a) **(b)**

Figure - 46 Potentiodynamic polarization of MS in (a) 0.5 M H_2SO_4 and (b) 1 M HCl in presence or absence of BFS extract

Table – 39 Electrochemical parameters for the corrosion of MS in the presence of BFS in 0.5 M H_2SO_4 and 1 M HCl

Conc. (%v/v)	BFS in 0.5 M H_2SO_4					BFS in 1 M HCl				
	I_{corr} (µA/ cm^2)	$-E_{corr}$ (mV/ SCE)	b_a (mV/ dec)	b_c (mV/ dec)	IE (%)	I_{corr} (µA/ cm^2)	$-E_{corr}$ (mV/ SCE)	b_a (mV/ dec)	b_c (mV/ dec)	IE (%)
Blank	634	505	192	151	-	696	504	196	152	-
0.5	287	502	168	108	54	271	497	169	126	61
1.0	264	505	164	105	58	238	501	164	126	65
1.5	205	498	151	98	67	192	502	163	121	72
2.0	162	493	146	91	74	169	503	154	119	75
2.5	91	486	143	78	85	144	502	148	104	79
3.0	74	484	141	84	**88**	121	502	119	103	**82**

b. Polarization studies of MS with the addition of BFLS extract

The effect of the inhibitor concentration is shown in Figure-47(a and b) which presents the anodic and cathodic polarization measurements of mild steel in 0.5 M H_2SO_4 and 1 M HCl solutions at room temperature with BFLS. Mild steel corrosion in the presence of BFLS in 0.5 M H_2SO_4 reveals as the concentration increased from 0.5%v/v to 3.0%v/v the inhibition efficiency increased from 46% to 97% with reduction in current density from 675 µA/cm^2 to 18 µA/cm^2 (Table-40). BFLS in 1 M HCl offered a maximum protection ability of 88% at 3.0%v/v concentration for the

decrease in I_{corr} values from 704 μA/cm^2 to 82 μA/cm^2 for 3.0%v/v concentration. The steady values of E_{corr} indicate that the BFLS extract might have predominantly acted as mixed inhibitor to retard both the rates of hydrogen ion reduction and anodic dissolution of mild steel.

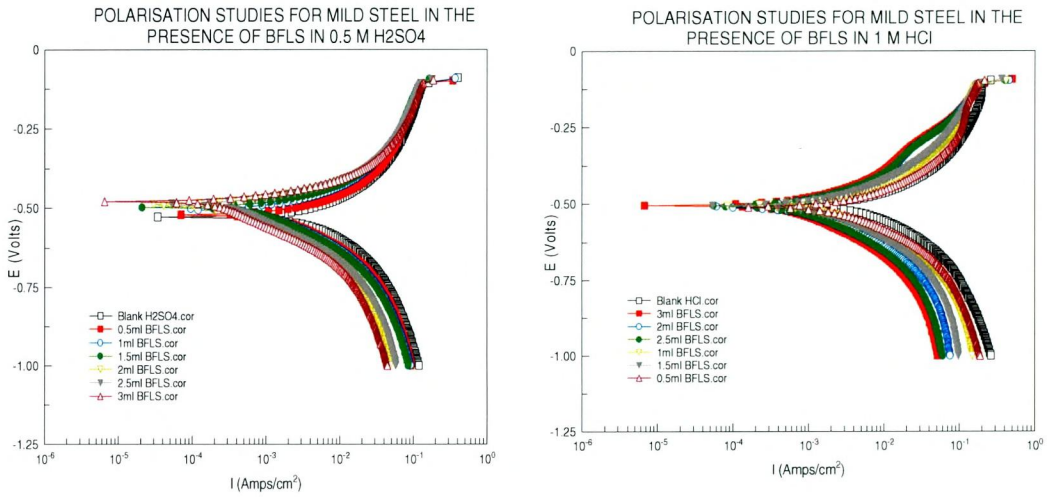

(a) **(b)**

Figure - 47 Potentiodynamic polarization of MS in (a) 0.5 M H_2SO_4 and (b) 1 M HCl in presence or absence of BFLS extract

Table – 40 Electrochemical parameters for the corrosion of MS in the presence of BFLS in 0.5 M H_2SO_4 and 1 M HCl

Conc. (%v/v)	BFLS in 0.5 M H_2SO_4					BFLS in 1 M HCl				
	I_{corr} (μA/cm^2)	$-E_{corr}$ (mV/SCE)	b_a (mV/dec)	b_c (mV/dec)	IE (%)	I_{corr} (μA/cm^2)	$-E_{corr}$ (mV/SCE)	b_a (mV/dec)	b_c (mV/dec)	IE (%)
Blank	675	507	236	192	-	704	510	177	144	-
0.5	359	501	226	140	46	391	503	158	127	44
1.0	178	503	177	109	73	240	506	144	119	65
1.5	125	498	126	86	81	149	504	138	107	78
2.0	84	493	183	96	87	129	509	150	123	81
2.5	67	497	175	79	90	113	506	162	118	83
3.0	18	496	108	60	**97**	82	505	154	109	**88**

The values of E_{corr} have not shifted to any particular direction from the blank values indicating again the mixed mode of inhibition. Tafel slope values b_a and b_c were not much affected and this suggests that BFLS extract molecules adsorb on the metal surface by blocking the active sites on the metal surface. From the values of inhibition efficiency, it is clear that the corrosion inhibition may be due to the increase in the adsorption of the inhibitor on the metal surface.

c. Polarization studies of MS with the addition of BFP extract

Potentiodynamic anodic and cathodic polarization scans were carried out at room temperature in 0.5 M H_2SO_4 and 11 M HCl with different concentrations of BFP extract. Anodic and cathodic polarization curves in the absence and in the presence of inhibitor at different concentrations after ½ h of immersion are shown in Figure-48(a and b). Reduction in I_{corr} values from 672 μA/cm^2 to 52 μA/cm^2 were noticed in the presence of BFP extract in 0.5 M H_2SO_4. Relatively the efficiency to protect mild steel surface increased from 50% to 92% (Table-41). For 1 M HCl, I_{corr} value decreases from 607 μA/cm^2 to 71 μA/cm^2 and a maximum protection efficiency of 88% for 3.0%v/v concentration was obtained.

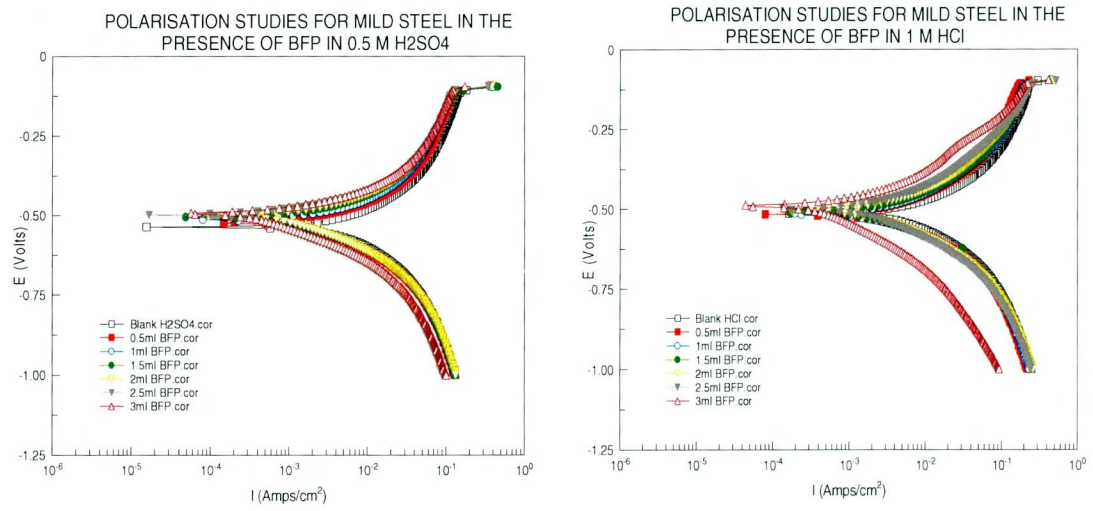

(a) **(b)**

Figure – 48 Potentiodynamic polarization of MS in (a) 0.5 M H_2SO_4 and (b) 1 M HCl in presence or absence of BFP extract

Table – 41 Electrochemical parameters for the corrosion of MS in the presence of BFP in 0.5 M H_2SO_4 and 1 M HCl

Conc. (%v/v)	BFP in 0.5 M H_2SO_4					BFP in 1 M HCl				
	I_{corr} (μA/ cm^2)	$-E_{corr}$ (mV/ SCE)	b_a (mV/ dec)	b_c (mV/ dec)	IE (%)	I_{corr} (μA/ cm^2)	$-E_{corr}$ (mV/ SCE)	b_a (mV/ dec)	b_c (mV/ dec)	IE (%)
Blank	672	536	222	186	-	607	517	144	136	-
0.5	333	522	179	135	50	362	515	148	143	40
1.0	213	512	149	112	68	252	514	144	136	58
1.5	184	516	144	108	72	126	510	141	128	79
2.0	174	513	149	98	74	106	505	146	129	82
2.5	67	514	128	76	90	93	500	147	126	84
3.0	52	521	135	81	**92**	71	509	193	98	**88**

E_{corr} values do not remarkably shift in the present system and hence, can be said to be a mixed type inhibitor. The values of Tafel slopes b_a and b_c are found to

change with BFP extract concentration which clearly indicated that the inhibitor controlled both reactions.

It is concluded apparently that I_{corr} decreases considerably in the presence of all the studied inhibitors, and decreases with increasing the inhibitor concentration correspondingly, IE(%) increased with the inhibitor concentration, due to the increase in the blocked fraction of the electrode surface by adsorption. Among the shell, leaf stalk and peduncle of CN, in 0.5 M H_2SO_4 and 1 M HCl, CNS is found to show maximum reduction in corrosion current followed by CNLS and then CNP (Figure-49.a)

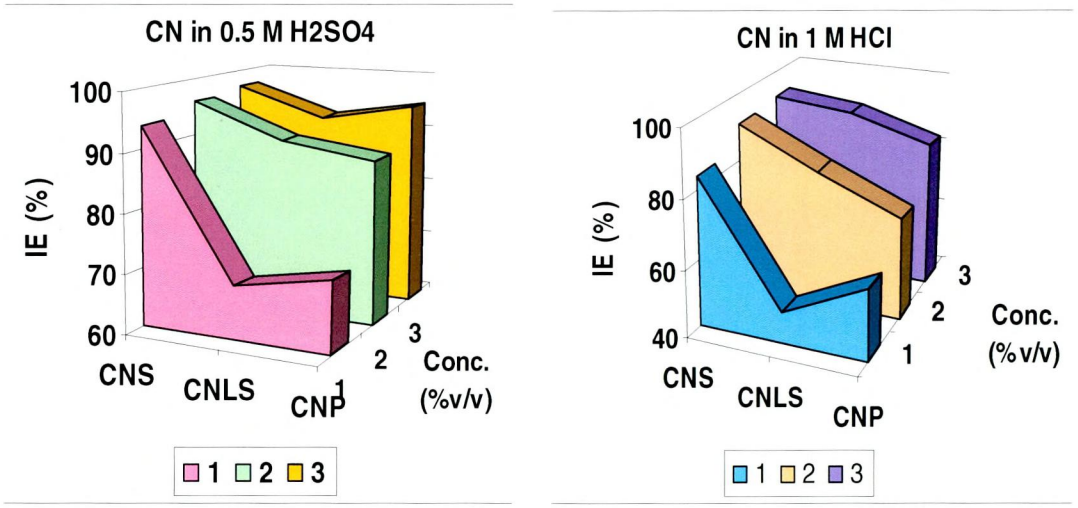

(a)

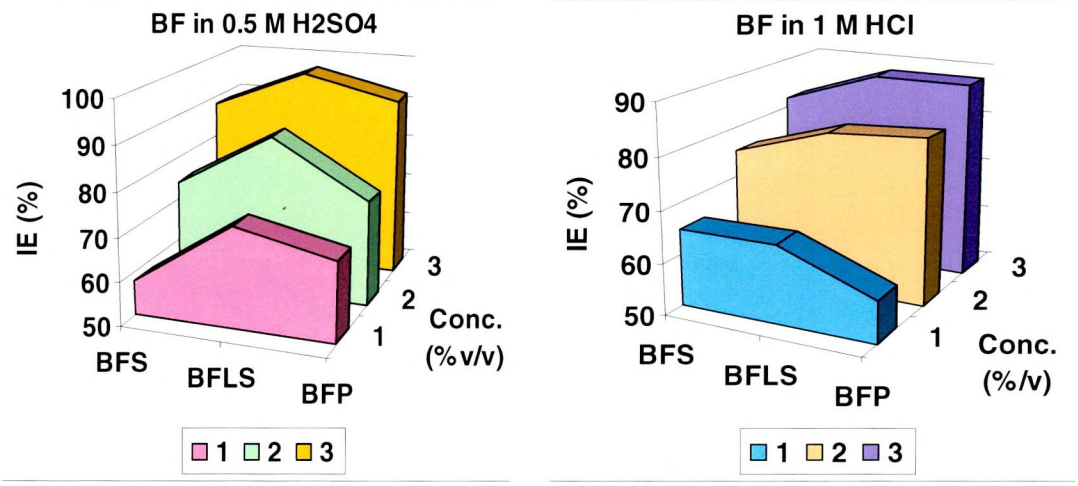

(b)

Figure - 49 Inhibitor efficiency of (a) CN and (b) BF inhibitors in 0.5 M H_2SO_4 and 1 M HCl

Among the shell, leaf stalk and peduncle of BF, in 0.5 M H_2SO_4, BFLS was found to show maximum reduction and in 1 M HCl, both BFLS and BFP were found to show the maximum corrosion current. (Figure-49.b).

Values of corrosion inhibition efficiency for these compounds also follow a similar order in the both acid media. It is seen from the Tables-(36-41) that mild steel corrodes to a greater extent in 1 M HCl, than in 0.5 M H_2SO_4, as seen from the values of I_{corr} for mild steel in these acids **(Muralidharan *et al.*, 1995)**.

Figures-(43 – 48) represent the anodic and cathodic Tafel polarization curves of mild steel in different concentrations of 0.5 M H_2SO_4 and 1 M HCl solutions on shell, leafstalk and peduncle for CN and BF extract of mild steel. In literature **(Satapathy *et al.*, 2009; Ahamad *et al.*, 2010)**, it has been reported that if the displacement in E_{corr} is >85mV the inhibitor can be seen as a cathodic or anodic type inhibitor and if the displacement of E_{corr} is <85 mV, the inhibitor can be seen as mixed type. In this investigation, the maximum displacement in E_{corr} value was 53 mV for shell, leafstalk and peduncle for CN and BF extract which indicates that the inhibitors acted as mixed type inhibitors. The presence of shell, leaf stalk and peduncle of CN and BF in 0.5 M H_2SO_4 and 1 M HCl produced a parallel displacement of the cathodic and anodic Tafel lines. Analysis of Tafel slopes Figures-(43-48) indicated that CN and BF behaved as a mixed type inhibitors. However the shift in b_a vales found to be higher indicating that CN extracts behaves as mixed type with a slight anodic control.

Anodic and cathodic Tafel slopes were not very much influenced by the presence of inhibitors. This suggests that the inhibitors did not change the mechanism of metal dissolution. The CN and BF extracts adsorption on the surface prevented the dissolution of iron. At first the metal atom leaves the crystal lattice to form surface adsorptive complexes, and then those complexes are discharged to form hydrated ions which will diffuse into the bulk solution.

4.6.2 LINEAR POLARIZATION RESISTANCE METHOD (LPR)

4.6.2.1 Polarization resistance value (R_p) of MS in 0.5 M H_2SO_4 and 1 M HCl with various concentration of shell, leaf stalk and peduncle for CN

R_p can be used as an index of corrosion inhibition. The values of R_p increased with increase in concentration of CNS extract in 0.5 M H_2SO_4 and 1 M HCl under investigation. R_p values increased from 4.5 to 25.6 Ω/cm^2 (3.0%v/v) in 0.5 M H_2SO_4 acid medium and from 4.7 to 30.1 Ω/cm^2 in 1 M HCl respectively (Table-42).

The protection efficiencies calculated from the R_p values were found to be increased from 56% (0.5%v/v) to 82% (3.0%v/v) in 0.5 M H_2SO_4 and 49% (0.5%v/v) to 84% (3.0%v/v) for the same extract in 1 M HCl.

Analysis of R_p values in the presence of CNLS extract in both the acidic media reflected a similar increase from 7.2 to 32.4 Ω/cm^2 in 0.5 M H_2SO_4 and from

3.8 to 41.0 Ω/cm^2 in 1 M HCl. Maximum inhibition efficiency of 77% and 90% were noticed in the CNLS extract in 0.5 M H_2SO_4 and 1 M HCl respectively at a concentration of 3.0%v/v.

Table - 42 Linear Polarization Resistance parameters of MS in the presence of CNS, CNLS and CNP in 0.5 M H_2SO_4 and 1 M HCl

Conc. (%v/v)	0.5 M H_2SO_4						1 M HCl					
	CNS		CNLS		CNP		CNS		CNLS		CNP	
	R_p (Ω/ cm^2)	IE (%)	R_p (Ω/ cm^2)	IE (%)	R_p (Ω/ cm^2)	IE (%)	R_p (Ω/ cm^2)	IE (%)	R_p (Ω/ cm^2)	IE (%)	R_p (Ω/ cm^2)	IE (%)
Blank	4.5	-	7.2	-	6.7	-	4.7	-	3.8	-	6.2	-
0.5	10.3	56	11.9	39	11.1	39	9.2	49	7.7	50	11.8	47
1.0	18.1	75	14.8	51	13.2	49	10.9	57	9.1	57	15.0	58
1.5	21.7	79	18.5	61	15.3	56	18.3	74	18.7	79	16.1	61
2.0	23.7	81	23.0	68	23.8	71	23.5	79	21.9	82	17.2	63
2.5	24.1	81	29.4	75	28.1	76	26.0	81	27.1	85	25.7	75
3.0	25.6	**82**	32.4	**77**	35.1	**80**	30.1	**84**	41.0	**90**	32.8	**81**

Investigation of polarization resistance values due to the influence of CNP extract in the examined media indicated an increase in R_p values from 6.7 to 35.1 Ω/cm^2 in 0.5 M H_2SO_4 and from 6.2 to 32.8 Ω/cm^2 in 1 M HCl medium. Experimental results revealed a maximum protection ability of 80% in 0.5 M H_2SO_4 and a maximum IE of 81% in 1 M HCl at 3.0%v/v.

4.6.2.2 Polarization resistance value (R_p) of MS in 0.5 M H_2SO_4 and 1 M HCl with various concentration of shell, leaf stalk and peduncle for BF

Examination of the performance of BFS extract in 0.5 M H_2SO_4 and in 1 M HCl revealed an increase in R_p values from 5.9 to 21.7 Ω/cm^2 in 0.5 M H_2SO_4 and from 3.8 to 24.4 Ω/cm^2 in 1 M HCl. This remarkable increase in R_p values reflected an increase in IE from 32% to 72% for 3.0%v/v concentration in 0.5 M H_2SO_4 and from 46% to 84% concentration in 1 M HCl respectively (Table-43).

Table - 43 Linear Polarization Resistance parameters of MS in the presence of BFS, BFLS and BFP in 0.5 M H_2SO_4 and 1 M HCl

Conc. (%v/v)	0.5 M H_2SO_4						1 M HCl					
	BFS		BFLS		BFP		BFS		BFLS		BFP	
	R_p (Ω/ cm^2)	IE (%)	R_p (Ω/ cm^2)	IE (%)	R_p (Ω/ cm^2)	IE (%)	R_p (Ω/ cm^2)	IE (%)	R_p (Ω/ cm^2)	IE (%)	R_p (Ω/ cm^2)	IE (%)
Blank	5.9	-	5.2	-	6.5	-	3.8	-	4.5	-	6.0	-
0.5	8.8	32	9.9	47	9.9	34	7.1	46	7.7	41	11.5	47
1.0	9.2	35	15.4	66	11.1	41	10.3	63	11.9	62	13.3	55
1.5	10.6	44	17.5	70	13.7	52	15.5	75	16.6	72	15.1	60
2.0	12.7	53	24.1	78	15.1	56	18.3	79	22.9	80	20.8	71
2.5	19.7	69	29.8	82	24.9	73	20.9	81	26.3	82	29.7	79
3.0	21.7	**72**	33.1	**84**	26.5	**75**	24.4	**84**	29.6	**84**	35.5	**83**

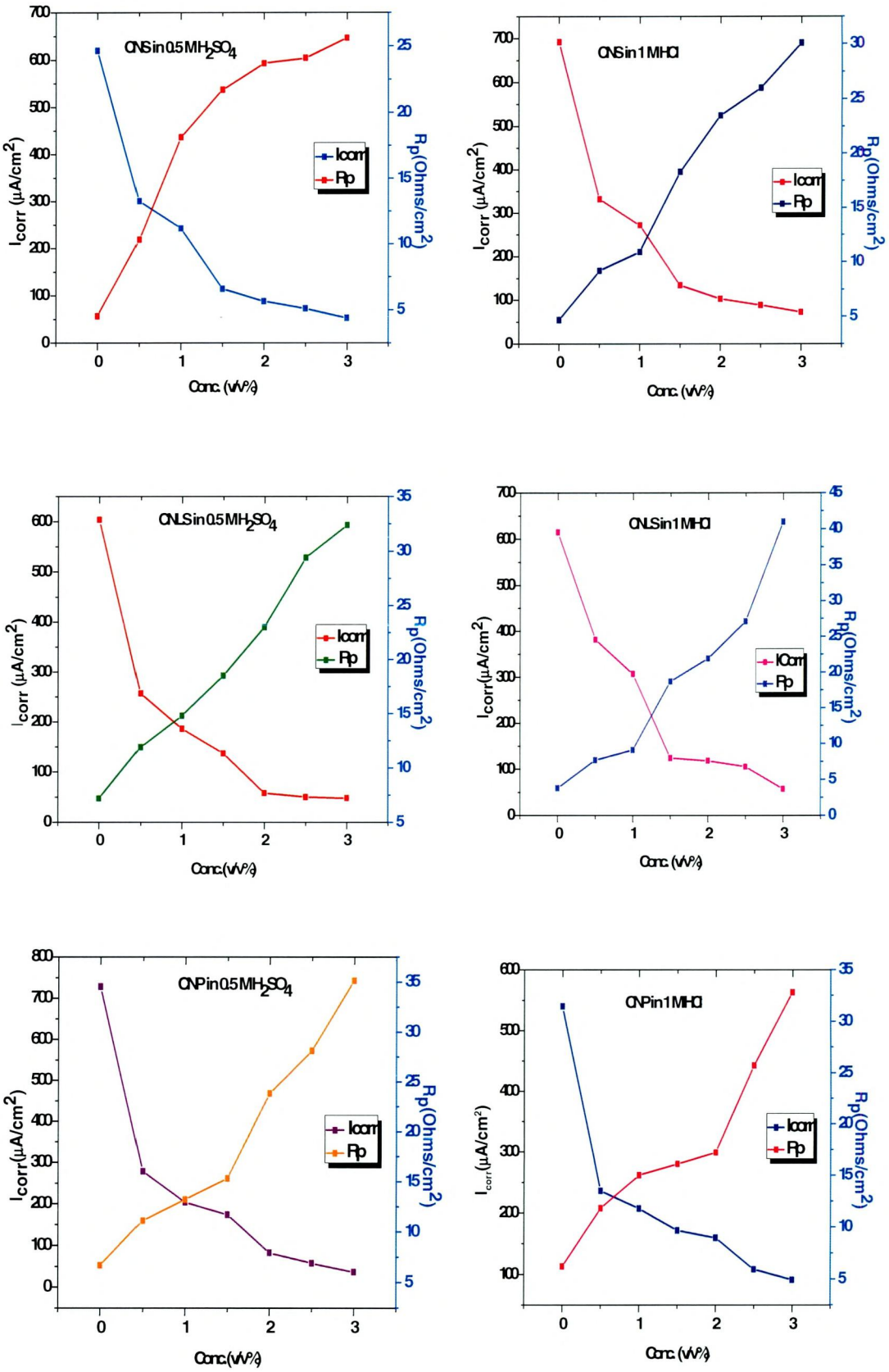

Figure-50.a Plot of I_{corr} and R_p with respect to concentrations of CN extracts

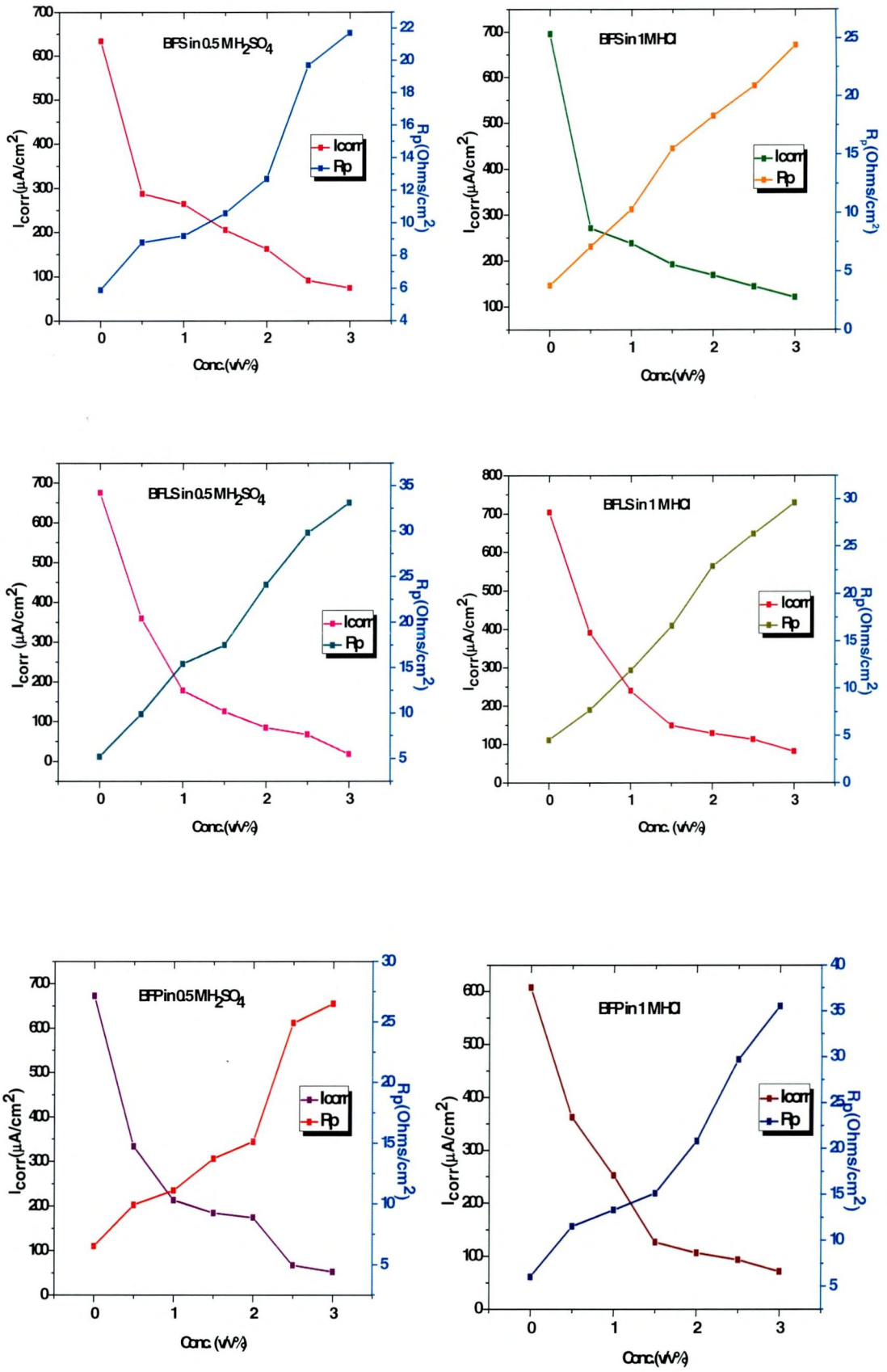

Figure – 50.b Plot of I_{corr} and R_p with respect to concentrations of BF extracts

The linear polarization resistance data confirmed an increase in R_p values with increase in concentration of BFLS extract in 0.5 M H_2SO_4 and 1 M HCl. Calculated protection ability using R_p was found to be 84% and 84% at 3.0%v/v concentration in 0.5 M H_2SO_4 and 1 M HCl for the maximum R_p values of 33.1 Ω/cm^2 and 29.6 Ω/cm^2 in 0.5 M H_2SO_4 and 1 M HCl respectively.

Protection ability evaluated from R_p values increased from 6.5 to 26.5 $\Omega/cm^2$and from 6.0 to 35.5 Ω/cm^2 for BFP extract in 0.5 M H_2SO_4 and 1 M HCl and inhibition efficiencies were found to be 75% and 83% at 3.0%v/v concentration respectively. The results of the study indicated that the addition of inhibitor increased the slope of the curve and hence the polarization resistance R_p distinctly increased when mild steel was exposed to the acid extracts of shell, leaf stalk and peduncle of CN and BF (Figure-50a and b).This supports that the plant extracts have excellent inhibitive action on the surface of mild steel. The greater inhibitive power of studied inhibitors can be explained by the presence of -OCH_3 and phenyl groups in the phytochemical constituents which are generally assumed to be active centre of adsorption **(Afidah A. Rahim, 2007)**. Another significant feature is that the current plant extracts have larger size of molecules. During the adsorption process, one molecule were expected to replace by much more water molecules and cover the metal surface more efficiently.

The enhanced inhibition ability of studied inhibitors was explained by the adsorption of molecules through the presence of unshared electron pairs of oxygen atom, π electrons of benzene ring and double bonds present in the phytochemical constituents.

4.6.3 ELECTROCHEMICAL IMPEDANCE SPECTROSCOPY (EIS)

Electrochemical impedance spectroscopy (EIS) is a well-established and powerful tool in the study of corrosion. Surface properties, electrode kinetics and mechanistic information can be obtained from the impedance diagrams **(Lorenz and Mansfeld, 1981)**. The influence of studied inhibitor on the impedance datas are discussed below.

4.6.3.1 Electrochemical impedance studies of MS by the addition of shell, leaf stalk and peduncle extracts for CN in 0.5 M H_2SO_4 and 1 M HCl

a. CNS extract

The electrochemical impedance measurements were carried out at open circuit potential. Figure-51 (a and b) show the EIS diagrams obtained as Nyquist plots in the absence and presence of different concentrations of CNS on mild steel corrosion in acid media. Table-44 summarized the parameters associated with the impedance diagrams. The obtained diagram for MS in both acid media as shown in

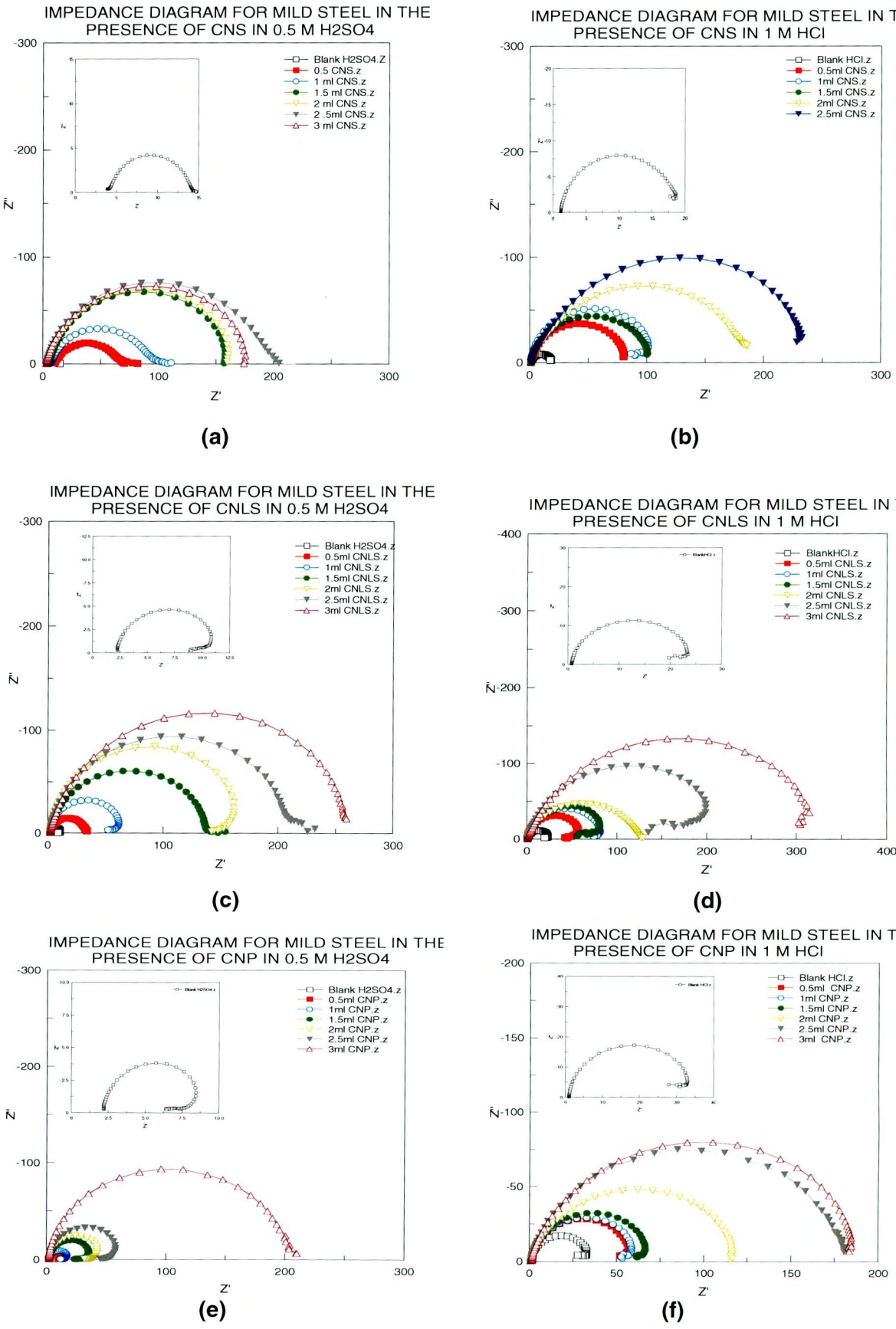

Figure – 51 Impedance diagram for mild steel in the presence of CN extracts in 0.5 M H_2SO_4 and 1 M HCl

Figure-51 (a and b) is not perfect semicircle, generally attributed to the frequency dispersion. The diameter of this capacitive loop increases with increasing concentration and then the charge transfer resistance R_{ct} increases from the value of 10.3 Ωcm^2 for the blank 0.5 M H_2SO_4 acid to 190.4 Ωcm^2 and 17.9 Ωcm^2 for the blank 1 M HCl to 296.5 Ωcm^2 for the highest concentration (3.0%v/v) of CNS extract, respectively. The interfacial double layer capacitance C_{dl} decreases from 271 $\mu F/cm^2$ for the blank 0.5 M H_2SO_4 to 90 $\mu F/cm^2$ and 241 $\mu F/cm^2$ for the blank 1 M HCl to 54 $\mu F/cm^2$, for CNS extract, respectively. Maximum IE afforded using CNS extract in 0.5 M H_2SO_4 and 1 M HCl media was found to be 94 % and 93% respectively. The analysis of the EIS parameters shows that the R_{ct} when the CNS extract concentration increases, giving consequently a decrease in the corrosion rate. It is important to emphasize that the values of C_{dl} decrease with increasing concentration of inhibitors for the same immersion time. The double layer between the charged metal surface and the solution is considered as an electrical capacitor. The adsorption of CNS extract on the steel decreases its electrical capacity because they displace the water molecules and others ions originally adsorbed on the surface. This decrease may be due to the adsorption of the CNS extract on the metal surface leading to a film formation on the steel surface **(Martinez and Stern, 2002)**.

Table - 44 Electrochemical impedance of MS in CNS extract in 0.5 M H_2SO_4 and 1 M HCl

Conc. (%v/v)	CNS in 0.5 M H_2SO_4				CNS in 1 M HCl			
	R_{ct} (Ωcm^2)	IE (%)	C_{dl} ($\mu F/cm^2$)	θ	R_{ct} (Ωcm^2)	IE (%)	C_{dl} ($\mu F/cm^2$)	θ
Blank	10.3	-	271	-	17.9	-	241	-
0.5	58.4	82	267	0.014	81.0	77	165	0.314
1.0	85.4	87	198	0.268	99.3	81	106	0.561
1.5	172.3	94	195	0.278	102.2	82	91	0.623
2.0	175.3	94	169	0.375	186.4	90	68	0.715
2.5	184.4	94	122	0.550	244.0	92	60	0.750
3.0	190.4	**94**	90	0.666	296.5	**93**	54	0.775

The decrease in C_{dl} values (Figure-51.a and b) may be due to a decrease of local dielectric constant **(McCafferty and Hackerman, 1972)** or by an increase of the thickness of the adsorbate layer of inhibitor at the metal surface **(Bastidas *et al.*, 2000)**. Surface coverage in 1 M HCl and 0.5 M H_2SO_4 was found to be 0.666 and 0.775 respectively.

b. Electrochemical impedance studies of MS in the presence of CNLS extract

The Nyquist plots for MS in the acid media in the presence and in absence of various concentrations of CNLS extract as shown in Figure-51(c and d) are is perfect

semicircles, which is attributed to non-homogeneity of the surface and roughness of the metal **(Bentiss *et al.*, 2009)**. From the plots, it could be seen that impedance response of mild steel is increased by the addition of CNLS extract **(Ahamad and Quraishi, 2009)**. The C_{dl} and R_{ct} values obtained from the Nyquist plots are listed in Table-45.

The R_{ct} values increases from the value of 8.9 Ωcm^2 for the blank 0.5 M H_2SO_4 acid to 263.9 Ωcm^2 and 23.1 Ωcm^2 for the blank 1 M HCl to 330.8 Ωcm^2 for the highest concentration (3.0%v/v) of CNLS extract, respectively, which shows protection of MS surface by the inhibitor.

Table - 45 Electrochemical impedance of MS in CNLS extract in 0.5 M H_2SO_4 and 1 M HCl

Conc.(%v/v)	CNLS in 0.5 M H_2SO_4				CNLS in 1 M HCl			
	R_{ct} (Ωcm^2)	IE (%)	C_{dl} ($\mu F/cm^2$)	θ	R_{ct} (Ωcm^2)	IE (%)	C_{dl} ($\mu F/ cm^2$)	θ
Blank	8.9	-	189	-	23.1	-	294	-
0.5	30.8	71	179	0.054	83.1	72	153	0.477
1.0	62.7	85	168	0.113	84.1	72	145	0.505
1.5	137.1	93	86	0.545	92.7	74	82	0.719
2.0	170.2	94	75	0.603	124.4	81	61	0.792
2.5	208.8	95	40	0.786	213.2	89	42	0.855
3.0	263.9	**96**	33	0.823	330.8	**92**	28	0.902

The interfacial double layer capacitance C_{dl} decreases from 189 $\mu F/cm^2$ for the blank 0.5 M H_2SO_4 to 33 $\mu F/cm^2$ and 294 $\mu F/cm^2$ for the blank 1 M HCl to 28 $\mu F/cm^2$ for the highest concentration (3.0%v/v) of CNLS extract, respectively, which is due to the increase in the thickness of protective layer at higher concentrations. Inhibition efficiency, calculated from the values of R_{ct}, was found to be maximum at a concentration of 3.0%v/v of the CNLS extract for the acid media. CNLS in 0.5 M H_2SO_4 and 1 M HCl could furnish 96% and 92% IE respectively. Surface coverage calculated using C_{dl} values was observed as 0.823 (in 0.5 M H_2SO_4) and 0.902 (in 1 M HCl).

c. Electrochemical impedance studies of MS in the presence of CNP extract

Figure-51 (e and f) show the Nyquist plot obtained at the open circuit potential (E_{corr}). Table-46 summarized the impedance data extracted from EIS experiments carried out both in the absence and presence of increasing concentrations of CNP extract in the acid media. The semicircular appearance of Nyquist plot indicated that the charge transfer process takes place during dissolution **(Muralidharan et al., 1995)**. From the curves it is clear that the impedance response for mild steel in uninhibited acid solution has significantly changed after the addition of inhibitor. The fact that impedance diagrams have an approximately semicircular appearance shows

that the corrosion of mild steel in both the acid media was controlled by a charge-transfer process. By increasing the inhibitor concentrations, the R_{ct} values increased from 4.6 Ωcm^2 for the blank 0.5 M H_2SO_4 acid to 202.7 Ωcm^2 and 33.4 Ωcm^2 for the blank 1 M HCl to 208.4 Ωcm^2 for the highest concentration (3.0%v/v) of CNP extract, respectively. R_{ct} values in the presence of CNP extract in 0.5 M H_2SO_4 and 1 M HCl yielded maximum IE of 97% and 83% respectively. The interfacial double layer capacitance C_{dl} decreases from 233 $\mu F/cm^2$ for the blank 0.5 M H_2SO_4 to 69 $\mu F/cm^2$ and 226 $\mu F/cm^2$ for the blank 1 M HCl to 52 $\mu F/cm^2$ for the highest concentration (3.0%v/v) of CNP extract, respectively, which causes an enhancement of inhibition efficiency. The most pronounced effect and the highest R_{ct} was obtained at 3.0%v/v concentration of inhibitor. The decrease in C_{dl} can result from the decrease of the local dielectric constant and/or from the increase of thickness of the electrical double layer, which suggests an adsorption of the inhibitor molecules on the mild steel surface. **McCafferty and Hackerman (1972)** attributed the change in C_{dl} values to the gradual replacement of water molecules by the adsorption of the organic molecules on the metal surface, decreasing the extent of metal dissolution. The increase in the C_{dl} values in the acid media in the presence of increasing CNP concentration may be a result of decreasing surface heterogeneity due to inhibitor adsorption on the most active adsorption sites **(Popova and Christov, 2007)**.

Table - 46 Electrochemical impedance of MS in CNP extract in 0.5 M H_2SO_4 and 1 M HCl

Conc. (%v/v)	CNP in 0.5 M H_2SO_4				CNP in 1 M HCl			
	R_{ct} (Ωcm^2)	IE (%)	C_{dl} ($\mu F/cm^2$)	θ	R_{ct} (Ω cm^2)	IE (%)	C_{dl} ($\mu F/$ cm^2)	θ
Blank	4.6	-	233	-	33.4	-	226	-
0.5	10.4	55	201	0.133	58.2	42	201	0.111
1.0	11.4	59	193	0.170	60.4	44	195	0.135
1.5	27.9	83	121	0.480	68.7	51	173	0.235
2.0	33.7	86	85	0.634	120.1	72	79	0.651
2.5	47.9	90	76	0.673	181.6	81	66	0.704
3.0	202.7	**97**	69	0.702	208.4	**83**	52	0.769

4.6.3.2 Electrochemical impedance studies of MS in the addition of shell, leaf stalk and peduncle extract of BF in 0.5 M H_2SO_4 and 1 M HCl

a. BFS extract

Corrosion behaviour of mild steel in both corrosive media in the presence of BFS extract was investigated by EIS at room temperature and is given in Figure-52

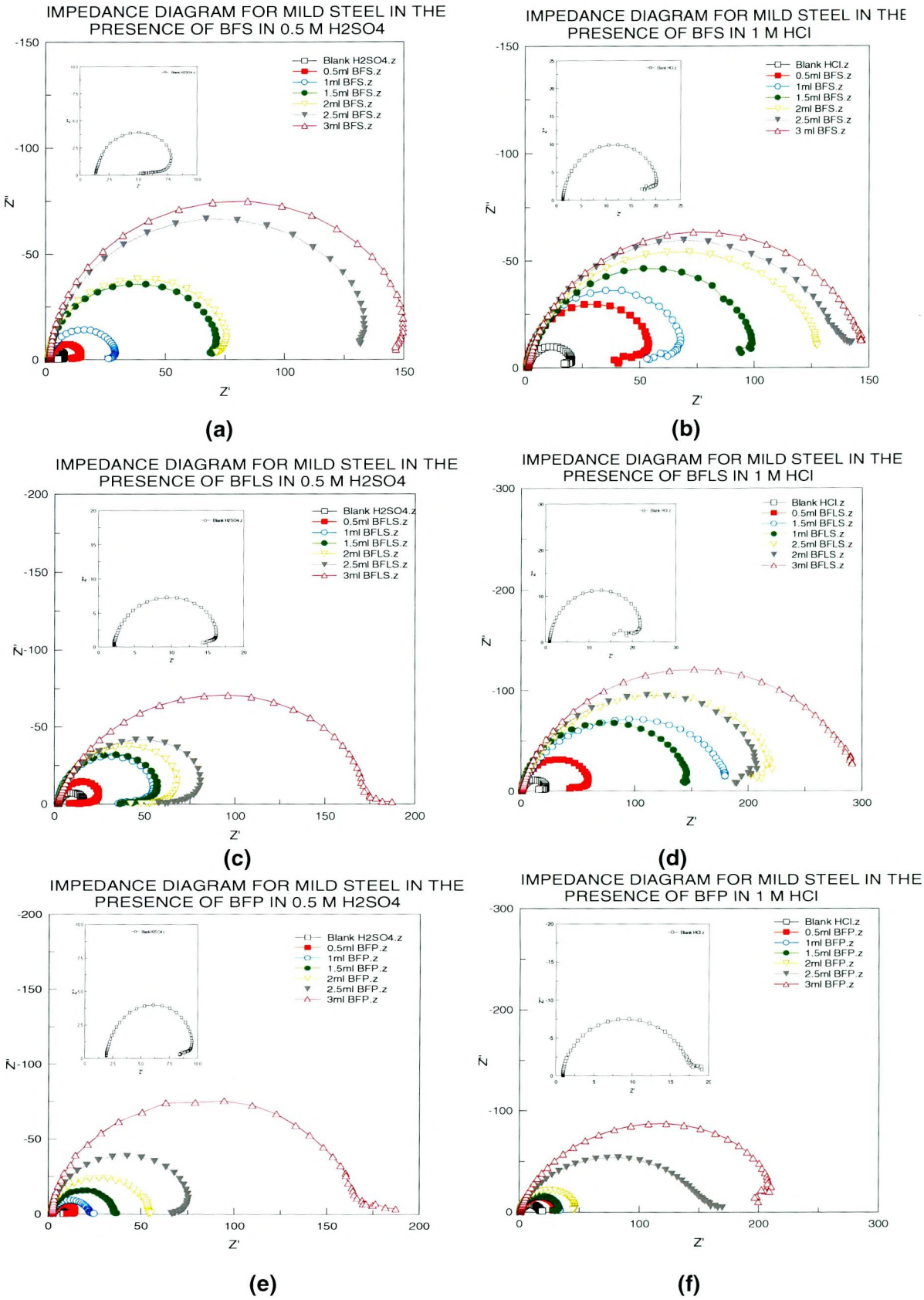

Figure - 52 Impedance diagram for mild steel in the presence of BF extracts in 0.5 M H_2SO_4 and 1 M HCl

(a and b). Various impedance parameters such as charge transfer resistance (R_{ct}), double layer capacitance (C_{dl}) and IE (%) are given in Table-47. The impedance diagrams obtained are not perfect semicircles. This feature had been attributed to frequency dispersion. The results can be interpreted in terms of equivalent circuit of the double layer shown in Figure-52 (a and b) which has been used previously to model the iron/acid interface.

Table - 47 Electrochemical impedance of MS in BFS extract in 0.5 M H_2SO_4 and 1 M HCl

Conc. (%v/v)	BFS in 0.5 M H_2SO_4				BFS in 1 M HCl			
	R_{ct} (Ωcm^2)	IE (%)	C_{dl} ($\mu F/ cm^2$)	θ	R_{ct} (Ω cm^2)	IE (%)	C_{dl} ($\mu F/ cm^2$)	θ
Blank	6.6	-	245	-	20.0	-	222	-
0.5	14.1	53	219	0.106	55.2	63	157	0.289
1.0	28.6	76	210	0.142	70.3	71	148	0.331
1.5	68.4	90	159	0.349	101.6	80	129	0.415
2.0	72.3	90	157	0.357	130.6	84	105	0.524
2.5	131.0	94	139	0.433	138.2	85	92	0.582
3.0	147.2	95	**95**	0.612	149.0	86	**87**	0.605

The semicircle in all cases corresponds to a capacitive loop. The semicircle radii depend on the concentration of BFS extract. The diameter of the capacitive loop increases with increasing the concentration of BFS extract. It should be noted from Table-58 that R_{ct} values increase from 6.6 Ωcm^2 for the blank 0.5 M H_2SO_4 acid to 147.2 Ωcm^2 and 20 Ωcm^2 for the blank 1 M HCl to 149.0 Ωcm^2 for the highest concentration (3.0%v/v) of BFS extract, respectively furnishing 95% IE in 0.5 M H_2SO_4 and 87% IE in 1 M HCl. The interfacial double layer capacitance C_{dl} decreases from 245 $\mu F/cm^2$ for the blank 0.5 M H_2SO_4 to 95 $\mu F/cm^2$ and 222 $\mu F/cm^2$ for the blank 1 M HCl to 87 $\mu F/cm^2$ for the highest concentration (3.0%v/v) of BFS extract with increase in concentration of inhibitor, and the decrease in capacitance values indicated the formation of a surface film. θ values were found to be 0.612 in 0.5 M H_2SO_4 and 0.605 in 1 M HCl.

b. Electrochemical impedance studies of MS in the presence of BFLS extract

The Nyquist plots of the impedance behaviour of MS in 0.5 M H_2SO_4 and 1 M HCl in the presence of various concentrations of BFLS extract is shown in Figure-52 (c and d). The existence of a single semicircle shows the presence of single charge transfer process during dissolution which is unaffected by the presence of inhibitor molecule. The slightly depressed nature of semicircle is the characteristic for solid electrodes and such frequency dispersion has been attributed to roughness and other inhomogeneties of the solid electrode. The charge transfer resistance (R_{ct}) and the interfacial double layer (C_{dl}) values derived from these curves are listed in Table-

48. From the Table-48 it is obvious that R_{ct} values increase from 15.0 Ωcm^2 for the blank 0.5 M H_2SO_4 acid to 175.0 Ωcm^2 and 20.5 Ωcm^2 for the blank 1 M HCl to 298.3 Ωcm^2 for the highest concentration (3.0%v/v) of BFLS extract, respectively.

Table - 48 Electrochemical impedance of MS in BFLS extract in 0.5 M H_2SO_4 and 1 M HCl

Conc. (%v/v)	BFLS in 0.5 M H_2SO_4				BFLS in 1 M HCl			
	R_{ct} (Ωcm^2)	IE (%)	C_{dl} ($\mu F/ cm^2$)	θ	R_{ct} (Ω cm^2)	IE (%)	C_{dl} ($\mu F/ cm^2$)	θ
Blank	15.0	-	198	-	20.5	-	264	-
0.5	25.4	40	176	0.110	60.0	65	170	0.353
1.0	57.1	73	168	0.152	150.0	86	150	0.430
1.5	68.4	77	157	0.208	191.9	89	129	0.510
2.0	71.0	78	94	0.525	224.7	90	91	0.654
2.5	85.0	82	79	0.600	232.3	91	85	0.678
3.0	175.0	**91**	64	0.676	298.3	**93**	80	0.694

Accordingly the IE(%) of BFLS was found to be 91% and 93% in 0.5 M H_2SO_4 and 1 M HCl respectively. The interfacial double layer capacitance C_{dl} decreases from 198 $\mu F/cm^2$ for the blank 0.5 M H_2SO_4 to 64 $\mu F/cm^2$ and 264 $\mu F/cm^2$ for the blank 1 M HCl to 80 $\mu F/cm^2$ for the highest concentration (3.0%v/v) of BFLS extract with increase in the inhibitor concentration. BFLS extract shows maximum inhibition efficiency (91% in 0.5 M H_2SO_4 and 93% in 1 M HCl) at the maximum concentration (3.0%v/v).

c. Electrochemical impedance studies of MS in the presence of BFP extract

The corrosion behaviour of mild steel in 0.5 M H_2SO_4 and 1 M HCl with and without BFP extract is also investigated by the electrochemical impedance spectroscopy (EIS) at room temperature. The charge-transfer resistance (R_{ct}) values are calculated from the difference in impedance at lower and higher frequencies, as suggested by **Tsuru *et al.*, (1978)**. Nyquist plots for mild steel in acid media at

Table - 49 Electrochemical impedance of MS in BFP extract in 0.5 M H_2SO_4 and 1 M HCl

Conc.(%v/v)	BFP in 0.5 M H_2SO_4				BFP in 1 M HCl			
	R_{ct} (Ω cm^2)	IE%	C_{dl} ($\mu F/$ cm^2)	θ	R_{ct} (Ω cm^2)	IE%	C_{dl} ($\mu F/$ cm^2)	θ
Blank	7.8	-	349	-	16.6	-	382	-
0.5	12.6	38	306	0.123	30.8	45	294	0.230
1.0	20.6	61	284	0.186	33.6	50	251	0.342
1.5	34.0	76	255	0.269	34.0	54	182	0.523
2.0	51.9	84	141	0.595	46.6	64	123	0.678
2.5	75.7	89	106	0.696	157.9	89	59	0.845
3.0	164.5	**95**	82	0.765	221.1	**92**	53	0.861

various concentrations of BFP extract is presented in Figure-52 (e and f). Table-49 gives values of charge transfer resistance, R_{ct} double layer capacitance, C_{dl}, derived from Nyquist plots and inhibition efficiency. Figure-52 (e and f) reveals that the impedance spectra exhibit one single depressed semicircle, and the diameters of

semicircle increases with the inhibitor concentration. The single semicircle can be attributed to the charge transfer that takes place at electrode/solution interface, and the transfer process controls the corrosion reaction of steel and the presence of inhibitor does not change the mechanism of dissolution of steel **(Larabi *et al.*, 2004)**. It is also clear that these impedance diagrams consists of one large capacitive loop and they are not perfect semicircles and this difference has been attributed to frequency dispersion **(Mansfeld *et al.*, 1981)** and the heterogeneity of the metal surface **(Juttner, 1990)**.

From the electrochemical impedance data (Table-49), it is clear that the R_{ct} values increase from 7.8 Ωcm^2 for the blank 0.5 M H_2SO_4 acid to 164.5 Ωcm^2 and 16.6 Ωcm^2 for the blank 1 M HCl to 221.1 Ωcm^2 for the highest concentration (3.0%v/v) of BFP extract, respectively. The interfacial double layer capacitance C_{dl} decreases from 349 $\mu F/cm^2$ for the blank 0.5 M H_2SO_4 to 82 $\mu F/cm^2$ and 382 $\mu F/cm^2$ for the blank 1 M HCl to 53 $\mu F/cm^2$ for the highest concentration (3.0%v/v) with increase in the inhibitor concentration and consequently the inhibition efficiency increases to 95% in 0.5 M H_2SO_4 and 92% in 1M HCl at 3.0%v/v concentration of the BFP extract. In fact, the presence of BFP extract is accompanied by the increase of the value of R_{ct} in acidic solution confirming a charge transfer process mainly controlling the corrosion of mild steel. Values of double layer capacitance are also brought down to the maximum extent in the presence of inhibitor and the decrease in the values of C_{dl} follows the order similar to that obtained for I_{corr} in this study. The decrease in C_{dl} is due to the adsorption of the inhibitor on the metal surface leading to the formation of film or complex from acidic solution **(Bentiss *et al.*, 1999)**.

Variation of R_{ct} and C_{dl} of MS in Shell, Leaf Stalk and Peduncle for CN and BF extracts in 0.5 M H_2SO_4 and 1 M HCl

The values of R_{ct} and C_{dl} of MS by addition of different concentrations of Shell, Leaf Stalk and Peduncle for CN and BF extracts in 0.5 M H_2SO_4 and 1 M HCl, respectively are shown in Figure-53 (a and b). The data's indicate that increasing charge transfer resistance is associated with a decrease in the double layer capacitance. The decrease in the C_{dl} values could be attributed to the adsorption of the chemical constituents of CN and BF extracts, respectively, at the MS surface. It has been reported that the adsorption process on the metal surface is characterized by a decrease in C_{dl} **(Abdel-Gaber *et al.*, 2006b)**.

The phenomenon for these extracts can be explained on the basis that different chemical compounds could be extracted from CN and BF plant. Since, it is well known that the adsorption process depends on the electronic characteristics of the inhibitors. The natural substances are very complex and also very active.

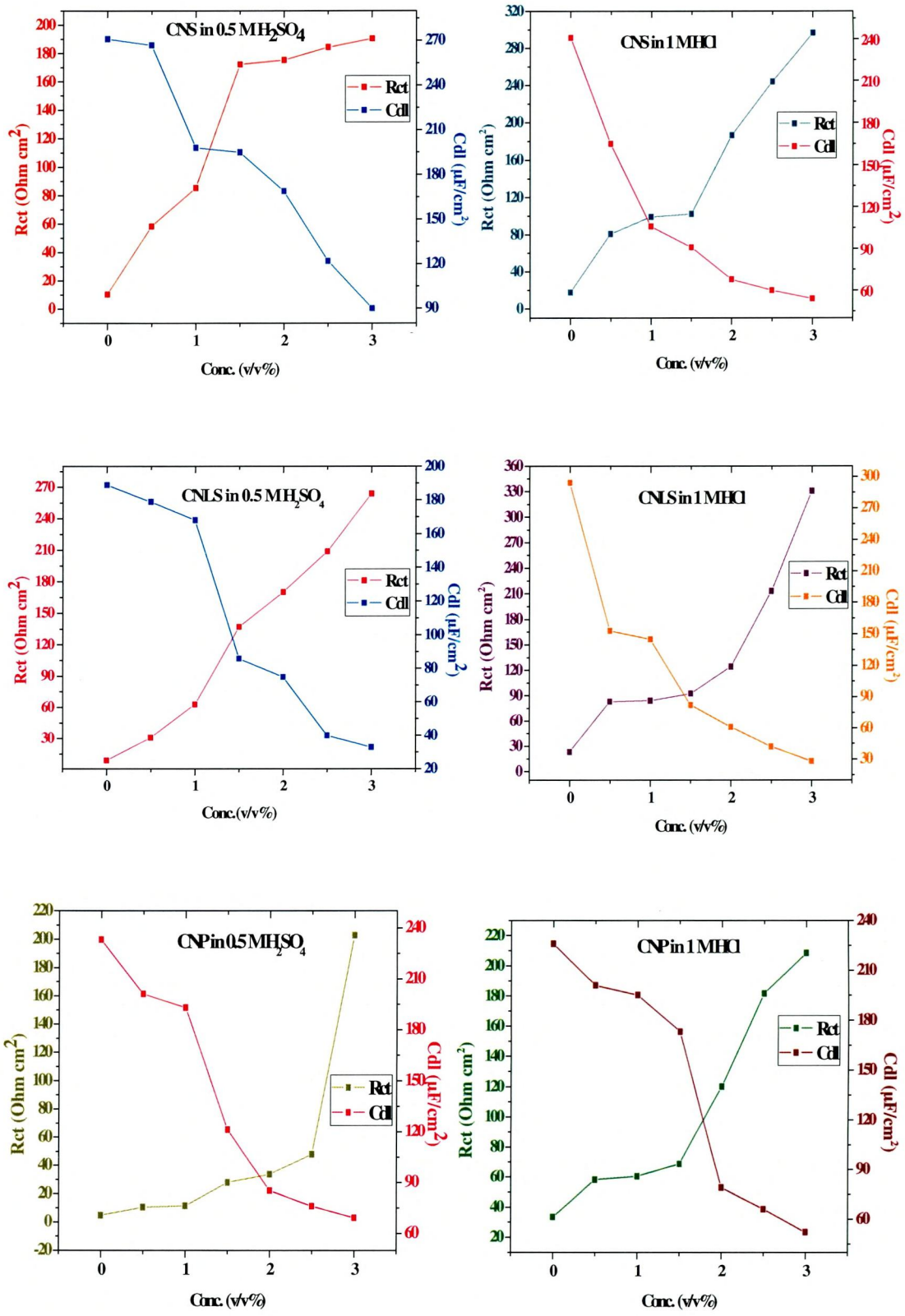

Figure – 53.a Variation of R_{ct} and C_{dl} values against the various concentration of CN extracts

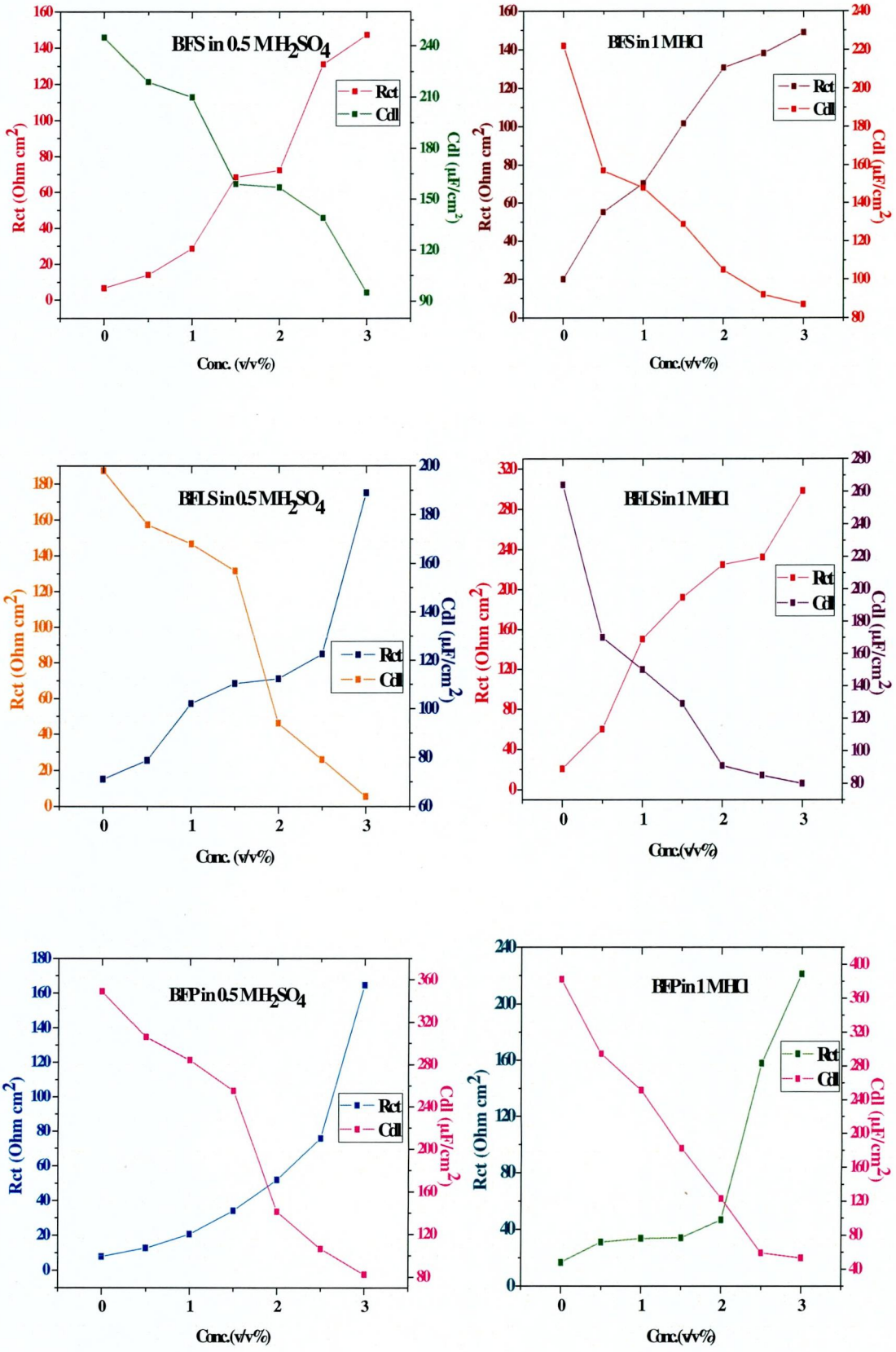

Figure - 53.b Variation of R_{ct} and C_{dl} values against the various concentration of BF extracts

Variation of C_{dl} versus surface coverage (θ) of MS in Shell, Leaf Stalk and Peduncle for CN and BF extracts in 0.5 M H_2SO_4 and 1 M HCl

The analysis of the EIS parameters shows that the R_{ct} when the CNS concentration increases, giving consequently a decrease in the corrosion rate. It is important to emphasize that the values of C_{dl} decrease with increasing concentration of inhibitors for the same immersion time. The double layer between the charged metal surface and the solution is considered as an electrical capacitor. The adsorption of CNS on the steel decreases its electrical capacity because they displace the water molecules and others ions originally adsorbed on the surface. This decrease may be due to the adsorption of the inhibitor on the metal surface leading to a film formation on the steel surface **(Martinez and Stern, 2002).** The decrease of the double layer capacitance C_{dl} may be discussed using the following relation:

$$C_{dl} = \frac{\varepsilon_o \varepsilon}{\delta} S \qquad (4.17)$$

where δ is the thickness of the deposit, S is the surface of the electrode, ε_o is the permittivity of the air and ε is the medium dielectric constant. The relation shows that the decrease in C_{dl} values (Figure-54 a and b) may be due to a decrease of local dielectric constant ε **(McCafferty and Hackerman, 1972)** or by an increase of the thickness of the adsorbate layer of inhibitor at the metal surface **(Bastidas *et al.*, 2000)**.

A plot of C_{dl} values in the presence of inhibitor concentration versus surface coverage (θ) is drawn. A straight line is obtained. The linear decrease of C_{dl} with the surface coverage means that the capacitance contribution from the inhibitor covered surface is solely due to the flat-adsorbed molecules at low surface coverage **(Martinez and Metikos-Hukovic, 2003)** (Figure-54 a and b). Similar plots are drawn for all the studied inhibitors, which confirm that the inhibitor molecules that are adsorbed flatly on the metal surface.

The values of IE(%) obtained from EIS, polarization and gravimetric methods are in good agreement.

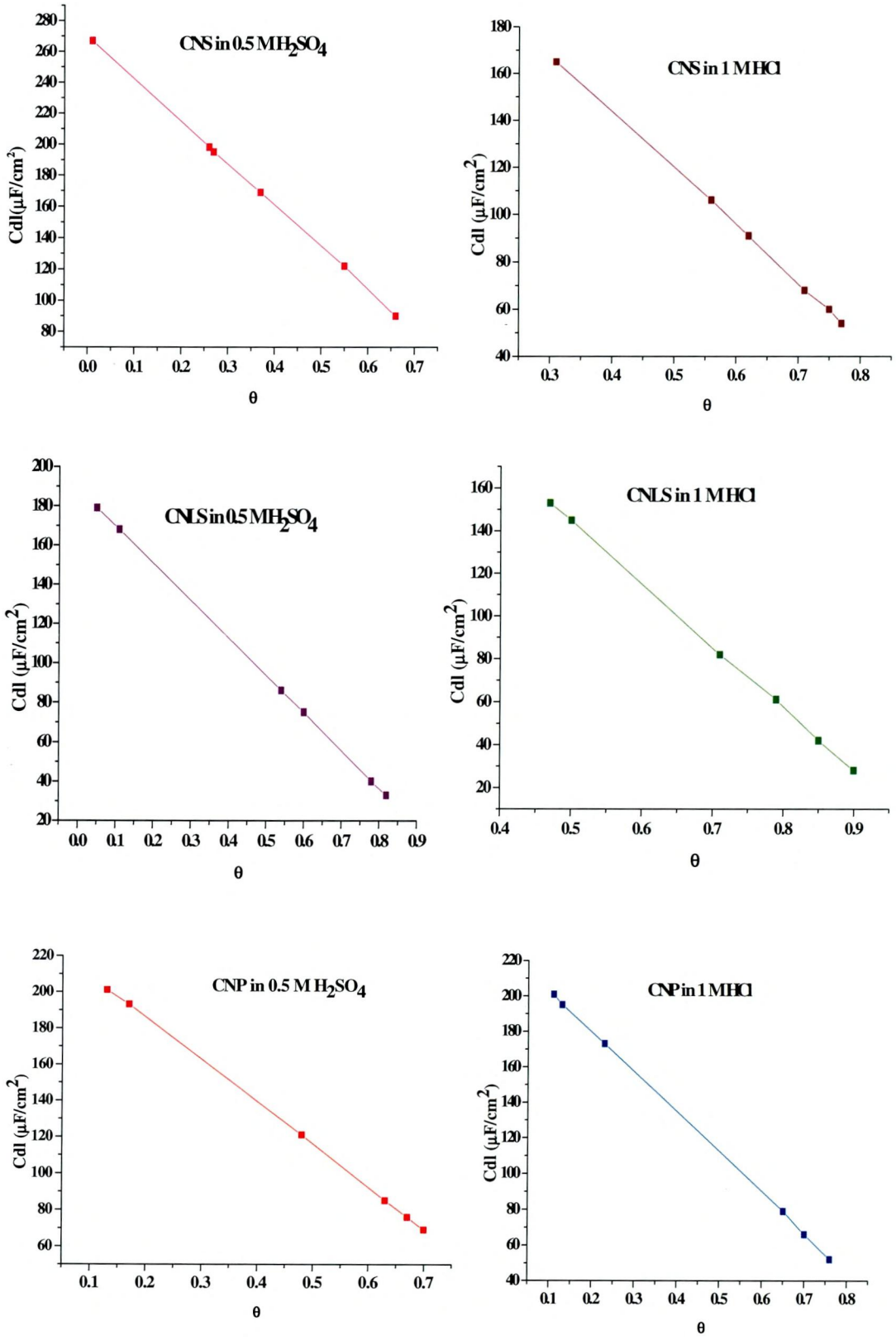

Figure – 54.a Variation of C_{dl} versus surface coverage (θ) of MS for CN extracts in 0.5 M H_2SO_4 and 1 M HCl

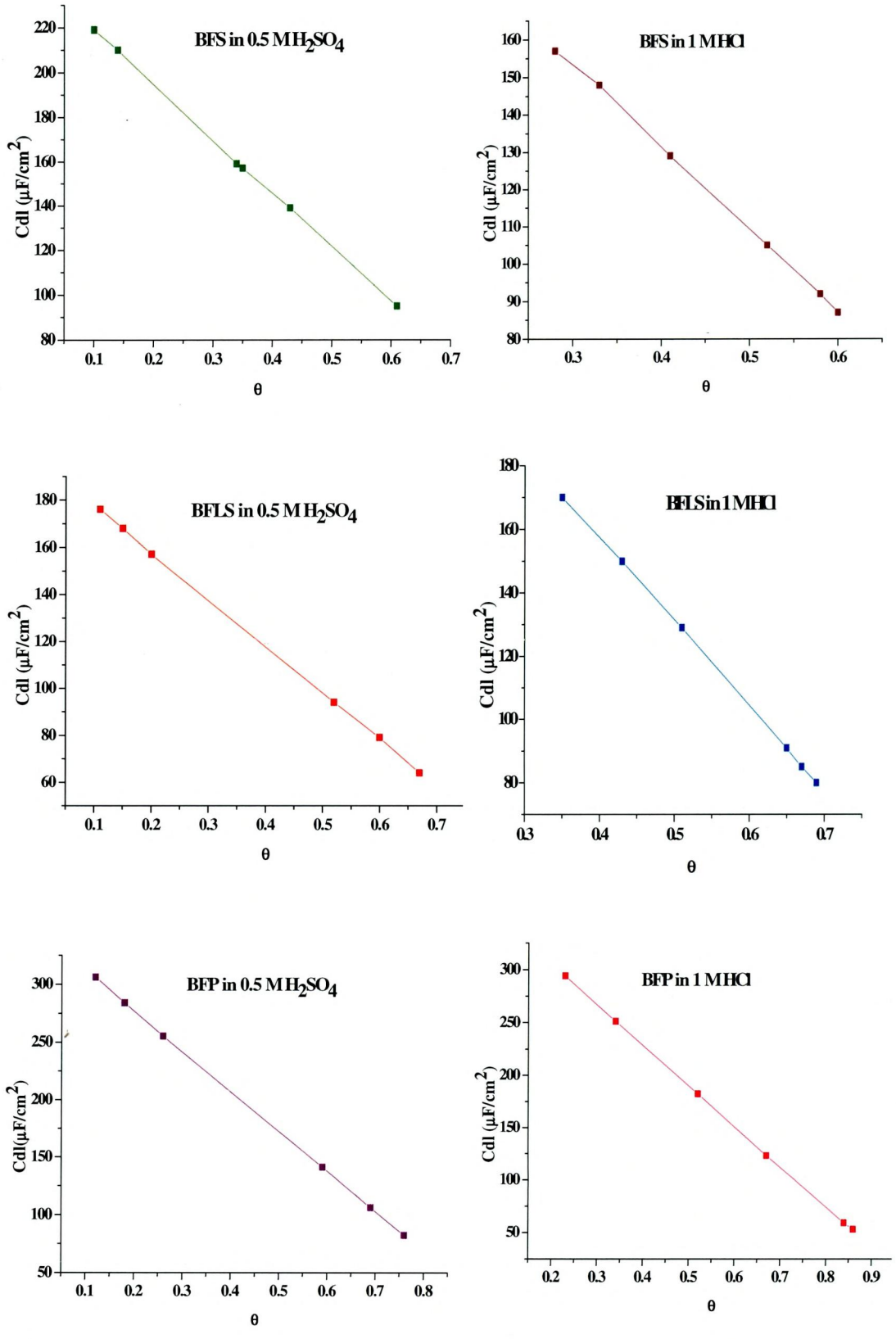

Figure – 54.b Variation of C_{dl} versus surface coverage (θ) of MS for BF extracts in 0.5 M H_2SO_4 and 1 M HCl

Performance evaluation of CN and BF extracts on MS acid corrosion in both acidic media by various techniques

Figure-55 revealed that the results of mass loss and electrochemical measurement methods are in good agreement within the experimental error. The difference in inhibition efficiency values obtained by mass loss and electrochemical techniques can be attributed to the fact that mass loss method gives average corrosion rates, whereas the electrochemical measurement gives instantaneous corrosion rates. The difference may be expected to arise because of the difference in time required to form an adsorbed layer, which brings down corrosion **(Vijayalakshmi *et al.*, 2011)**.

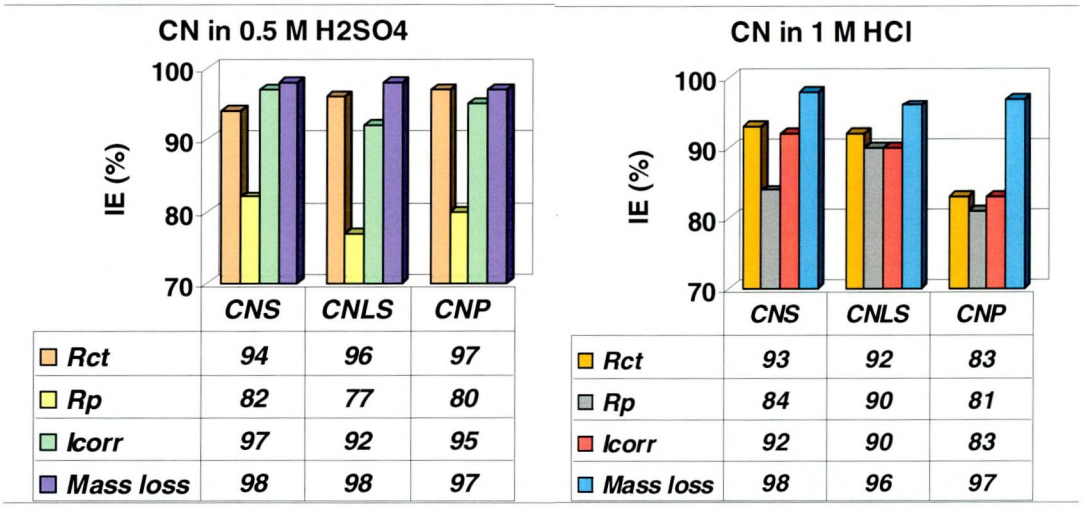

(a)

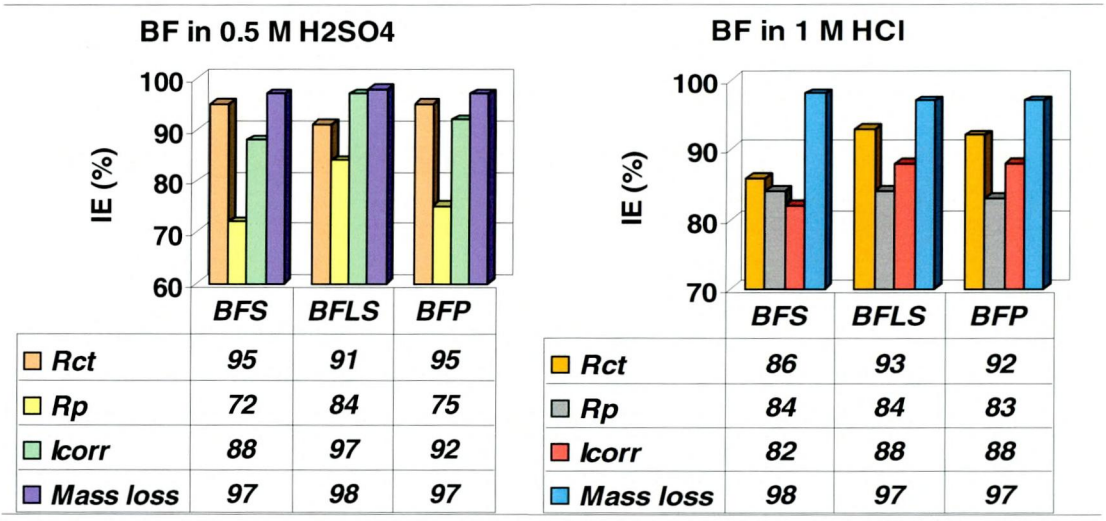

(b)

Figure- 55 Comparison of inhibition efficiencies obtained from different methods for (a) CN and (b) BF extracts in 0.5 M H_2SO_4 and 1 M HCl

4.7 SURFACE ANALYTICAL TECHNIQUES

In the present investigation, surface of mild steel specimen exposed to the uninhibited and inhibited solutions have undertaken to supplement the results. The following surface analytical techniques have been used to study the surface of the mild steel in the presence and absence of the inhibitors.

- ✶ **Fourier Transform Infra Red Spectroscopy (FT-IR)**
- ✶ **Scanning Electron Microscope (SEM)**

4.7.1 FT-IR SPECTRAL STUDY OF THE INHIBITORS

FT-IR spectrum has been used to analyze the functional groups present in the corrosion product formed on metal surface.

4.7.1.1 FT-IR spectra of CN extract and corrosion product of CN extracts on MS surface in 0.5 M H_2SO_4 and 1 M HCl

Table-5 shows that FT-IR spectrum of CN extracts Figure-56 shows the corrosion product of CN extracts on mild steel surface in 0.5 M H_2SO_4 and 1 M HCl. Observed IR frequencies for the corrosion product of CN extracts are presented in Table-50. By comparing the spectrum of scratched film with that of CN extract, it can be interpreted as:

a. In 0.5 M H_2SO_4:

Analysis of FT-IR spectra of **CNS** and corrosion products of CNS are presented in Figure- 56.a, it is noted that the O-H stretch has shifted from 3434.69 cm^{-1} to 3367.0 cm^{-1}, the C=C stretching frequency has slightly shifted from 1639.44 to 1637.7 cm^{-1}, the C-O stretch has shifted from 1054.39 to 1117.7 cm^{-1}. In Figure-56.b (**CNLS** and corrosion products of CNLS), the IR spectra of the phytochemical compounds adsorbed on the metal surface reveal the presence of functional group peaks whose absorption frequencies corresponds to O-H stretch (shifted from 3423.14 to 3367.3 cm^{-1}), C=C stretch (shifted from 1637.11 to 1637.4 cm^{-1}), C-O stretch (shifted from 1055.86 to 11181. cm^{-1}). Figure-56.c represents the FT-IR spectrum of **CNP** and corrosion products of CNP. The shift in the O-H stretch frequency (3389.17 cm^{-1}) to lower wavenumber (3367.7 cm^{-1}), the shift in the C=C stretch (1595.82 cm^{-1}) to higher wavenumber. (1636.6 cm^{-1}) and the shift in the C-O stretch (1057.61 cm^{-1}) to higher wavenumber (1119.50 cm^{-1}). The shift in these absorption frequencies of the studied inhibitors on the mild steel surface strongly supports the interaction between the phytochemical compounds of the inhibitor and metal surface.

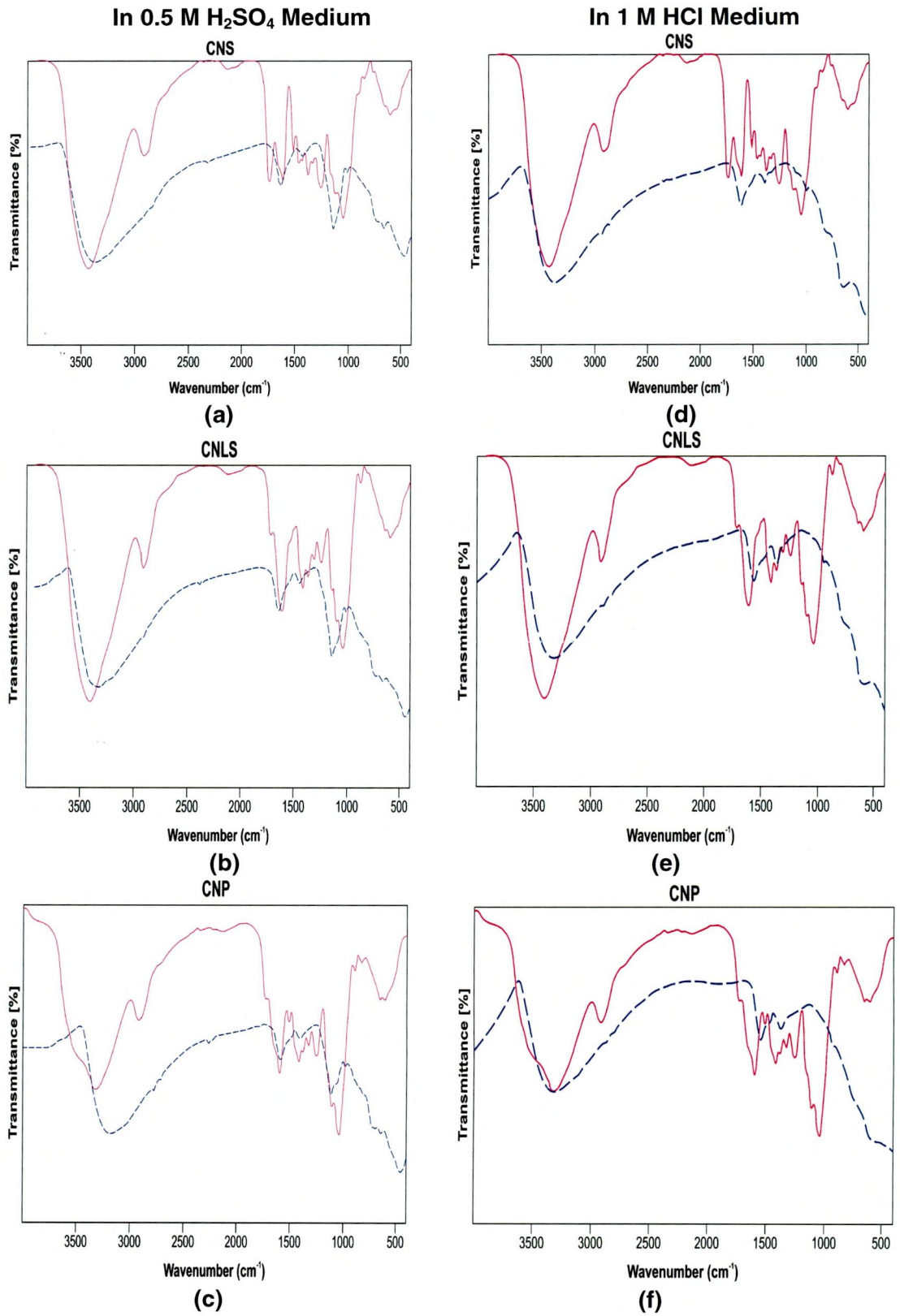

FT-IR spectra of CN extract.

FT-IR spectra of corrosion product of CN extract on MS surface.

Figure - 56 FT-IR spectra of CN extracts and corrosion product of CN extracts on MS surface in 0.5 M H_2SO_4 and 1 M HCl

However, for CNS the C-H stretch frequencies (2964.11 and 1377.29 cm^{-1}), the C=O stretch frequency (1714.97 cm-1), the C-O-C stretch frequency (1244.34 cm-1) have disappeared in the spectrum of the corrosion product indicating that these bonds might have been used for bonding between the vacant d orbital of Fe and the inhibitor. Similarly IR frequencies in the corrosion product of CNLS and CNP extracts on mild steel surface in 0.5 M H_2SO_4 have also been observed. The band at 400-700 cm^{-1} probably originates mainly from γ-Fe_2O_3 (680 cm^{-1}) **(Chauhan *et al.*, 2007).** This particular peak corresponding to γ-Fe_2O_3 has been found to be present in CNS, CNLS and CNP corrosion product also.

Table - 50 FT-IR peak values for corrosion product of CN extract in 0.5 M H_2SO_4 and 1 M HCl

Observed FT-IR frequency, (cm^{-1})						Assignment	Reference
0.5 M H_2SO_4			1 M HCl				
CNS	CNLS	CNP	CNS	CNLS	CNP		
3367.0	3367.3	3367.7	3367.1	3349.4	3368.2	O-H stretch	Chauhan, *et al.*, **2007**
1637.7	1637.4	1636.6	1637.8	1618.5	1618.3	C=C stretch	Ebenso, *et al.*, **2008**
1117.7	1118.1	1119.5	-	-	-	C-O stretch	Eddy, *et al.*, **2009a**
448.44	422.24	437.47	-	-	-	γ-Fe_2O_3	Chauhan, *et al.*, **2007**

b. In 1 M HCl

Figure-56.d represents the FT-IR spectra of **CNS** and corrosion products of CNS. It is observed that the O-H stretching frequency has shifted from 3434.69 cm^{-1} to 3367.1 cm^{-1} and the C=C stretching frequency has slightly shifted from 1639.44 to 1637.7 cm^{-1}. Figure-56.e. shows the FT-IR spectra of **CNLS** and corrosion products of CNLS. From the results, the O-H stretch at 3423.14 cm^{-1} has shifted to 3349.4 cm^{-1} and the C=C stretch at 1637.11 cm^{-1} has shifted to 1618.5 cm^{-1}. Analyzing the FT-IR spectra of **CNP** and corrosion products of CNP (Figure-56.f), it is noted that the O-H stretching frequency has shifted from 3389.17 cm^{-1} to 3368.2 $cm^{-1}$and the C=C stretch at 1595.82 cm^{-1} to 1618.3 cm^{-1}. These shifts in frequencies indicated that there are interaction between the studied inhibitors and the surface of mild steel. **(Eddy *et al.*, 2009d).**

However, for CNS,CNLS and CNP the C-H stretch, C=O stretch, C-H bend, C-O-C, C-O stretch and aromatic substituents frequency have vanished in the spectrum of the corrosion product indicating that these bonds might have used for the adsorption of the inhibitor on the surface of mild steel.

4.7.1.2 FT-IR spectra of BF extract and corrosion product of BF extracts on MS surface in 0.5 M H_2SO_4 and 1 M HCl

The peak observed for BF extracts shown in Table-10 and the corrosion product of BF extract on mild steel surface in 0.5 M H_2SO_4 and 1 M HCl shown in Figure-57. The peak values obtained from FT-IR analysis are shown in Table-51. By comparing the spectra of BF extract with that of scratched film it can be interpreted as:

a. In 0.5 M H_2SO_4

From the FT-IR spectra of the phytochemical compounds present in **BFS** and corrosion products of BFS (Figure-57.a) reveal the presence of functional group peaks whose absorption frequencies correspond to O-H (shifted from 3408.94 to 3368.0 cm^{-1}), the C=C (shifted from 1596.36 to 1637.4 cm^{-1}), the C-O (shifted from 1053.45 to 1120.8 cm^{-1}). FT-IR spectra of **BFLS** and corrosion products of BFLS are shown in Figure-57.b. The O-H stretching frequency has shifted from 3409.38 to 3367.3 cm^{-1}. The C=C stretching frequency has slightly shifted from 1642.86 to 1637.4 cm^{-1} and the C-O stretching frequency has also shifted 1053.22 cm^{-1} to 1121.4 cm^{-1}. Analysis of FT-IR spectra of **BFP** and corrosion products of BFP (Figure-57.c), it is noted that the O-H stretch has shifted from 3452.62 to 3368.8 cm^{-1}, the C=C stretching frequency has slightly shifted from 1639.54 to 1637.7 cm^{-1} and the C-O stretching frequency has also shifted 1055.18 cm^{-1} to 1121.5 cm^{-1}. The shift in these absorption frequencies of the studied inhibitors on the metal surface strongly supports the interaction between the phytochemical compounds of the inhibitor and metal surface.

The absorption frequencies pertaining to C-H stretch, C=O, C-H bend and C-O-C have disappeared from the spectrum of corrosion product of BFS. Hence the adsorption of BFS extract on mild steel might have taken place through these missing linkages. **(Bahrami *et al.*, 2010)**. Similarly IR frequencies in the corrosion product of BFLS and BFP extracts on mild steel surface in 0.5 M H_2SO_4 have also been observed. The band at 400-700 cm^{-1} probably originates mainly from γ-Fe_2O_3 (680 cm^{-1}) **(Abdel-Gaber *et al.*, 2006a)**. This particular peak corresponding to γ-Fe_2O_3 has been found to be present in BFS, BFLS and BFP corrosion product also.

b. 1 M HCl

From the spectra of **BFS** and corrosion products of BFS (Figure-57.d), it is observed that the O-H stretching frequency has shifted from 3408.94 to 3367.4 cm^{-1} and the C=C stretching frequency has also shifted from 1596.36 to 1618.3 cm^{-1}.

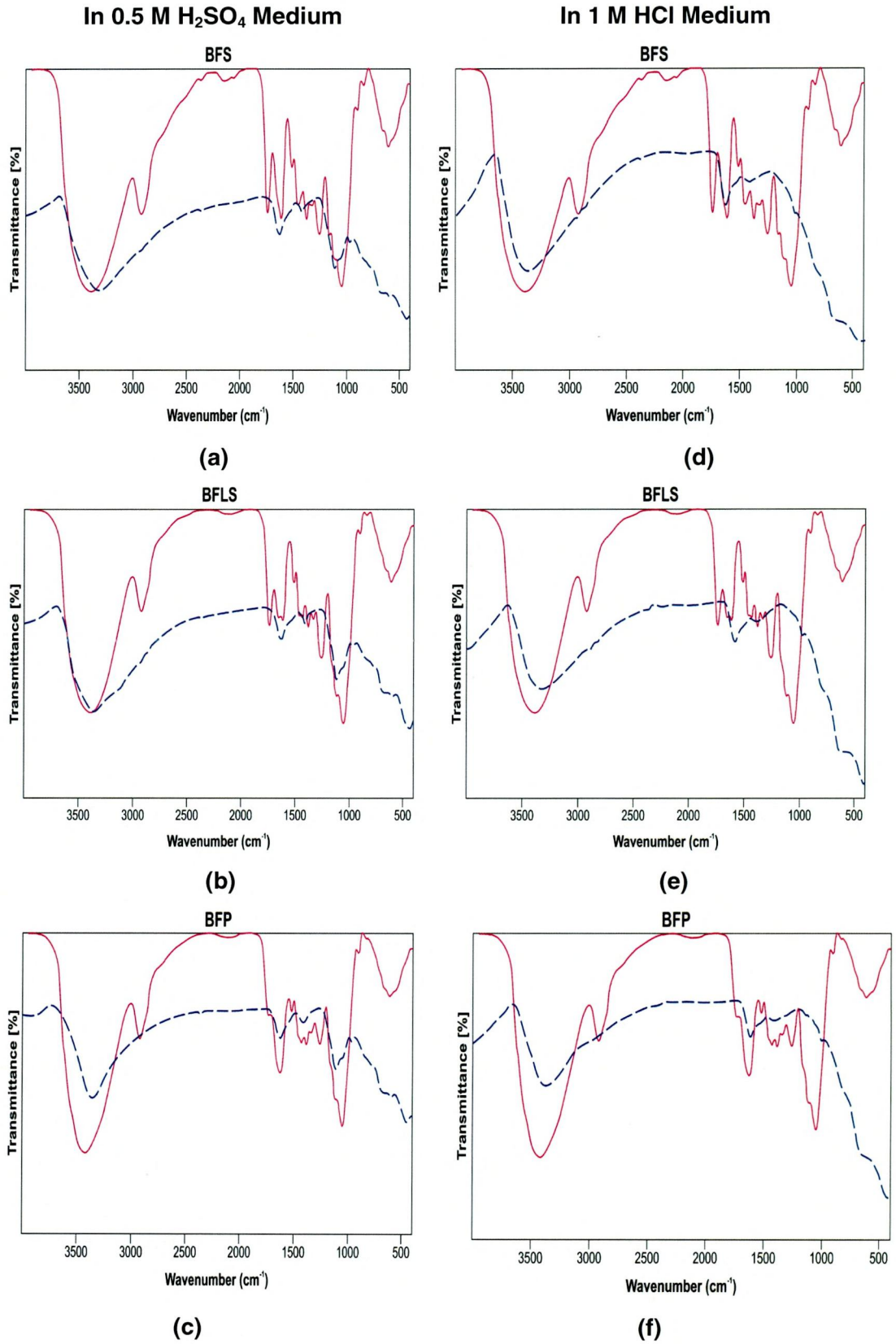

FT-IR spectra of BF extract.

FT-IR spectra of corrosion product of BF extract on MS surface.

Figure - 57 FT-IR spectra of BF extracts and corrosion product of BF extracts on mild steel surface in 0.5 M H_2SO_4 and 1 M HCl.

In **BFLS** and corrosion products of BFLS (Figure-57.e), it is experiential that the O-H stretching frequency has shifted from 3409.38 to 3367.3 cm^{-1} and the C=C stretching frequency is also shifted from 1642.86 to 1615.4 cm^{-1}. Analysis of FT-IR spectra of **BFP** and corrosion products of BFP (Figure-57.f), it is noted that the O-H stretching frequency has shifted from 3452.62 to 3362.9 cm^{-1}. The C=C stretching frequency is also shifted from 1639.54 to 1622.0 cm^{-1} **(Ebenso *et al.*, 2008).** In BFS, BFLS and BFP the functional groups ranging in frequencies C-H stretch, C=O stretch, C-H bend, C-O-C, C-O stretch and aromatic substituents frequency disappeared in the spectrum suggesting that the adsorption of the studied inhibitor on the surface of mild steel might have occurred through the missing bonds.

Table - 51 FT-IR peak values for corrosion product of BF extract in 0.5 M H_2SO_4 and 1 M HCl

Observed FT-IR frequency, (cm^{-1})						Assignment	Reference
0.5 M H_2SO_4			1 M HCl				
BFS	BFLS	BFP	BFS	BFLS	BFP		
3368.0	3367.3	3368.8	3367.4	3367.3	3362.9	O-H stretch	Chauhan, *et al.*, **2007**
1637.4	1637.4	1637.7	1618.3	1615.4	1622.0	C=C stretch	Ebenso, *et al.*, **2008**
1120.8	1121.4	1121.5	-	-	-	C-O stretch	Eddy, *et al.*, **2009**
460.27	439.96	461.24	-	-	-	γ-Fe_2O_3	Chauhan, *et al.*, **2007**

The shift in the absorption frequencies of the CN and BF extracts on the metal surface strongly has supported the interaction between the phytochemical compounds of the inhibitor and metal surface, thus confirming the inhibitors were the adsorptive type. FT-IR analysis of the CN and BF extracts and corrosion products of CN and BF extracts on mild steel surface reveals the iron-CN and iron-BF complex **(Jaen *et al.*, 1999).** Again the IR patterns of corrosion products are similar to the CN and BF extracts, though some shift in the frequencies of some functional groups and missing bonds are observed. This might be due to the formation of complexes on iron surface.

4.7.2 SEM STUDY OF MS IN THE PRESENCE OF INHIBITORS

The surface morphology has taken in order to study the changes that occur on mild steel surface during the corrosion of MS in the presence of and absence of CN and BF extracts in 1 M HCl.

4.7.2.1 Scanning electron microscopy of MS in the presence of CN extracts

SEM photographs obtained for mild steel surface immersed in 1M HCl solutions at room temperature for 6 h in the absence and presence of 4.0%v/v concentration of CN extract are shown in Figure-58. Parallel features on the polished steel surface before exposed to the corrosive solution, which have associated with polished scratches, have observed (Figure-58.a). The corroded metal surface with etched grain boundaries is clearly seen in Figure-58.b, due to the direct attack of aggressive acids.

a. In CNS:

The SEM photograph in Figure-58.c shows the formation of a film by the active CNS constituents on the MS surface which is responsible for the corrosion inhibition. The inhibition properties of CNS extract may be due to the adsorption of phytochemical constituents in the extract on the MS surface present in the extract. These may be responsible for the formation of an oriented film layer by the adsorption of the active constituents of the extract on the MS surface, which essentially blocks discharge of H^+ and dissolution of metal ions. These results support the electrochemical impedance analyses and mass loss measurements **(Niketan Patel *et al.*, 2010)**.

b. In CNLS

Figures-58.d display images of mild steel surface after immerse in 1 M HCl in the presence of CNLS. Close examination of the SEM images revealed that the specimens immersed in the inhibitor solutions are in better conditions with smooth surfaces compared with those of corroded rough and coarse uneven surfaces of mild steel immersed in 1 M HCl. This observation indicated that corrosion rate is reduced to a very low value in the presence of the inhibitors. This might be due to the adsorption of phytochemical constituents on the MS surface as a protective layer **(Bothi Raja and Sethuraman, 2010).**

c. In CNP

The scanning electron micrographs of mild steel specimens exposed to 1 M HCl in the presence of 4.0%v/v of CNP is presented in Figure-58.e. In presence of CNP the surface of mild steel is less corroded in 1 M HCl than mild steel in 1 M HCl. The inhibitor molecule fully covers the metal surface, giving it a high degree of protection against corrosion, as proved by the absence of pits on the surface. Scanning electron microscopic studies reveal that the extent of corrosion of mild steel decreases with the increase of concentration of the inhibitors. This is in agreement with electrochemical results **(Ramananda Singh *et al.*, 2008)**.

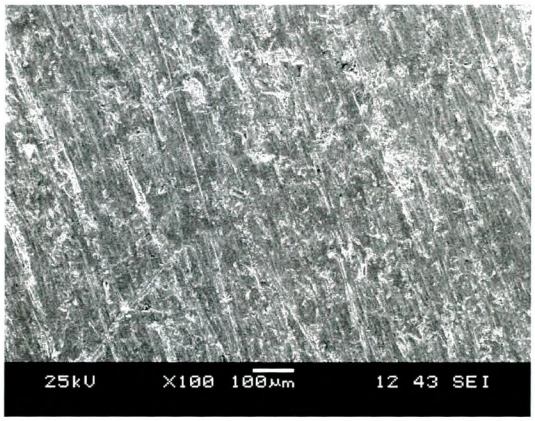

Figure-58.a Plain Mild Steel

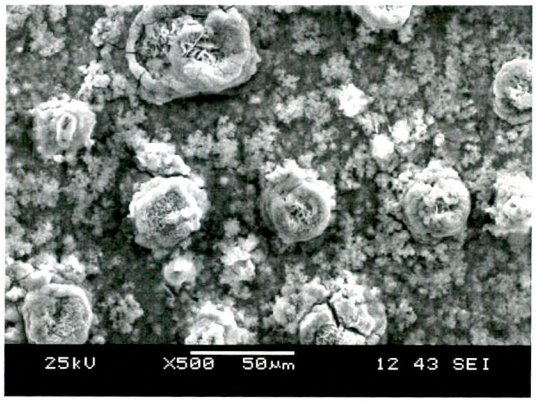

Figure-58.b Blank I M HCl

Figure-58.c Mild steel-CNS

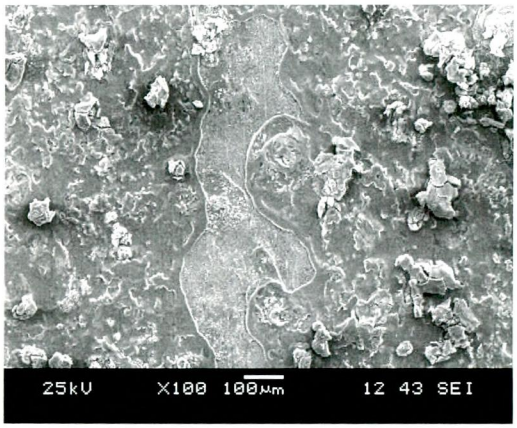

Figure-58.d Mild steel-CNLS

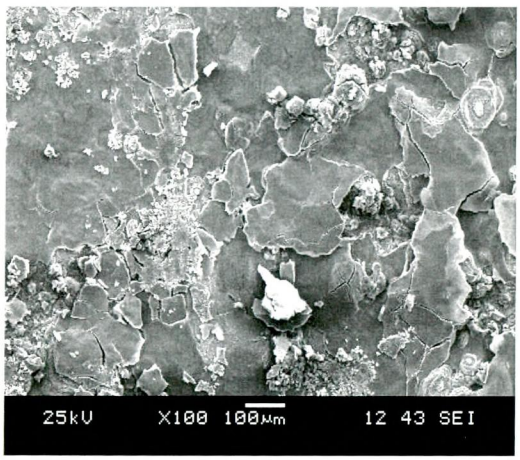

Figure-58.e Mild steel-CNP

Figure - 58 SEM micrograph of MS in 1 M HCl and in the presence of CN extracts

4.7.2.2 Scanning electron microscopy of MS in the presence of BF extracts

The SEM photographs for BF are depicted in Figure-59. The surface morphology of the sample before immersion in 1 M HCl solutions show a freshly polished steel surface (Figure-59.a), and the scratches are from the mechanical polishing treatment. Figure-59.b shows the surface morphology of the corroded mild steel surface in 1 M HCl.

a. In BFS

The SEM images (Figure-59.c) exhibited the features of mild steel surface after 6 h in 1 M HCl in presence of 4.0%v/v BFS at 313 K. The SEM images revealed that the mild steel specimens immersed in inhibited solution is in better condition having smooth surface, while the metal surface immersed in blank acid solution is rough covered with corrosion products and appeared like full of pits and cavities. This may be due to the phytochemical constituents present in BFS hinder the dissolution of iron by forming protective film on mild steel surface and thereby reduce the corrosion rate **(Bothi Raja *et al.*, 2010).**

b. In BFLS

SEM micrographs of the mild steel samples exposed to inhibited (1M HCl + 4.0%v/v BFLS) solutions for 6 h are displayed in Figure-59.d. The metal surface was fully covered with the inhibitor molecules and a protective inhibitor film was formed. The surface analysis result suggested higher adsorption of BFLS extract on the surface, which support the mass loss, EIS and polarization results **(Praveen *et al.*, 2009).**

c. In BFP

Surface examination using SEM (Figure-59.e) has carried to investigate the effect of inhibitor on the surface morphology of the mild steel. Figure 59.e shows SEM image of the surface of the mild steel specimens after immersion in 1 M HCl solution with BFP extract for 6 h. This can be viewed from Figure-59.e, the surface damage has diminished in the presence of inhibitors. It is revealed that the metal surface was highly covered with the protective layer formed by BFP extract which prevents the metal from further attack of acid media thus inhibiting corrosion **(Pandian Bothi Raja, 2009)**.

For the studied inhibitors the inhibited metal surface is smoother than the uninhibited surface indicating a protective layer of adsorbed inhibitor preventing acid attack. SEM images prove that CN and BF extracts could adsorb onto steel surface to form a dense and more tightly protective film. The film covered with anodic and cathodic reactive sites on the steel surface and inhibited both reactions at the same time.

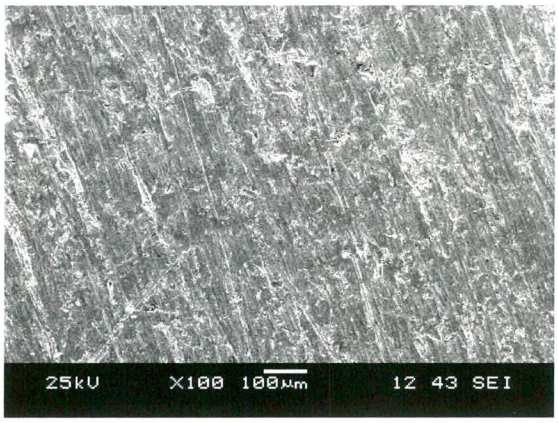

Figure-59.a Plain Mild steel

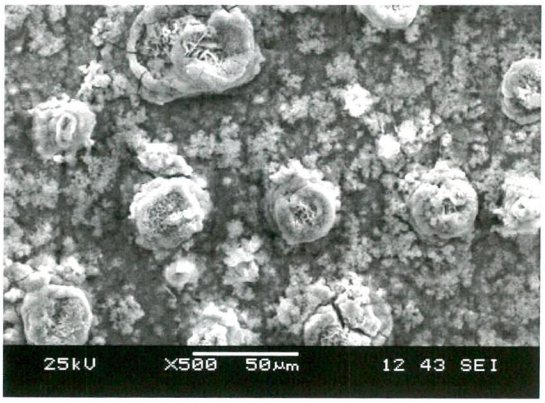

Figure-59.b Blank I M HCl

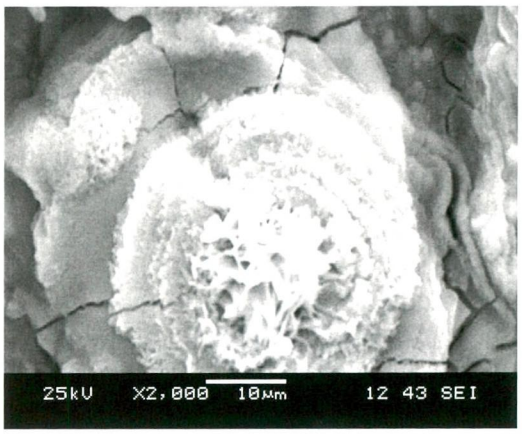

Figure-59.c Mild steel- BFS

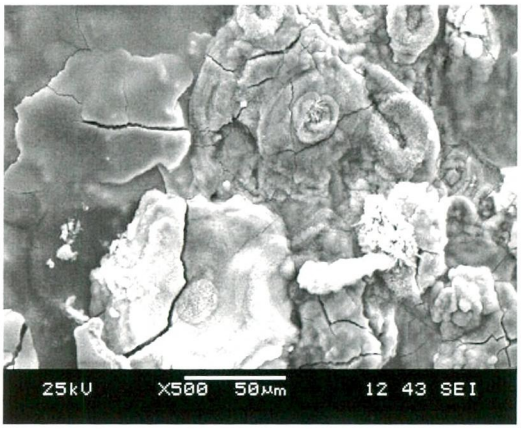

Figure-59.d Mild steel-BFLS

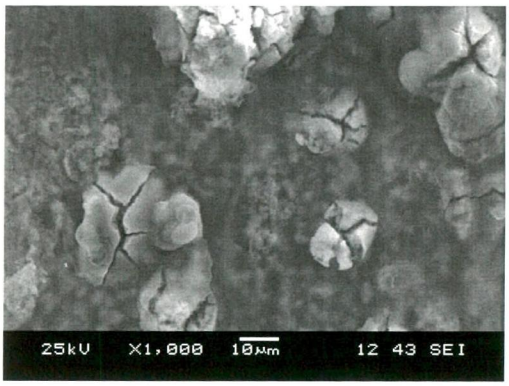

Figure-59.e Mild steel-BFP

Figure - 59 SEM micrograph of MS in 1 M HCl and in the presence of BF extracts

4.8 QUANTUM CHEMICAL CALCULATION

In the last few years, theoretical investigations based on quantum chemical calculations have been proposed as a powerful tool for predicting a number of molecular parameters directly related to the corrosion inhibiting property of any chemical compound **(Khaled and Hackerman, 2003; Bouayed *et al.*, 1999; Kutej *et al.*, 1995)**. Among several theoretical methods available, the density functional theory (DFT) is one of the most important theoretical models used in explaining the science of solids and chemistry. A number of chemical concepts have been correlated within the framework of DFT **(Parr and Yang, 1995).** The most fundamental parameter in DFT is the electron density ρ(r) upon which all the chemical quantities are expressed **(Parr and Yang, 1989).** Recently, the density functional theory (DFT) has been used to analyze the characteristics of the inhibitor/surface mechanism and to describe the structural nature of the inhibitor on the corrosion process **(Lashkari and Arshadi, 2004; Sein *et al.*, 2004; Blajier and Hubin, 2004)**. Furthermore, DFT is considered a very useful technique to probe the inhibitor/surface interaction as well as to analyze the experimental data.

Quantum chemical methods and molecular dynamic simulation have become an effective way to study the correlation between molecular structure and inhibition properties. Quantum chemical calculations have proved to be a very powerful tool for studying corrosion inhibition mechanism and helped to design the novel high efficiency inhibitors by the Quantitative Structure-Activity Relationship (QSAR) method. Molecular dynamic simulation is adopted as a beneficial supplement of quantum chemical method, which is applied to study the interaction between inhibitors and metal surface

One of the aspects of recent corrosion inhibition studies is the use of quantum chemical methods to calculate electronic properties possibly relevant to explain the inhibiting action. Among all computer simulation methods, quantum chemistry calculation has been widely used to evaluate the inhibition performance of corrosion inhibitors, which can quantitatively study the relationship between inhibition efficiency and molecular reactivity. With this method, the capability of inhibitor molecules to donate or accept electrons can be predicted with analysis of global reactivity parameters, such as energy gap between Highest Occupied Molecular Orbital (HOMO) and Lowest Unoccupied Molecular orbital (LUMO), chemical potential, hardness, softness, dipole moment etc.,

Quantitative structure-activity and structure property relationship studies are unquestionably of great importance in modern chemistry and biochemistry. The

concept of Quantitative Structure Activity Relationship (QSAR) and Quantitative Structure Activity and Structure Property Relationship Studies (QSPR) is to transform searches for compounds with desired properties using chemical intuition and experience into mathematically quantified and computed form. Once a correlation between structure and activity/property is found, any number of compounds, including those not yet synthesized, can readily be screened on the computer. **(Jun Zhang *et al.*, 2010)**

The reactive ability of the inhibitor is considered to be closely related to their frontier molecular orbitals, the HOMO and LUMO. Higher HOMO energy (E_{HOMO}) of the molecule means a higher electron donating ability to appropriate acceptor molecules with low-energy empty molecular orbital and thus explains the adsorption on metallic surfaces by way of delocalized pairs of π-electrons. E_{LUMO}, the energy of the lowest unoccupied molecular orbital signifies the electron receiving tendency of a molecule.

In general, significant differences can be appreciated referring to the inhibitory efficiency of phenolic derivatives. The understanding that the corrosion inhibition efficiency of organic compounds is related to their adsorption properties allows us to propose a possible mechanism. The inhibition efficiency depends strongly on the structures and chemical properties of the species formed under the experimental conditions studied. The extent of adsorption is dependent upon the electronic structure of the metal and the inhibitor.

In research on organic corrosion inhibitors, attention is paid to the mechanism of adsorption and also to the relationship between inhibitor structures and their adsorption properties. It has been observed that the adsorption depends mainly on the electronic and structural properties of the inhibitor molecule such as functional groups, steric factors, aromaticity, electron density on donor atoms and π orbital character of donating electrons **(Martinez, 2002)**.

In the present investigation, efforts has been taken to characterize the CN and BF extracts obtained by destructive distillation using FT-IR and GC-MS studies (Table-52 and 53). Based on these results, the major components present in CN and BF extracts were found to be 2-Methoxy 4-methylphenol (I), 2,6-Dimethoxy phenol (II), 2-Methoxy phenol (III) and Phenol (IV). Literature survey on the constituents present in CNS, CNLS, CNP & BFS, BFLS and BFP revealed the presence of phenolic compounds in *Cocos nucifera* L. and *Borassus flabellifer* L. plant parts. Analyzing these aspects, to suggest a suitable mechanism for inhibitive action of CN and BF extracts on mild steel surface, efforts are undertaken to perform theoretical calculations for 2-Methoxy-4-methylphenol (I), 2,6-Dimethoxy phenol (II), 2-Methoxy

phenol (III) and Phenol (IV) and these have been fully optimized using Gaussian 03 code of programs using the B3LYP hybrid functional and the 6-31 G (d) basis set.

The following quantum chemical parameters which indicate the structural characteristics of these common phytochemical constituents were considered: E_{HOMO}, E_{LUMO}, ΔE and μ. The optimized geometry of the corresponding Frontier Molecular Orbital density distribution of 2-Methoxy-4-methylphenol (I), 2,6-Dimethoxy phenol (II), 2-Methoxy phenol (III) and Phenol (IV) are depicted in Figure (60-63) It shows the values of some quantum chemical parameters, namely the energy of the highest occupied molecular orbital (E_{HOMO}), energy of the lowest unoccupied molecular orbital (E_{LUMO}), the energy gap (E_{LUMO}-E_{HOMO}) and dipole moment (μ) for selected major components in the investigated CN and BF extracts.

The major constituents of CN and BF were found to be I, II, III and IV. Quantum chemical calculation for these four major constituents were subjected to potential energy surface scans at the B3LYP/6-31 G(d) level of theory. All structures were drawn and optimized using the Chemcraft 1.6 and presented in Figure 60-63.

Analyzing the optimized geometry and frontier molecular orbital density distribution of main phytochemical constituents, it is clear that the phenyl ring being plane thus helping the interaction of phenolic derivatives with the metal surface. The ground state geometry of the inhibitor as well as the nature of its molecular orbitals, namely the HOMO and LUMO is involved in the activity properties of the inhibitors. When the frontier molecules are analyzed, the HOMO are localized over the oxygen, $-OCH_3$, -OH and the phenyl ring, consequently this is the preferred zone of the molecular interaction with the metal surface. Both the $-OCH_3$ and -OH can coordinate with mild steel. The effectiveness of a corrosion inhibitor can be related to its molecular spatial structure, molecular electronic structure as well as to its hydrophobicity, solubility and dispersibility **(Sastri and Paerumareddi, 1997)**. The optimized molecular structure for 2-Methoxy-4-methyl phenol, 2,6-Dimethoxy phenol, 2-Methoxy phenol and phenol as a major constituent of CN and BF are depicted in Figures-60a-63a. Quantum chemical parameters such as the energy (E_{HOMO}, E_{LUMO}) of the highest occupied molecular orbital (HOMO) and the lowest unoccupied molecular orbital (LUMO), the energy gap $\Delta E_{HOMO-LUMO}$ between HOMO and LUMO and the molecular dipole μ are listed in Table-52 and 53.

a. 2-Methoxy-4-methyl phenol:

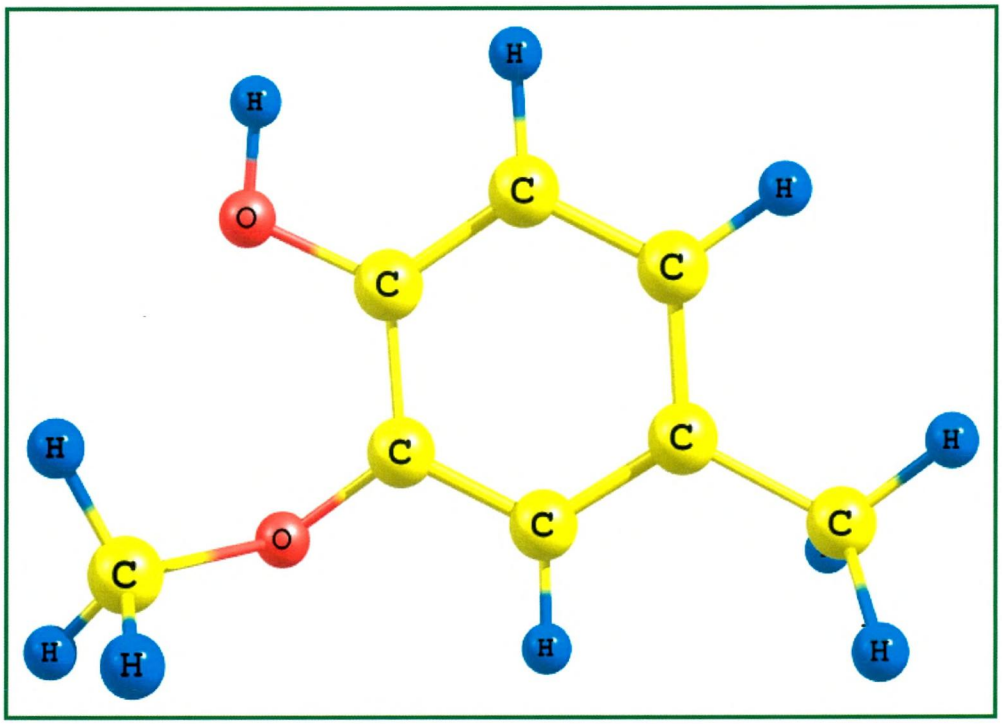

Figure – 60.a Optimized structure of 2- Methoxy-4-methyl phenol

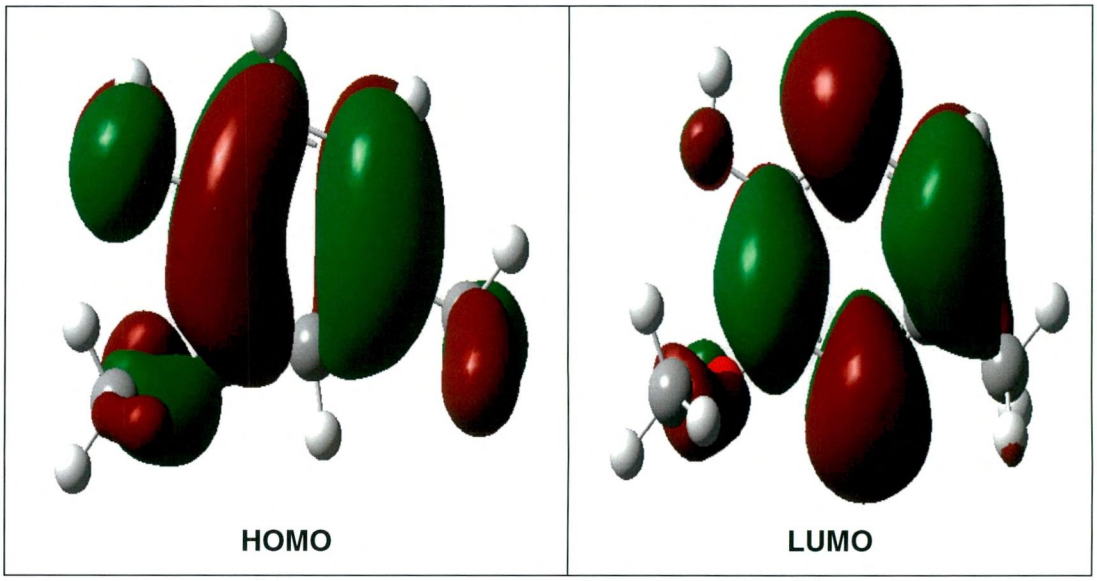

(b) (c)

Figure – 60 (b and c) Frontier Molecular orbital density distribution of 2-Methoxy-4-methyl phenol

b. 2, 6-Dimethoxy phenol:

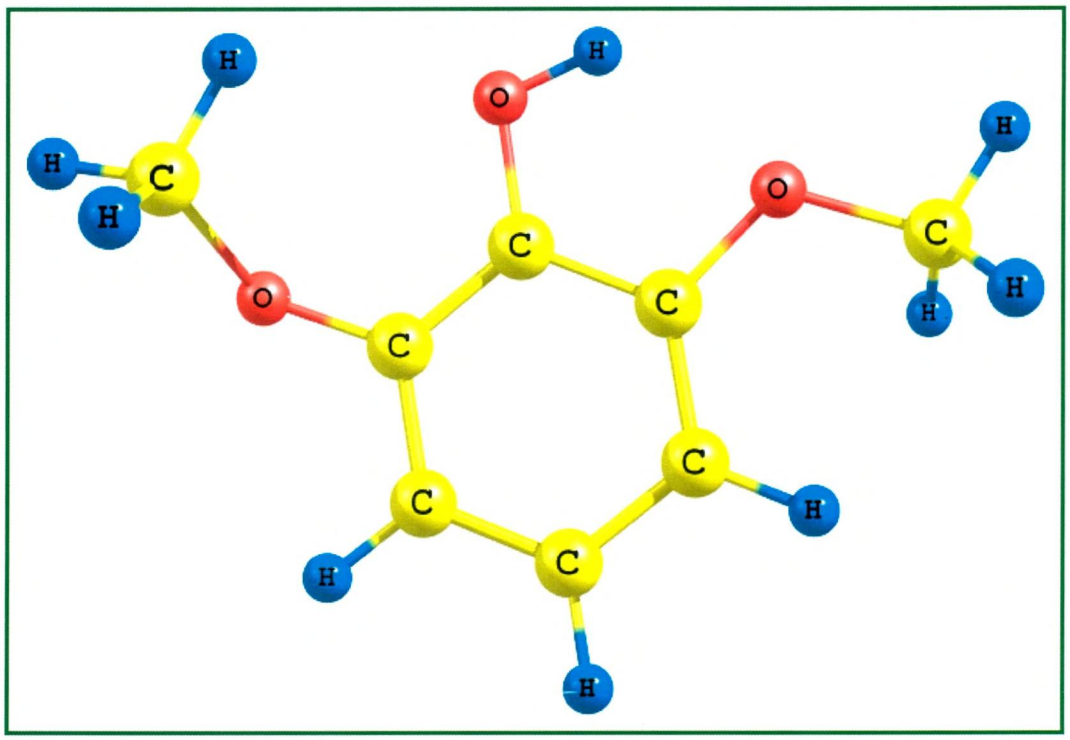

Figure – 61.a Optimized structure of 2, 6-Dimethoxy phenol

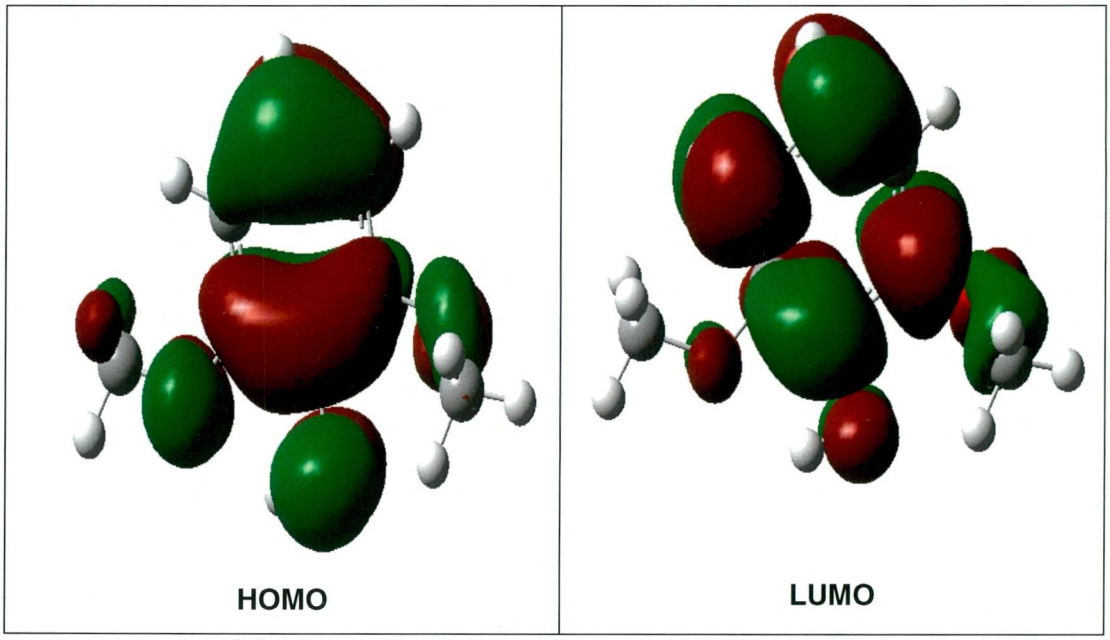

(b) (c)

Figure –61 (b and c) Frontier Molecular orbital density distribution of 2, 6 - Dimethoxy phenol

c. 2- Methoxy phenol:

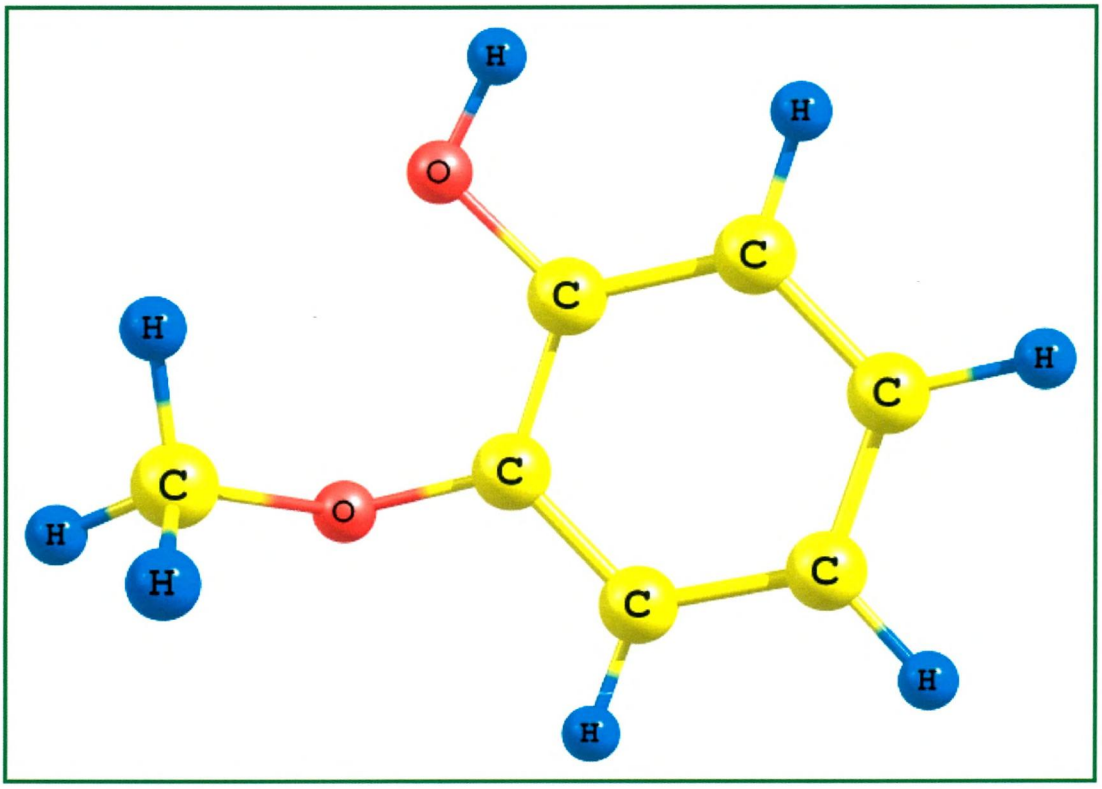

Figure –62. a Optimized structure of 2- Methoxy phenol

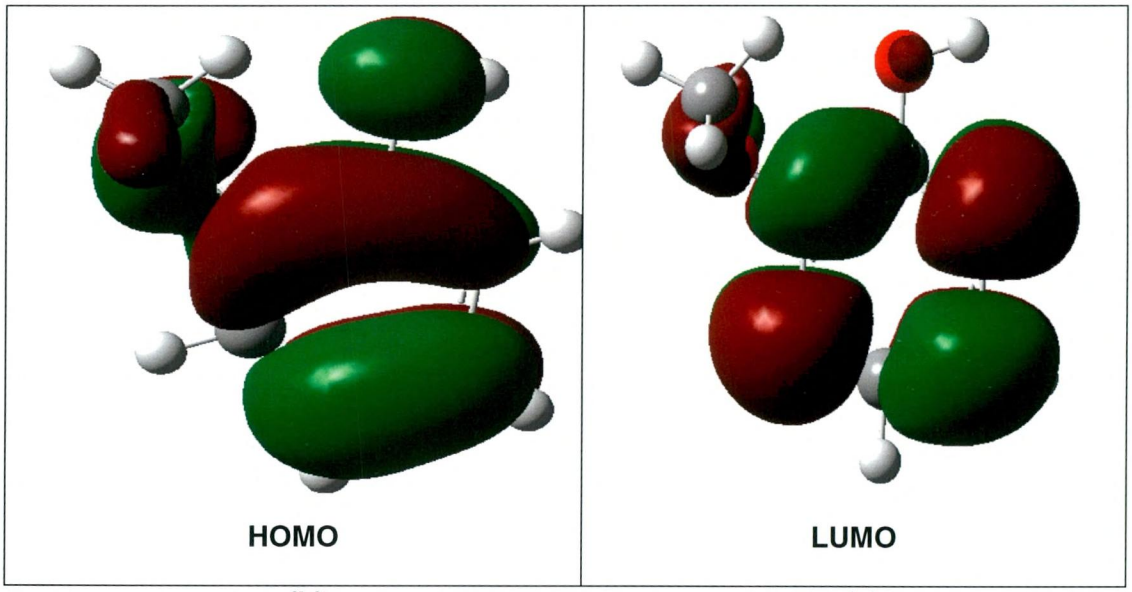

(b) **(c)**

Figure – 62 (b and c) Frontier Molecular orbital density distribution of 2-Methoxy phenol

d. Phenol:

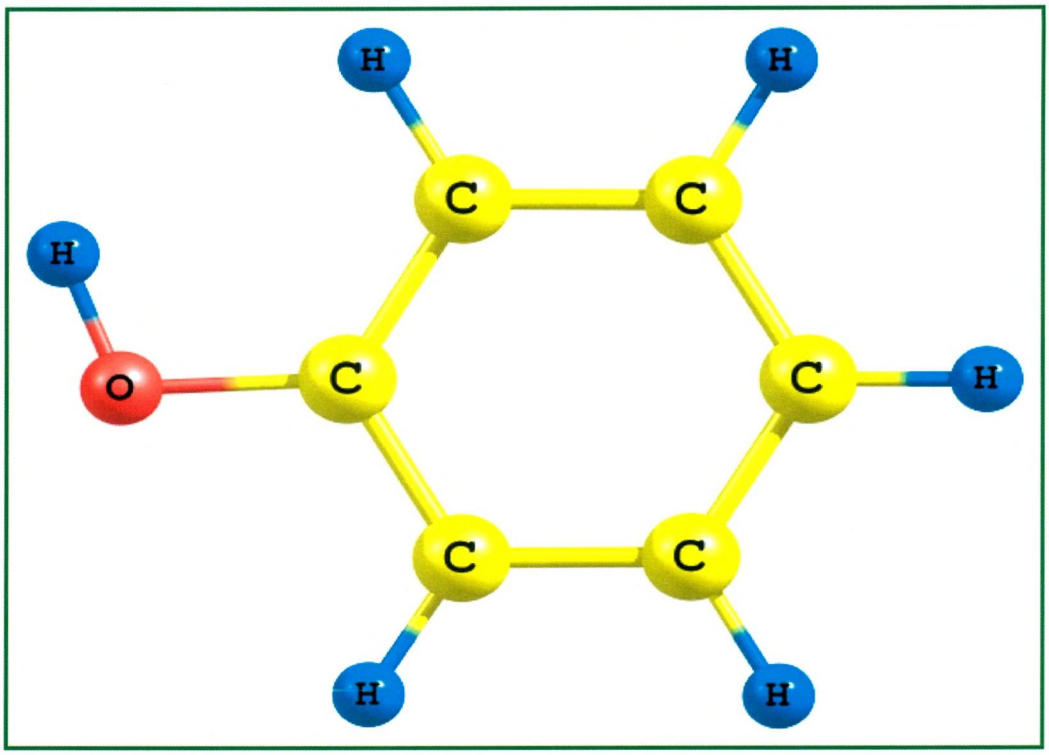

Figure – 63.a Optimized structure of Phenol

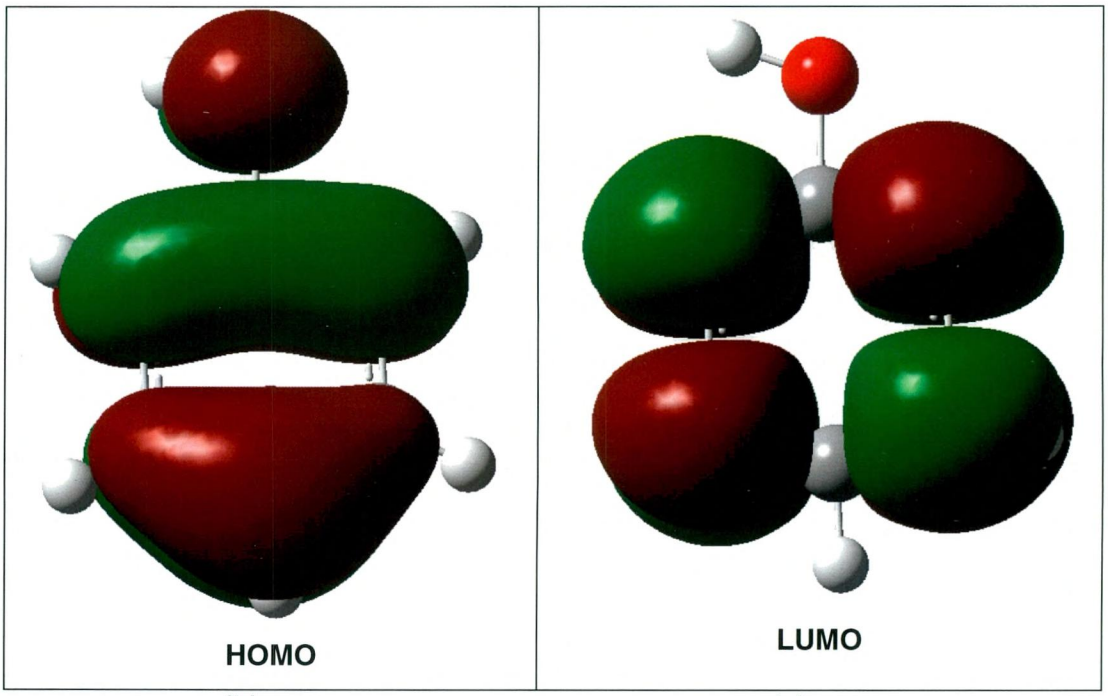

(b) **(c)**

Figure – 63 (b and c) Frontier Molecular orbital density distribution of Phenol

Table - 52 Quantum chemical parameters for the selected phenolic derivatives using Gaussian 03 code of programs using B3LYP hybrid functional and the 6-31 G (d) basis set

Inhibitor	HOMO (eV)	LUMO (eV)	HF (eV)	ΔE (eV)	Dipole Moment (Debye)	ΔN
2-Methoxy-4-methyl phenol	-5.6608	-0.1499	-12552.64	-5.5109	2.0424	1.4860
2,6-Dimethoxy phenol	-5.5372	-0.4348	-14599.13	-5.1024	3.1789	1.5733
2-Methoxy phenol	-5.8211	-0.1308	-11482.74	-5.6902	2.1391	1.4143
Phenol	-5.9571	-0.0359	-8366.61	-5.9212	1.3514	1.3522

4.8.1 Dipole Moment

The dipole moment (μ) is an index that can also be used for the prediction of the direction of a corrosion inhibition process. Dipole moment is the measure of polarity in a bond and is related to the distribution of electrons in a molecule. Although literature is inconsistent on the use of 'μ' as a predictor for the direction of a corrosion inhibition reaction, it is generally agreed that the adsorption of polar compounds possessing high dipole moments on the metal surface should lead to better inhibition efficiency.

In the current study, the dipole moment values were in the order 2,6-Dimethoxy phenol > 2-Methoxy-4-methyl phenol > 2-Methoxy phenol > Phenol. The observed increase of the dipole moment with the increase in the number of –OH and $–OCH_3$ groups (Table-52) is in accordance with the assumption that oxygen lone-pair electrons are major contributors to the overall dipole moment of the molecule **(Lukovits *et al.*, 2001).** Dipole moment values of the selected phytochemical constituents confirmed the adsorption of all these phenolic derivatives onto mild steel surface

4.8.2 E_{HOMO} & E_{LUMO}

The HOMO energy (E_{HOMO}) is often associated with the electron density ability of the molecule, whereas the (E_{LUMO}) indicates the ability of the molecule to accept electron. The regions of highest electron density (HOMO) are the sites at which electrophiles attack and represent the active centers, with the utmost ability to bond to the metal surface, whereas the LUMO orbital can accepts the electrons in the orbital of the metal using antibonding orbitals to form feedback bonds **(Martinez and stagljar, 2003)**. Therefore, high values of the E_{HOMO} indicate an increased tendency

of the inhibitor to donate electron to the vacant d orbital of Fe in mild steel. Similarly, E_{LUMO} represents the ability of the molecule to accept electrons.

Table - 53 Calculated Quantum chemical parameters for the selected phenolic derivatives using Gaussian 03 code of programs using B3LYP hybrid functional and the 6-31 G (d)basis set

Inhibitor	IP (eV)	EA (eV)	η (eV)	S (eV)	X (eV)	ω
2-Methoxy-4-methyl phenol	5.6608	0.1499	2.7554	0.1814	2.9053	1.5316
2,6-Dimethoxy phenol	5.5372	0.4348	2.5512	0.1959	2.986	1.7474
2-Methoxy phenol	5.8211	0.1308	2.8451	0.1757	2.9759	1.5563
Phenol	5.9571	0.0359	2.9606	0.1688	2.9965	1.5164

The lower the values of E_{LUMO}, the more probable it is that the molecule would accept electrons. Increasing values of E_{HOMO} and decreasing value of E_{LUMO} suggest efficient adsorption process. Generally, the lower the energy gap, the better the electron transfer process. According to **Mihit *et al.*, (2010)** high values of the E_{HOMO} facilitate adsorption and enhance inhibition efficiency by influencing the transport process through the adsorbed layer. Large values of energy gap ($E_{L-H} = E_{LUMO} - E_{HOMO}$) implies increased electronic stability and low reactivity, while low values render good inhibiting efficiency because the energy to remove an electron from the last occupied orbital will be low.

Analysis of Table-52, indicated that the values of E_{HOMO} of I, II, III and IV compounds increased in the following order: **II > I > III >IV**.

The values of ΔE decreased in the following order: **II< I < III <IV.** The values of HOMO pertaining to the main phytochemical constituents – I, II, III and IV indicate the greater tendency of these phytochemical constituents to donate the electron to the vacant d-orbital of the iron atom. Therefore CN and BF extracts had the tendency to bind with the metal surface. The HOMO and LUMO electronic density distributions of these molecules (2,6-Dimethoxy phenol (I), 2-Methoxy 4-methyl phenol (II), 2-Methoxy phenol (III) and Phenol (IV)) were plotted in Figure-64. For the HOMO of the studied compounds, it canbe observed that the π electrons in benzene ring, -O,-OCH_3 have a large electron density. Figure-64 shows the size and position of the HOMO-LUMO gap.

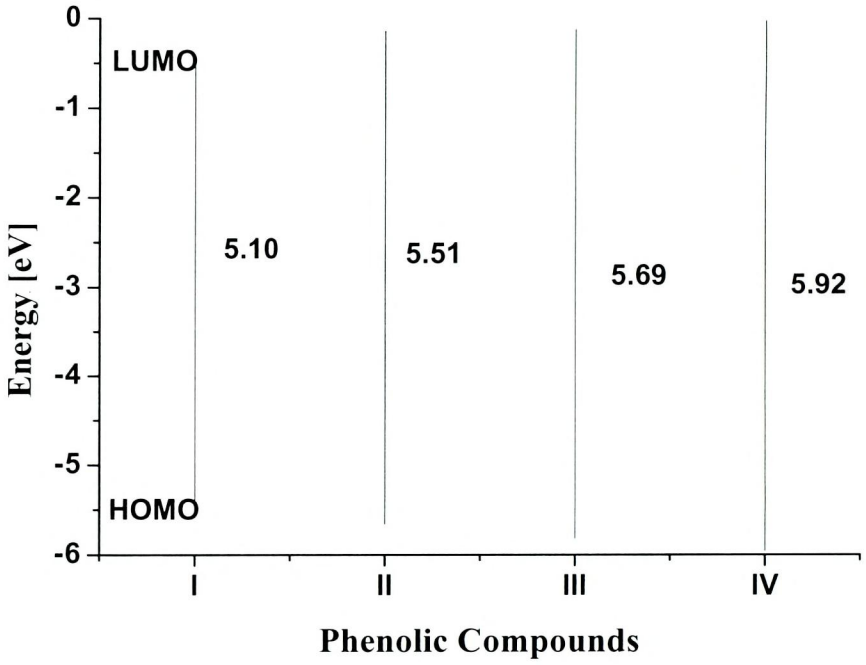

Figure- 64 Relation between frontier molecular orbitals of I, II, III & IV and their gap energy.

4.8.3 ΔN (number of electrons)

If bulk iron metal and the inhibitor molecule are brought together, the flow of electrons will occur from the molecule of lower electronegativity to the iron that has higher electronegativity until the value of the chemical potential becomes equal **(Martinez, 2002)**.

The number of electrons transferred (ΔN) from the inhibitor molecule to the metallic atom was also calculated using the following equation:

$$\Delta N = (\chi_{Fe} - \chi_{inh}) / 2(\eta_{Fe} + \eta_{inh}) \quad (4.18)$$

where χ_{Fe}, χi_{nh} represent the absolute electronegativity of iron and the inhibitor molecule, respectively and $\eta_{Fe} + \eta_{inh}$ represent the absolute hardness of iron and the inhibitor molecule. These quantities are associated with electron affinity (EA) and ionization potential (IP) which are useful in their ability to help chemical behaviour.

$$\chi = \frac{IP + EA}{2} \quad (4.19)$$

$$\eta = \frac{IP - EA}{2} \quad (4.20)$$

where IP and EA are related in turn to E_{HOMO} and E_{LUMO} as following equations:

$$IP = - E_{HOMO} \quad (4.21)$$

and $$EA = - E_{LUMO} \quad (4.22)$$

Inorder to calculate ΔN, a theoretical value for the electronegativity of bulk iron was used $\chi_{Fe} \approx 7$ eV and global hardness of $\eta_{Fe} \approx 0$, by assuming that for a metallic bulk IP = EA, because they are softer than the neutral metallic atoms. The values of ΔN for I, II, III and IV are represented in Table- 52.

If $\Delta N < 3.6$, the inhibition efficiency increased with increasing electron donors ability at the metal surface. It can be inferred from the results that inhibitors investigated in this current study were donating electrons and the iron surface was the acceptor.

4.8.4 Global Softness

As expected, there are some similarities in the trends between the above parameters and frontier orbital molecular energies. The global softness S for the investigated inhibitors is the same, suggesting that softer molecules are stronger inhibitors. Calculated values of S and η are also presented in Table -53. From Table-53, it is evident that the inhibitor with the least value of global hardness (hence the highest value of global softness) is the best and *vice versa*. This is because a soft molecule is more reactive than a hard molecule. This frontier orbital may be also be used to predict the adsorption centers of the inhibitor molecule. For the easiest transfer of electrons, adsorption should occur at the part of the molecule where the softness σ, which is a local property, has the highest value **(Martinez, 2002)**.

4.8.5 Ionization Potential and Electron Affinity

Values of *IP* and *EA* calculated are presented in Table -53. The results obtained indicate that the inhibition efficiencies of the inhibitors increase with increasing ionization energy but decrease with decreasing value of electron affinity. This is because IP is directly related with the E_{HOMO}, while *EA* is related to the E_{LUMO}. This explains why the trend for the variation of inhibition efficiencies of the inhibitors with IP and EA are similar to those obtained for E_{HOMO} and E_{LUMO} data. According to the data the trend in IE and EA are as follows:

II > I > III > IV

Figure (60-63) represents the optimized structures and the HOMO and LUMO diagrams of I, II, IIII and IV. The spatial distribution of the HOMO and the LUMO are important for understanding the adsorption preferences of the inhibitors. Considering that the inhibitors would be electron donors with respect to the steel surface, the HOMO distribution would be of particular importance. The HOMO distribution maps of I, II, III and IV are very similar and the HOMO is localized on the phenyl ring suggesting strong docking to the phenyl ring **(Martinez, 2002)**. DFT – based

quantum chemical computations of parameters associated with the electronic structures of specific components of the extract confirmed their inhibiting potentials.

Analyzing the quantum chemical parameters obtained the inhibition process can be explained as follows:

In a corrosion system containing inhibitor, the inhibitor and the metal act as a lewis base and a lewis acid, respectively, therefore the frontier orbital theory may be used to determine possible modes of interaction between the inhibitor and metal **(Sastri, 1998)**. If bulk iron metal and the inhibitor molecule are brought together, the flow of electrons will occur from the molecule of lower electronegativity to the iron that has higher electronegativity until the value of the chemical potential becomes equal.

The stability of the adsorption bond may further be related to the pearson's HSAB principle **(Pearson, 1989)**. Bulk metals are soft acids, thus soft base inhibitors are most effective for metals corroding in acid solutions. **Klopman, (1968)** relates the hard-hard at soft-soft bond character, respectively, to electrostatic (charge controlled) and covalent (Frontier controlled) reactions. In case of the soft-soft inhibitor-metal interaction, the bond is largely covalent in character and is accomplished by a favorable overlap of the frontier orbitals, i.e., HOMO and LUMO. The results obtained by the above analysis (Table – 52) imply the possibility of soft-soft interaction between metal acting as a soft acid and inhibitor acting as a soft base in the investigated system as described by **Martinez and Stagljar, (2003)**.

Frontier orbital theory may also be used to predict the adsorption centers of the inhibitor molecules. For the easiest transfer of electron, adsorption should occur at the part of the molecule where the softness σ, which is a local property, has the highest value. Characterization of CN and BF revealed the presence of many phytochemical constituents (Table – 3-4 & 6-9). The adsorption centers in the present system were found to be $-OCH_3$, -OH and phenyl ring.

Quantum chemical studies were conducted for the main constituents present in both the extracts. Hence it is reasonable to assume that the higher mass fraction of CN and BF extracts, not included in the present analyses would contain even more polar compounds and more complicated geometric structures. Thus the suggested adsorption mechanism would also apply to this fraction of extract **(Martinez and Stagljar, 2003)**.

4.9 MECHANISM OF INHIBITION PROCESS

Mechanism of the inhibition process for studied inhibitors can be discussed on the basis of the experimental findings from mass loss, electrochemical measurements and surface analytical techniques.

In the present investigation corrosion inhibition of mild steel in 0.5 M H_2SO_4 and 1M HCl using CN and BF extracts could furnish the following results:

- ✶ All the investigated CN and BF extracts obey Frumkin adsorption isotherm besides other adsorption isotherms indicating that the CN and BF extracts are of adsorptive type. The inhibition process is due to the adsorption of the inhibitor molecules onto the mild steel surface.
- ✶ The negative values of ΔG°_{ads} could confirm that the adsorption process is not merely physical adsorption or chemical adsorption but a mixed adsorption.
- ✶ Inspection of the data from El-Awady adsorption isotherm shows that the 'x' is the number of inhibitor molecules occupying one active site (or the number of water molecules replaced by one molecule (1/y = x). Values of 'x' less than one and are approximately equal to one mean that the studied inhibitor molecule will occupy more than one active site. Values indicate that the phytochemical constituents present in the studied inhibitors molecules occupy more than one active site **(Abd-El Rehim *et al.*, 2001).**
- ✶ Values of cathodic and anodic Tafel constant confirm that the investigated CN and BF extracts under study act as mixed type of inhibitors.
- ✶ Surface analytical techniques' using FT-IR spectroscopic studies confirmed that FT-IR analysis of the CN and BF extracts and corrosion products of CN and BF extracts on mild steel surface reveals the iron-CN and iron-BF complex **(Jaen *et al.*, 1999).** Again the IR patterns of corrosion products are similar to the CN and BF extracts, though some shift in the frequencies of some functional groups and missing bonds are observed. This might be due to the formation of complexes on iron surface and SEM investigate that the images prove that CN and BF extracts could adsorb onto steel surface to form a dense and more tightly protective film. The film covered both anodic and cathodic reactive sites on the steel surface and inhibited both reactions at the same time. Thus CN and BF extracts on the mild steel surface prevents corrosion in acid medium.
- ✶ DFT-based quantum chemical computations of parameters associated with the electronic structures of specific components of the extract confirmed their inhibiting potentials.

✶ Analyzing the optimized geometry and frontier molecular orbital density distribution of main phytochemical constituents, it is clear that the phenyl ring being plane thus helping the interaction of phenolic derivatives with the metal surface. The ground state geometry of the inhibitor as well as the nature of its molecular orbitals, namely the HOMO and LUMO is involved in the activity properties of the inhibitors. When the frontier molecules are analyzed, the HOMO are localized over the oxygen, $-OCH_3$, -OH and the phenyl ring, consequently this is the preferred zone of the molecular interaction with the metal surface. Both the $-OCH_3$ and -OH can coordinate with mild steel.

The use of corrosion inhibitors increases continually **(Antropov *et al.*, 1981)**. The mechanism of their action can be different, depending on metal, the medium and the structure of the inhibitor. Generally, two modes of adsorption are considered on the metal surface in acid media. In one mode, the neutral molecules may be adsorbed on the surface of mild steel through the chemisorption mechanism, involving the displacement of water molecules from the mild steel surface and the sharing of electrons between the hetero atoms and iron. The inhibitor molecules can also adsorb on the mild steel surface on the basis of donor-acceptor interactions between π-electrons of the aromatic ring and vacant d-orbitals of surface iron atoms. In second mode, since it is well known that the steel surface bears positive charge in acid solution **(Mu *et al.*, 1996)**, it is difficult for the protonated molecules to approach the positively charged mild steel surface (H_3O^+/metal interface) due to the electrostatic repulsion. Since chloride ions have a smaller degree of hydration, they could bring excess negative charges in the vicinity of the interface and favor more adsorption of the positively charged inhibitor molecules, the protonated inhibitors adsorb through electrostatic interactions between the positively charged molecules and the negatively charged metal surface. Thus, there is a synergism between adsorbed Cl^- ions and protonated inhibitors.

The main constituents of extracts of CN/BF are listed in Table-(3-5 & 7-9) **(Khanna and Seshadri, 1964)**. The high performance of CN/BF extracts could also be due to synergistic effect of all constituents which covers wide areas on the metal surface and thus retarding the corrosion **(Trabenelli and Mansfeld, 1987).** It is not possible to consider a single adsorption mode between inhibitor and metal surface because of the complex nature of adsorption and inhibition of a given inhibitor. The adsorption of main constituents of CN/BF extracts can be attributed to the presence

of O-atom, π-electrons and aromatic rings. Presence of methoxy group also enhances the inhibition efficiency. Therefore, the possible reaction centers are unshared electron pair of hetero-atoms and π-electrons of aromatic ring which was also confirmed from quantum chemical studies.

In aqueous acidic solutions, main constituents exist either as neutral molecules or as protonated molecules (cations). The inhibitors may adsorb on the metal/acid solution interface by one and/or more of the following ways:

- ✶ Electrostatic interaction of protonated molecules with already adsorbed chloride ions,
- ✶ Donor-acceptor interactions between the π-electrons of aromatic ring and vacant d orbital of surface iron atoms,
- ✶ Interaction between unshared electron pairs of hetero atoms and vacant d-orbital of iron surface atoms.

The corrosion of mild steel in aqueous acidic solutions can be inhibited by the extract of shell, leaf stalk and peduncle of CN/BF. It is often not possible to assign a single general mechanism of action to an inhibitor, because the mechanism may change with experimental conditions. Thus, the predominant mechanism of action of an inhibitor in acidic solutions may vary with factors such as concentration of the extracts, the nature of the anion of the acid, the presence of other species in the solution, the extent of reaction to form secondary inhibitors and the nature of the metal **(Shreir *et al.*, 1994)**.

Another possible mechanism is the adsorption of the inhibitor, which blocks the metal surface and thus do not permit the corrosion process to take place **(Christov and Popova, 2004).** In the current investigation using CN and BF extracts as corrosion inhibitors for MS in both acid media, CN/BF might be protonated in the acid media as follows:

$$CN / BF + x\, H^{+} \leftrightarrow [CN / BFH_x]^{x+} \qquad (4.23)$$

Thus, in aqueous acidic solutions, the CN/BF exists either as neutral molecules or in the form of cations (protonated CN/BF). In general, two modes of adsorption could be considered. The neutral CN/BF may adsorb onto the metal surface via the chemisorption mechanism, involving the displacement of water molecules from the metal surface and sharing electrons between the O atoms and Fe. The CN/BF

molecules can also adsorb on the metal surface on the basis of donor-acceptor interactions between π-electrons of aromatic ring and vacant d-orbitals of Fe. On the other hand, it is well known that the steel surface charges positive charge in acid solution, so it is difficult for the protonated CN/BF to approach the positively charged steel surface (H_3O^+/metal interface) due to the electrostatic repulsion. Since chloride ions have a smaller degree of hydration, being specifically adsorbed, they create an excess negative charge toward the solution and favor more adsorption of the cations **(Bentiss *et al.*, 2000)**. The protonated CN/BF may adsorb through electrostatic interactions between the positively charged molecules and the negatively charged metal surface. In other words, there may be a synergism between Cl^- and CN/BF, which improves the inhibitive capability of the inhibitor. When protonated CN/BF is adsorbed on metal surface, a coordinate bond may be formed by partial transference of electrons from polar atoms (O atoms) to the metal surface. In addition, owing to lone-pair electrons of O atom in CN/BF, CN/BF or protonated CN/BF may combine with freshly generated Fe^{2+} ions on steel surface forming metal inhibitor complexes:

$$Fe \rightarrow Fe^{2+} + 2e \qquad (4.24)$$

$$CN / BF + Fe^{2+} \leftrightarrow [CN / BF\text{-}Fe]^{2+} \qquad (4.25)$$

$$[CN / BFH_x]^{x+} + Fe^{2+} \leftrightarrow [CN / BFH_x\text{-}Fe]^{(2+x)+} \qquad (4.26)$$

Similar type of mechanism was also proposed by **Xiang-Hong Li *et al.*, (2010).** These complexes might be adsorbed onto steel surface by vander Waals force to form a protective film to prevent mild steel from corrosion.

Electrochemical mechanism was proposed by **Graeme Wright, (1998).** This adsorption model can also be suggested for CN/BF extracts in mild steel acid corrosion. The anodic and cathodic reactions involved in the corrosion of metal in acidic solutions are:

$$M \rightarrow M^{n+} + ne^- \qquad \text{Anodic} \qquad (4.27)$$

$$H^+ + e \rightarrow H \qquad \text{Cathodic} \qquad (4.28)$$

$$H + H \rightarrow H_2 \qquad (4.29)$$

Another adsorption model can also be suggested for the adsorption of CN/BF extracts on mild steel surface in acidic media. The adsorbed inhibitor blocks either the anodic or cathodic reaction or both (Figure-65). Adsorption is the primary step in

achieving inhibition in acid solutions. This is a consequence of the fact that the corroding metal surface to be inhibited is usually oxide-free allowing the inhibitor ready access to retard the cathodic and/or the anodic electrochemical processes of corrosion. Once the inhibitor has adsorbed on the metal surface it can then affect the corrosion reactions in a number of ways: by offering a physical barrier to the diffusion of ions or molecules to or from the metal surface; direct blocking of anodic and/or cathodic reaction sites; interaction with corrosion reaction intermediates; change the make-up of the electrical double layer which develops at the metal/solution interface and so affect the rate of electrochemical reactions **(Graeme Wright, 1998).**

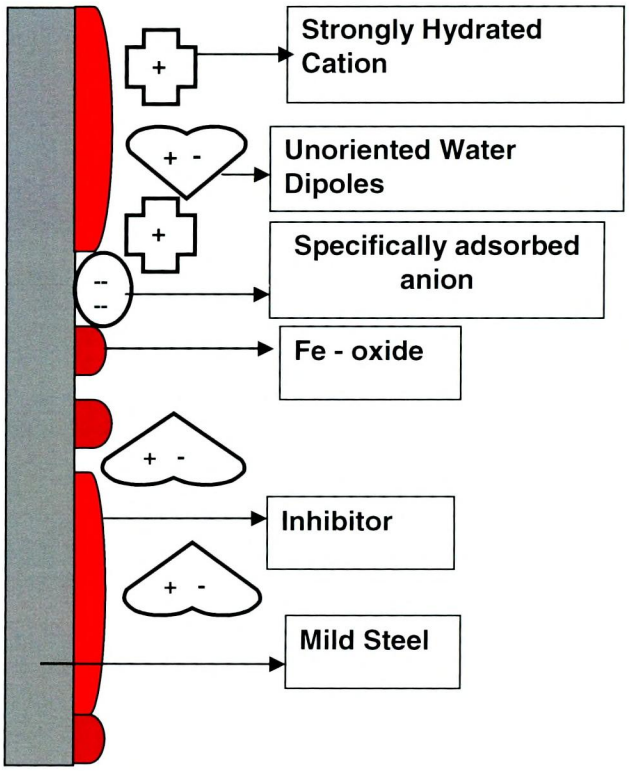

Figure -65 Adsorption model of MS in the presence of CN/BF extracts

While considering electrostatic interaction of the inhibitors with the metal surface the question arises whether the inhibitor molecule exits, in a solution, in a molecular or a protonated form. Analyzing the values of ΔG and E_a it may be concluded a mixed adsorption involving physical as well as chemical adsorption. The phytochemical constituents in CN and BF extracts interact with metal surface both in a molecular form as well as protonated form **(Martinez and Stagljar, 2003)**. Similar type of mechanism was also proposed by **Ehteram A. Noor, 2007 and Emeka E. Oguzie, 2008b.**